Dose Verification of a Stereotactic IMRT Treatment Planning System

by

Zheng Xian

B.Sc., Peking University, 2005

A THESIS SUBMITTED IN PARTIAL FULFILMENT OF
THE REQUIREMENTS FOR THE DEGREE OF

Master of Science

in

The Faculty of Graduate Studies

(Physics)

The University Of British Columbia

(Vancouver)

April, 2010

Abstract

In this project, ion chamber measurement and film dosimetry were used to verify dose distributions for a new stereotactic IMRT (Intensity Modulated Radiation Therapy) treatment planning system. This technique combines the principles of stereotactic radiosurgery and IMRT to significantly increase the positioning accuracy compared with conventional IMRT . Ion chamber measurements reveal that the discrepancy between the measured and the calculated dose at the isocenter can be up to 2 %. Angular dependence of ion chamber sensitivity and the tissue equivalence of the phantom material were determined to be the main sources of this discrepancy. Radiochromic film was used as the film dosimeter in the project. A set of performance tests of Gafchromic EBT film indicated that the uncertainty in Gafchromic EBT film dosimety was expected to be 2.5 %. However, the discrepancies we found in measurements of clinical cases using the film were much larger than this. And further investigation into this discrepancy was beyond the scope of this thesis.

Table of Contents

Appendices

List of Tables

List of Figures

Acknowledgements

Chapter 1

Introduction

Radiation therapy or radiotherapy, is the medical application of radiation most commonly as part of cancer treatment. External beam radiotherapy is the most frequently used form of radiotherapy, during which, the patient usually lies on a couch and the radiation beam coming from the therapeutic equipment is directed to the patient's body to kill the malignant cells within the target volume. A more detailed introduction to the physics of radiation therapy is given in Chapter 2, Section 2.1.1. The radiation beam causes damage to both malignant cells and healthy tissue, therefore, different treatment techniques are used to confine the dose (which is the energy per unit mass deposited by the radiation beam) to the target volume. From the most simple square field irradiation to more complex techniques such as RapidArc™[1], radiotherapy techniques have improved along with advances in equipment to increase the accuracy, flexibility and efficiency of beam delivery. Intensity modulated radiotherapy or IMRT for short, is one of the modern radiotherapy techniques that can dramatically improve the dose coverage and normal tissue sparing. This technique not only confines the beam outline but is capable of modulating the beam intensity across the plane perpendicular to the beam axis. By projecting multiple beams from different angles, three dimensional dose modulation can be achieved. This technique is particularly useful and necessary in some situations such as when the target volume is close to critical organs that must be protected, or the shape of the target volume is highly irregular. The hardware that is used to achieve the modulation is called a multi-leaf collimator or MLC, which is nowadays a standard build-in part of most medical accelerators. The leaves of the MLC travel dy-

namically while the beam is being delivered, blocking different parts of the field at different moments. The relation between the leaf sequence and dose distribution is complicated. (Further discussions about IMRT are found in 2.3.2.)

Quality control is important for radiation therapy. The ultimate goal of quality control is to ensure the desired dose distribution is delivered as planned. Quality control for radiation therapy includes: commissioning of new equipment, periodic quality assurance (QA) on hardware and software and dose verification of individual patients' treatment plans. Dose verification is an essential part of both commissioning and patient plan dose verification. For IMRT the dose calculation depends on accurate modeling of the MLC leaves. Most MLC leaves have specially designed rounded leaf tips to follow the beam divergent line for different field sizes. The MLC leaf cross section is also not rectangular, but is designed in a tongue and groove style to minimize the inter-leaf leakage[2]. For most of the time during beam delivery the MLC opening is small compared to the range of electrons set in motion by the photon beam, therefore electron disequilibrium may be significant and this is difficult for the treatment planning software to account for. The dose delivery is also affected by the mechanical performance of the MLC. Considering all these factors, the agreement between the dose distribution calculated from the treatment planning system and the delivered result is usually worse than for simpler techniques. A thorough dose verification is thus required for both commissioning purposes and individual patient plan verification to ensure that any discrepancies are within clinical tolerance.

Ideally, a three dimensional dose measurement method would be the most comprehensive test, however, currently there is no such three dimensional measurement technique that can meet the requirements of both spatial resolution and accuracy. A gel dosimeter[3] and an accurate tomography technique may be a solution but gel dosimeters are not routinely used due to a number of practical issues. The most commonly used methods of IMRT dose

verification include ion chamber measurement, film dosimetry and Monte Carlo simulation[4]. An ion chamber measurement provides the most reliable and accurate dose reading but cannot easily provide information about the dose distribution, therefore it is usually used to acquire a single reference point dose reading. Film dosimetry can be used to measure the two dimensional dose distributions. Unfortunately, the absolute dose reading for film dosimetry is in general inaccurate, and is the result of several factors such as limitations of the film itself, the performance of the optical scanner and chemical processing. (Detailed discussion of film dosimetry is given in Chapter 2.) Monte Carlo techniques can simulate particle interactions and transport from the linac to and within the patient's body and therefore can calculate dose distributions accurately[5]. One option for verification of the treatment planning dose calculation is to do an independent simulation of the dose using Monte Carlo techniques. Additionally, the performance of the treatment unit can be incorporated into the simulation using the information from the MLC log file, which records the leaf position as a function of time during treatment delivery. This method is generally more accurate than film dosimetry. Also, a three dimensional dose distribution can be acquired. But, Monte Carlo simulation is not a measurement method, but a highly accurate calculation method. Monte Carlo algorithms therefore need to be verified by direct dose measurement prior to clinical use. As a result, a direct two-dimensional dose measurement is still necessary. (More discussions about dose measurement techniques can be found in Chapter 4.3.)

BrainLAB AG (Feldkirchen, Germany) provides iPlan® RT treatment planning software which is a stereotactic radiotherapy dose planning software program capable of doing IMRT treatment planning. This software, is particularly suitable for stereotactic planning. (Stereotactic radiotherapy is introduced in Chapter 2, Section 2.3.1.) iPlan comes as part of the BrainLAB stereotactic radiosurgery system and is designed to be compatible to the m3® High-Resolution multi-leaf collimator. With the help of this sys-

tem the patient can benefit from both IMRT and stereotactic techniques, which is quite necessary for some difficult intra-cranial and head and neck cases where small irregularly shaped target volumes are very close to critical structures[6–10]. As mentioned in previous paragraphs, dose verification is an essential part of commissioning and QA processes. Dose verification for the iPlan system has its unique challenges, primarily because the field size is smaller than for more conventional IMRT techniques. Detailed discussion about this is given in Chapter 2, Section 2.4.

The overall scope of this project is to evaluate a radiochromic film dosimetry system and use it together with the ion chamber measurement to achieve dose verification for the iPlan stereotactic IMRT treatment planning system. Radiochromic film is a self- developing and light insensitive alternative to radiographic film. The Gafchromic® EBT film is specially designed for IMRT QA purposes. It does not have to be handled in a dark room thus can be easily cut and loaded under normal room lighting conditions. The lack of chemical processing not only reduces the post irradiation work load but also removes one of the more problematic aspects of traditional film dosimetry. Gafchromic film may be used with a flatbed scanner, which is accessible and affordable. Finally, the composition of radiochromic film is much closer to water or tissue and thus gives a more representative measure of dose in these materials compared with silver bromide radiographic film. For these benefits, it is of great interest to replace radiographic film with radiochromic film. Before radiochromic film can be clinically used, its performance has to be tested and a proper procedure for using it as a dosimeter has to be established, because the performance also depends on how the film is scanned and analyzed. Detailed discussions and performance tests of Gafchromic EBT film are reported in Chapter 3.

The EBT film technique is tested on three clinical cases following a commissioning process. In Chapter 4, the treatment planning and delivery system for the stereotactic IMRT technique used for the three cases is explained in

detail. The last section of Chapter 4 describes in the methods used in dose verification and commissioning, including MLC performance tests , phantom structure, ion chamber measurement and the film dosimetry technique. Chapter 5 summarizes the experimental data and discussion. Final conclusions are presented in Chapter 6. Future work is described in the last chapter.

Chapter 2

Theory

This chapter serves to introduce some theoretical background to provide a general understanding of radiation therapy and some specific radiotherapy techniques. The chapter is divided into three sections. In Section 2.1, physical and biological effects of ionizing radiation are discussed as well as the general principles of radiation therapy. In Section 2.2, two important radiotherapy instruments, the linear accelerator and the multi-leaf collimator are introduced. Stereotactic radiotherapy and intensity modulated radiation therapy which are the major techniques used in this project, are discussed in Section 2.3.

2.1 Introduction to Radiation Therapy Physics

Radiation can cause biological damage to living tissue, including acute radiation illness at high doses, and cancer induction or genetic damage at low doses. Radiation is also widely used in health care for medical imaging and tumor treatment. In order to utilize radiation for therapeutic and diagnostic purposes, it is important to understand how radiation interacts with living tissue.

2.1.1 Radiation Interactions with Matter

In general the term radiation refers to subatomic particles or photons that are directed at a target. Typically, radiation can be categorized as non-ionizing

or ionizing. The difference being whether the energy of the impinging individual particle is high enough to detach electrons from atoms or molecules. The ability of radiation to ionize depends on the energy, and the type of the individual particle but not on the number of particles. A beam of intense low energy radiation, although possibly possessing a large amount of energy, may not be able to cause any ionization. Different kinds of particles interact with a medium through different mechanisms. . Some particles interact with soft tissue strongly, losing energy rapidly, thus have limited penetration depth. Some particles, on the other hand, can travel for a long distance without undergoing interaction. Detailed descriptions of how particles interact with matter can be found in many publications[11, 12]. For the purpose of this thesis, a 6 MV photon beam is used, thus only photon and electron interactions in this energy range will be discussed in the following paragraphs.

Photons interact with matter primarily through four mechanisms in the energy range from several hundred keV to several MeV, including Rayleigh scattering, the photoelectric effect, Compton scattering and pair production (or more precisely pair and triplet production). The probability of occurrence of these interactions depends both on photon energy and atomic number of the medium.

Rayleigh Scattering

Rayleigh scattering, which is sometimes referred to as coherent scattering, occurs when a photon travels through a medium in which the particles are much smaller than the wavelength of the incoming photon. In Rayleigh scattering, only the direction of incident photons changes. The photon energy is conserved and not transfered to the medium. The probability of occurrence for Rayleigh scattering decreases with the incident photon energy, but it increases with the atomic number of the medium. The atomic cross section

for Rayleigh scattering ($_a\sigma_R$) is approximately given by Equation 2.1,

$$_a\sigma_R \propto \frac{Z^2}{(h\nu)^2} \tag{2.1}$$

Rayleigh scattering has more practical importance in the low energy regime, partly because the probability is higher, partly because the scattering angle is greater. Rayleigh scattering does not contribute to dose, since no energy is transferred during this interaction. Rayleigh scattering is thus more important in imaging application than in radiation therapy.

The Photoelectric Effect

The photoelectric effect is a phenomenon where the incident photon is absorbed by the atom and an electron is emitted. The photoelectric effect is more dominant in the energy range of several eV to around 0.5 MeV. In order for the photoelectric effect to occur, the incident photon energy has to be higher than a threshold, which is the binding energy of the electron. The incident photon with enough energy interacts with the bound electron in an atom and gets absorbed. The energy of the photon is transferred to the electron. Part of the energy is used to overcome the binding energy and free the electron from the atom. The residual energy is transferred to the kinetic energy of the escaping electron. The probability of occurrence for the photoelectric effect is roughly proportional to the third power of the reciprocal of the photon energy provided it is higher than the binding energy. Similar to Rayleigh scattering the probability of occurrence is also strongly dependent on the atomic number of the medium. The atomic interaction cross section, $_a\tau$, is approximately given by Equation 2.2,

$$_a\tau \propto \frac{Z^4}{(h\nu)^3} \tag{2.2}$$

Compton Scattering

Compton scattering is the dominant mode of interaction in the energy range from several hundred keV to several MeV. When Compton scattering occurs, the incident photon transfers part of its energy to an electron and changes its direction. The electron which receives the energy and a certain amount of momentum is called a recoiling electron. In Compton scattering, the photons only interact with loosely bound electron such as the outer shell electrons or free electrons. During the process, the overall energy and momentum of both particles are conserved, and are used to derive the relationship between the scattering angle and energy transferred. Compton scattering is the only type of interaction that is not highly dependent on the Z of the medium. The probability of occurrence of Compton scattering only depends on incident photon energy, and decreases with increasing photon energy. The interaction cross section follows the Klein-Nishina function[11]. Since all other types of interaction are highly Z-dependent and the probability of occurrence increases with respect of the atomic number, Compton effect turns out to be more important for media with low Z, such as carbon and hydrogen. For soft tissue, Compton scattering contributes most to the dose deposition for megavoltage photons[13].

Pair Production

Pair production refers to the creation of an electron and a positron pair from a photon. In order for this interaction to occur, the photon energy should be greater than the rest energy of the electron-positron pair it is going to create. In order to conserve the momentum, pair production can only occur in the vicinity of the nucleus so that part of the momentum can be absorbed by the recoiling nucleus. For photon energies close to the threshold, the created electron and positron travel almost in opposite directions to each other. For energy well above the threshold, the pair could travel more in the forward direction. The probability of occurrence of pair production increases rapidly

as the photon energy increases, and it is also strongly dependent on the atomic number. The interaction cross section per unit mass is approximately proportional to the atomic number. The positron created in a pair production process slows down by interacting with the surrounding environment, and eventually annihilates with another slow electron creating a pair of 511 keV photons.

Summary of Photon Interactions

The probability of occurrence for these interactions depends both on the photon energy and the atomic number of the medium. This is why high atomic number materials have very different absorption characteristics compared with low atomic number materials. For media that have high atomic number, the photoelectric effect and pair production have relatively higher interaction cross sections compared to Compton scattering. Compton scattering thus is dominant only for a very narrow energy range. At low energy, since the photoelectric effect is strong, high atomic number media absorb the photon much more strongly than low atomic number media. For media that have low atomic number, Compton scattering is the most dominant mode of interaction for wider spectrum of a few hundred keV to several MeV. This makes it of great importance for radiotherapy, since soft tissue is primarily made up of low atomic number media and the photon energy used in radiotherapy is just in that energy range.

Electron Interactions

In all the above interactions, secondary electrons and or positrons are created, and it is those electrons and or positrons that eventually deposit the energy in the medium by causing ionization and excitation. Because electrons are charged particles, electron interactions differ greatly from photon interactions. and are described using different terminology. For example, the attenuation of photons is logarithmic and the probability of interaction for

photons is often described by cross sections. Due to the Coulomb force, electrons are strongly influenced by the surrounding environment and typically interact and loose energy continuously as they travel through a medium and come to rest. Stopping power, which is the amount of energy transferred to the medium per unit thickness of travel, is used to characterize electrons.

Electron interactions can be categorized into three classifications: ionizational, radiative and scattering interactions. In ionizational interactions, the electron's kinetic energy is transferred to an atom causing ionization or excitation. For non-relativistic electrons the energy transferred in ionizational interactions is inversely proportional to the kinetic energy of the incident electron. For high energy electrons, since the velocities are closer to the speed of light, relativistic effects must be considered. The mass stopping power is relatively constant within the energy range from 0.1 MeV to 100 MeV. During radiative interactions, electrons accelerate rapidly within an atomic nucleus' electric field and part of the kinetic energy is transferred as a radiated photon (bremsstrahlung). In scattering interaction, the electron is deflected by the strong Coulomb force without loss of its kinetic energy.

Electron Equilibrium

Notably, this chain of interactions does not happen locally, thus the dose distribution is not proportional to the photon flux at any given point in the medium. The exception is a condition called electronic equilibrium, where the secondary electrons set in motion inside and outside a small volume element reach a dynamic balance. This means the same number of electrons with same energy distribution enter and exit this volume element. When electronic equilibrium is present, the energy deposition by the secondary electrons is locally dependent and is proportional to the photon flux, which simplifies dose calculation and measurement in most cases. Electronic equilibrium dose not hold close to field and medium boundaries. For example, when a beam crosses a discontinuity in the medium or at the edge of a photon beam,

the number of electrons entering and exiting the volume is different. This is called electronic disequilibrium.

2.1.2 Radiation Biology

Radiation causes cell damage in different ways. Ionization of DNA molecules can break chemical bonds, causing the strand to break up. Moreover, ionization can create highly reactive radicals. Free radicals are highly reactive due to the presence of unpaired valence shell electrons. They can cause damage to cell structure as well as DNA. Usually DNA damage can lead to three different results. In some cases DNA damage can be repaired by DNA repair enzymes with the aid of the opposite strand. Sometimes, DNA damage cannot be repaired, and this leads to cell death. In this situation, the single cell is lost preventing potential genetic damage from being transferred to the next generation. In other cases, DNA damage is unable to be repaired but is also non-lethal. In these cases, the genetic mutations will be passed on to subsequent generations of cells. If the mutation happens to be critical, they can cause cancer or other illness. During each phase of the cell cycle, cells have different sensitivity to radiation due to the fact that DNA is being replicated in some phases and is not paired. Generally, if the cells are actively undergoing cell division they are more vulnerable to radiation damage. Fractionation of dose delivery is beneficial because radiation from different sessions has more chance to catch all cancer cells in the most sensitive cell division phase, thus resulting in better tumor control. Research also shows that healthy tissue tends to resist more radiation damage compared with cancer cells if dose per fraction is kept below a certain level. For the susceptibility of radiation on an organ level, the volume effect has to be to take into account. Parallel organs, in which the functional units work in parallel, for example the liver, can tolerate high dose if a relatively small portion is irradiated. For serial organs, such as the spinal cord, on the other hand, the tolerance is almost independent of irradiated volume.

2.1.3   General Principles of Radiation Therapy

The goal of cancer treatment is to control the malignant cells, either cura-
tively or palliatively. This goal is the same for radiation therapy. Radiation
therapy uses ionizing radiation to treat cancer by killing the malignant cells
to achieve local tumor control. Radiation therapy can be used as a primary
curative treatment, or it can be used as an adjuvant treatment. As radiation
can damage both malignant cells and healthy cells, effort has to be made to
protect the healthy surrounding tissue. Radiation therapy can be categorized
as: External Beam Radiotherapy, where the source of radiation is outside of
the body; brachytherapy, where a sealed source is implanted into the tu-
mor target and radioisotope therapy, where an unsealed radioactive source
is given by infusion or oral ingestion. The subject of this thesis is related to
external beam radiotherapy and further discussion will be restricted to this
method.

For external beam radiation therapy, because radiation from the external
source has to travel through a patient's body to reach the clinical target in
most cases, dose deposition along the path is inevitable. An external beam
treatment unit not only functions as a radiation source but most importantly
as a guidance system to direct and confine the radiation damage to clinical
targets. Usually the radiation is given from several different angles so that
unnecessary dose deposition for each field to any point in normal tissue is
only a small fraction of the tumor dose. The shape of each field can be ad-
justed according to the projection of the tumor target(s). The application
of medical linear accelerators and high tech accessories allows more sophis-
ticated techniques to be realized, including Intensity Modulated Radiation
Therapy (IMRT), Rapidarc™, Image Guided Radiation Therapy (IGRT) and
Stereotactic Radiosurgery (SRS). But the purpose of all these improvements
is simple, achieving better tumor control while sparing healthy tissue as much
as possible.

2.2 Equipment

2.2.1 Linear Accelerator

Radiation therapy has over one hundred years of history. Originally X-ray
tubes were used to treat superficial malignancies due to a limited penetration
depth. Most deep target treatments used radioactive isotopes as the radiation
source, until the medical linear accelerator was invented in the 1960's[14].

A medical linear accelerator (Linac) uses a tuned-cavity waveguide, in
which the radio frequency eletromagnetic fields are used to accelerate elec-
trons to high energy. Usually the wave guide is horizontally mounted so that
a magnetic bending device is used to turn the electron beam vertically to-
ward the patient. The direct output is a monoenergetic electron beam from
4 MeV to 25 MeV. If a photon beam is needed, the electron beam is directed
into a high-density metal target (usually made of tungsten alloy) to create an
x-ray beam with a continuous energy spectrum of maximum energy equal to
the electron energy. X-rays are generated by rapid slowing down of the elec-
trons inside the target (Bremmstrahlung radiation). A collimation system is
located in the head of the gantry, including two pairs of jaws and usually an
integrated multi-leaf collimator (The integrated MLC can be seen on Figure
2.1). The jaws are used to define the basic rectangular field size, while a
multi-leaf collimator defines the actual field shape.

Figure 2.2 shows a photograph of a medical linac. Notice the gantry can
rotate about a horizontal axis. The collimator can rotate about the central
beam axis. The patient couch can rotate about a vertical axis. All these
three axes intersect at one particular point named the isocenter which is in
most cases 100 cm away from the source. Other accessories include position-
ing lasers, and immobilization devices that are used to increase positioning
accuracy.

The flexibility, accuracy and safety of linacs are the most significant ad-
vantages over the older generation of therapeutic isotope machines. The linac
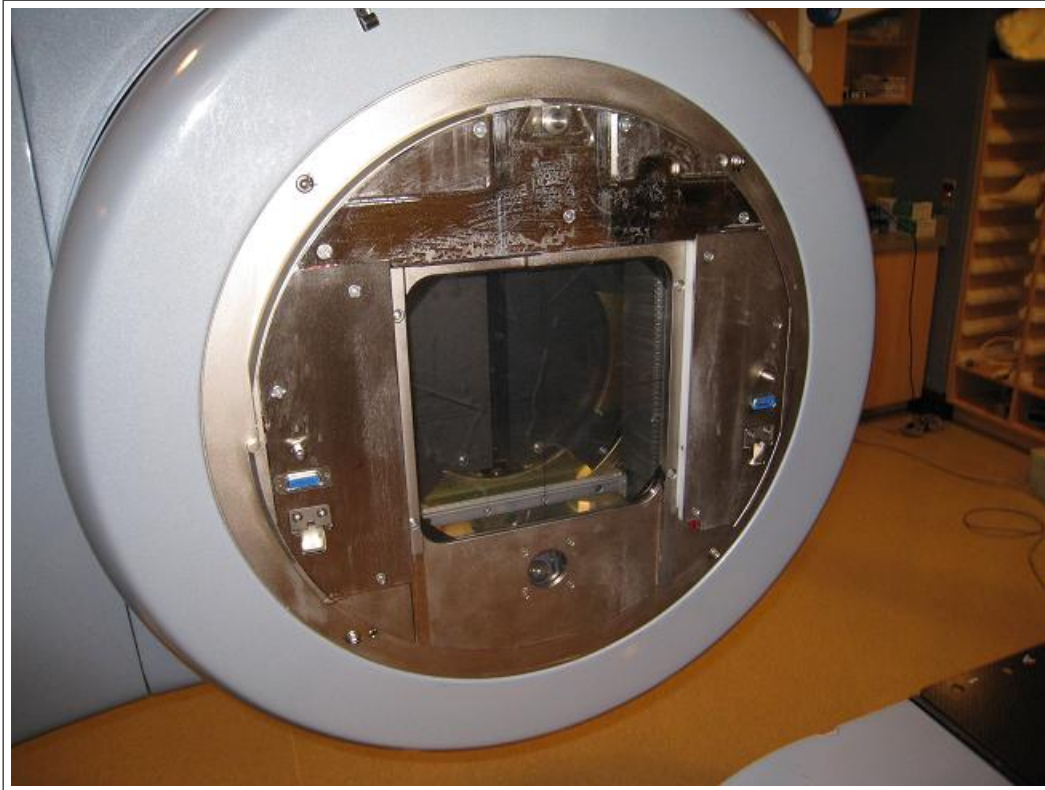
Figure 2.1: This is a photograph of a linac gantry head. Inside the window at the right edge, a line of tungsten leaves is visible. This is the integrated Varian Millennium MLC. The visible leaves are from a single bank and are all fully retracted. At the center of the window, there are two visible blocks which are the second pair of the jaws.

Figure 2.2: This is a photograph of a linac system. Under the currently setup condition, the couch angle is in zero position, as well as the gantry angle. The collimator angle is 90 °.

can simply be powered off when not in use. There is no permanent source requiring heavy shielding and there is no need to worry about radiation leakage when the machine is powered off. There are numerous built-in interlocks preventing accidental operation of the machine. System redundancy is high in monitoring the dose delivery to make sure no excess dose is given. The Linac is the most frequently used machine for delivery of many advanced techniques including IMRT[15].

2.2.2 Multi-leaf Collimator

An multi-leaf collimator (MLC) is a collimation system capable of shaping a radiation field in an arbitrary shape. MLCs consist of two opposing sets of tungsten leaves which travel across the field to shape and modulate the radiation beam. The position and speed of each leaf can be programmed individually. The number of leaf pairs varies from model to model. All leaves are parallel and move in a plane perpendicular to the beam axis. Ideally, in the vertical direction the MLC leaf edges follow a divergent line from the source to minimize the penumbra. In actual fact, MLC leaves have round tips to make the size of penumbra independent of leaf position. Tongue and groove design is used to counter inter-leaf leakage. Initially, MLCs were used as static shaping accessories, replacing the hand-crafted lead block, reducing work load. Around the 1980's, MLC was first used as a dynamic modulating device in IMRT delivery. The requirement for real time response of MLCs has pushed manufacturers to improve the design of MLCs to make them faster and more accurate. Nowadays, MLCs have become an essential part of a dynamic delivery system capable of delivering IMRT, dynamic arc and RapidArc™ radiation therapy. An MLC controller records real time internal monitoring data, providing a way to check the MLC performance. Monte Carlo simulation based on this dynamic log file is another important application that is discussed later in this thesis.

2.3 Techniques

2.3.1 SRT and SRS

Stereotactic radiosurgery (SRS) is a technique where an extremely high dose is given to a small, highly confined and precisely localized target usually located in the brain. The extremely high dose can be given in a single fraction, due to the fact that the targets are small and large volume of healthy tissue can be avoided by using beams from different angles. The benefit of delivering the dose in a single fraction is that it is easier to achieve precise target localization in one session[16, 17]. If the dose is delivered in several fractions the technique is called stereotactic radiotherapy (SRT). The intra-cranial environment is challenging for radiation therapy because of the existence of so many critical structures. In order to spare as much healthy brain tissue as possible, a sharp dose gradient outside the field edge is demanded. Special immobilization and positioning devices are used. These localization and positioning applications differentiate SRT from conventional radiation therapy.

Unlike conventional conformal radiotherapy techniques, a fixed coordinate system for SRS is set up by using a stereotactic frame and localization box used throughout the planning and treatment processes. The stereotactic frame is also used as an immobilization frame. It is physically screwed into the patient's skull and attached to the treatment couch, so that the relative position of the patient to the treatment couch does not change during the whole imaging and treatment process. The localization box can be mounted on the treatment couch and is located outside the patient's head. Prior to the treatment, a CT scan of the patient's cranium is performed with the localization box on. Metal rod markers are implanted on three surfaces of the box, which can be clearly seen on CT image. The planning system automatically recognizes these markers and sets up a fixed coordinate system based on these fiducials. Due to the fact that most intracranial tumors that

are treated with SRS are relatively small, conformal treatments are typically used.[18] For fractionated SRT a less invasive immobilization mask is used. For larger treatment volumes, IMRT in combination with SRT may provide therapeutic advantages[6–10].

2.3.2 Intensity Modulated Radiation Therapy

Intensity modulated radiation therapy (IMRT), as the name indicates, is used to modulate the intensity of incoming beams, adding flexibility (compared to conventional beams of uniform intensity) to achieve a higher degree of spatial conformity of dose distributions. Typically in IMRT, we reduce the intensity of rays that go through sensitive critical structures and increase the intensity of those rays that can primarily see the target volume. This modulation may result in highly non-uniform dose distribution associated with each individual field within the target volume, compared to traditional conformal treatment. For a single field, the modulated dose distribution may show unwanted cold spots and hot spots, but this would be compensated for by other fields. The overall effect is an additional degree of freedom for dose manipulation. A universally accepted definition of IMRT does not exist but an understanding agreed upon by most is that IMRT is a radiation treatment technique with multiple beams in which at least some of the beams are intensity-modulated and intentionally deliver a non-uniform intensity to the target. The desired dose distribution in the target is achieved after superimposing such beams from different directions. Because the calculation is done in a discrete manner and the MLC has limited spatial resultion, the modulation of each beam has finite resolution. The smallest division used in the optimization process is known as a beamlet. The additional degrees of freedom are utilized to achieve a better target dose conformality and/or better sparing of critical structures[19]. Generally, inverse planning techniques are used in IMRT.

History of Intensity Modulated Radiation Therapy

The earliest paper which is recognized as the cornerstone of IMRT development is published in 1982 by Brahme *et al* with the name "Solution of an integral equation encountered in rotation therapy."[20] In this paper, the author posed the central question:"Which is the desired lateral dose profile in the incident beam that produces a desired absorbed dose distribution in the body after one complete rotation?" Though this paper is mathematical in nature and the proposed model is rotational delivery rather than for static fields, it provides the most important conclusion:"a highly non-uniform intensity profile is needed to produce a uniform dose distribution in the target volume."

While the first theoretical inverse planning methods were developed in the 1980s, it was not at all clear at that time how IMRT would be practically delivered[19]. But a dynamic treatment technique called dynamic wedge, in use since 1978, gave an important indication of a possible solution. During the delivery of dynamic wedge, one leaf bank of an MLC, or at that time a single jaw, is stationary, while the opposing leaves move. The beam aperture becomes increasingly narrower as the treatment progresses. The dwell time of the jaw or leaves varies according to position, achieving a gradually decreasing dose distribution across the field, similar to the result we get from a physical wedge. By extending this idea, if the motion is independently modulated for each leaf, i.e. the speed of closing in is variable rather than a constant, an arbitrary intensity profile can be acquired. After solving several mechanical and quality assurance issues this idea of using MLC to deliver IMRT was quickly realized.

Inverse Planning and Forward Planning

The calculation of non-uniform intensity profiles for each individual field begins with the dose prescription to the target volume and dose limits for surrounding critical structures. Desired intensity profiles are derived by min-

imizing a cost function based on the dose volume constraints to both tumor and normal tissue. The process is known as 'inverse planning'. Actual leaf motion sequences are calculated based on beam intensity profiles taking into account physical MLC characteristics. The calculation of dose distributions based on MLC leaf sequences is called 'forward calculation'. Improvement in IMRT inverse planning algorithms and dose calculation continue to be made.

After some early attempts to apply inversely planned IMRT to certain sites such as lung, it was found that inverse planning based on simple dose objectives and constraints did not yield satisfactory results. This has led to or re-activated many discussions about the need for biologically-based IMRT planning. However, quite satisfactory results have been achieved for many sites such as head and neck and prostate using physical dose-volume based optimization. As a result, dose-volume limits are implemented in most commercial inverse planning systems today including the treatment planning system (TPS) used in this thesis. More and more detailed dosimetric issues are accounted for in modern systems, such as tongue and groove correction and hot beamlet correction (which is a correction method removing the spikes exceeding a certain threshold from the intensity profiles). Generally speaking, many of the recent developments in inverse planning aim at a better, more complete, representation of the clinical prescription and objectives, so that the resulting IMRT treatment plans become more clinically meaningful, rather than mathematically optimal.

Forward planning has also seen improvement due to increases in computational speed. Early pencil beam algorithms are being replaced by more sophisticated and reliable Monte Carlo algorithms, for which the computational efficiency is much better than before.

2.4　Treatment Plan Verification

The paper 'Comprehensive quality assurance for the delivery of intensity modulated radiotherapy with a multi-leaf collimator used in the dynamic mode' by LoSasso *et al*, is usually treated as a primary reference for IMRT quality assurance[4]. In this paper, the author proposed that IMRT QA should involve routine machine QA and verification of individual patient treatments. Routine machine QA focuses on a series of MLC basic performance tests, such as leaf positioning accuracy, leaf gap accuracy and stability. The verification of patient treatment plans includes ion chamber measurement, film dosimetry and MLC log file analysis. This thesis generally follows these recommendations.

For dose verification purposes, ion chamber measurement and film dosimetry are two main measurement methods. Due to the fact that the treatment technique to be tested in this thesis is a combination of IMRT and SRT techniques, there are several additional challenges compared to traditional IMRT dose verification. The primary cause of these challenges is the small field size. For SRT, a typical field size is approximately 20 mm in diameter, compared to a typical body IMRT field size which can be as large as 10 cm in diameter or more. The BrainLAB m3 MLC, designed for this purpose, has a maximum field opening of only 9.8 cm by 9.8 cm at 100 SAD. The MLC leaves are also narrower to provide a higher spatial resolution. As a result, electron disequilibrium is also more significant than for a traditional IMRT. The small field size and high degree of dose modulation causes significant electron disequilibrium. For individual fields, the dose distribution is usually highly modulated compared with the total accumulated dose. The influence of such high dose gradients on film dosimetry is still unclear. A special small size ion chamber should be used to measure the dose from such highly modulated small fields, otherwise the volume averaging effect will compromise the dose reading in high gradient regions. A direct consequence of using a smaller ion chamber is a relatively lower sensitivity, which is obviously a disadvantage.

Furthermore, as a direct consequence of high dose gradient and spatial resolution, the positioning tolerance for stereotactic techniques is much tighter. Special immobilization devices are used and mechanical performance errors have to be taken into consideration.

The detailed introduction of BrainLAB m3 micro MLC is given in Chapter 4, Section 4.2.2. The discussion of localization and immobilization devices is given in Chapter 4, Section 4.2.1. Detailed descriptions of the clinical dose verification are given in Chapter 4, Section 4.3. In this section, a highly suspected directional dependence for ion chamber response is investigated and ruled out. The numerical data of clinical case dose verification are presented in the Chapter 5, where related discussions are also presented.

Chapter 3

Film Dosimetry

Film dosimetry is a high resolution, two dimensional relative dosimetry method. As the spatial accuracy of a dose distribution is of great importance, film dosimetry is a useful tool for commissioning and verification of IMRT techniques. Conventional radiographic film is light sensitive, thus should be handled without exposing to light. In addition, the necessary chemical processing introduces uncertainty and is inefficient. The more recently developed radiochromic film is insensitive to room light and does not need chemical processing. Due to the nature of radiochromic film, readout may be conveniently performed using a flatbed optical scanner. In addition, radiochromic film is more tissue equivalent than radiographic film. In this project, we investigate the performance of radiochromic film and apply it to measure the dose distributions as part of the commissioning process for the stereotactic IMRT technique.

3.1   Introduction to Film Dosimetry

The principle of film dosimetry is that the micro particles within the active layer are sensitive to ionizing radiation. High energy particles deposit energy when they pass through the film interacting with those micro particles, and the deposited energy consequently changes the physical or chemical properties of the local micro structure. This usually results in a change of darkness or color of the film, which can be quantitatively measured by light detecting devices, such as optical scanners or densitometers. Depending on which scanning system was applied, the final dose distribution can be acquired either

as a fully continuous two dimensional distribution or dose points on a grid.

The traditional medical radiographic film relies on similar chemical reactions as in photographic film. Briefly speaking, the exposure to ionizing radiation causes the silver bromide in the film emulsion to decompose and create silver ions. Post-exposure chemical processing is a necessity to develop and fix the exposure pattern on the film and stop the film from possible future reaction to light. The darkness of the exposed film, or the optical density, is sensitive to the environmental conditions during chemical processing. The concentration of the developing solution, the duration of the development and the temperature all could influence the optical density. For example, variations of 1℃ in the developer bath can affect the optical density by as much as 10 %[12]. Because the chemical in the solution is continuously consumed during the process, no two pieces of film can be processed under exactly the same condition. The inconsistency of processing environment leads to fluctuation of film response. This drift theoretically restricts the accuracy of the dose information we get. Therefore, film dosimetry is believed to have relatively poor accuracy and usually should be used as a relative dosimetry method together with some absolute dosimetry techniques such as ion chambers. In this case, the ion chamber reading can be treated as an absolute dose reference point. The relative dose ratio among different pixels, which is less sensitive to variations in processing, can be used along with the reference point dose to calculate dose value for each pixel.

Despite the major difficulties mentioned above, film has several advantages that most other dosimetry methods do not have. The most obvious one is the high spatial resolution. The spatial resolution of radiographic or photographic film is theoretically limited by the size of light sensitive particles such as silver bromide grains in the active layer. In principle these particles are generally smaller than 0.1 mm. In practice, resolution is limited by the aperture of the scanning device or densitometer, which can be up to $\geq$ 0.3 mm. However, film resolution is still higher than other two dimen-

sional dosimetry methods such as EPID (Electronic Portal Imaging Device), or TLD (Thermoluminescent Dosimetry) grid. Another attractive feature is the robustness and the flexibility of film which can be easily cut into different sizes or shapes and fit into interior planes of phantoms. This could not be easily done by projective imaging modalities such as EPID.

3.1.1 General Considerations when Using Film

Generally, the following characteristics of film should be carefully evaluated since they will greatly influence the dose measurement: energy response (related to effective Z), dose rate dependence, dose range , linearity, directional dependence and sensitivity to ambient conditions.

Energy Response

Energy response is how sensitive the film is to incident photons of different energy. Ideally, energy response should be as uniform as possible. However, typically radiographic film is 10 times as sensitive to 0.1 MV photons than to 1 MV photons because of the stronger photoelectric interaction with AgBr below 150 keV[12]. Scattered components often have relatively low energy after the photons undergo several interactions and lose energy. Typical radiographic film thus tends to be much more sensitive to the scattered components, which is a drawback since the influence of the scattered components tends to be amplified. In some cases, where the energy spectrum dramatically changes with depth, one should expect the sensitivity will change accordingly.

Dose Rate Dependence

Dose rate dependence should be minimal in order for any film dosimetry system to work. If there were to be a strong dose rate dependence, one would be required to know the dose rate at any point in order to determine the dose distribution correctly, which is practically impossible. Most x-ray film

Type	Range (cGy)	Saturation (cGy)
Kodak EDR2	25~400	700
Kodak XV-2	0~100	200
XTL	1~15	30
Kodak PPL	0.25~5	10
MD55	0~3000	N/A
EBT	0~800	N/A

Table 3.1: Dose range and saturation level of different types of film

manufacturers claim their product is safe enough to be treated as dose rate independent. Several types of radiochromic film have been experimentally tested for dose rate dependence. Galante *et al* have reported that for polycarbonate, results show up to 10 % dose rate dependence for a dose rate range from 433 cGy/min to 4333 cGy/min. When radiochromic film is intended to be used for real-time dose monitoring, Rink *et al* have reported up to 4 % dose rate dependence.

Dose Range

The useful dose range determines which type of film is suitable for a particular application. Some data including dose range and saturation level of different types of film is listed in Table 3.1 [12].

Tissue Equivalence

Radiographic film usually has different effective Z from normal tissue. This could lead to different responses between the film and the tissue, and leads to inaccurate representation of dose to tissue. Gafchromic films (such as EBT) have effective Z much closer to normal tissue, within the range 6.0 to 6.5[21], compared with the effective Z of tissue which is 7.22.

Ambient Conditions

The film response can also be affected by environmental conditions such as humidity and temperature or storage conditions, storage time, post-exposure development time. Even more importantly, how scanning devices interact with film could bring more complexity to the problem. The general strategy is to acquire a calibration film each time and try to maintain all the control factors the same during the acquisition of both measurement films and calibration films. Some of these aspects of radiochromic film dosimetry will be discussed again in the following sections.

3.1.2 Introduction to Radiochromic Film

Radiochromic film is a relatively new type of film. During irradiation, its active component within the transparent layer undergoes a polymerization process and becomes dark blue. The optical absorption peak is at 670 nm for the darkened region. The color change induced by the radiation is stable and permanent. Unlike radiographic films, radiochromic films do not require post chemical processing, which eliminates the complication due to processing variations. Furthermore, radiochromic films have very low sensitivity to room light. Hence the change of optical density is negligible if exposed to room light for a reasonable duration, which brings convenience to the handling of film. The film can be cut or loaded under normal room light. The strong absorption peak in red visible light makes it compatible with RGB flatbed scanners, which could potentially save the investment in an expensive high quality medical film scanner. Due to these advantages, we decided to apply this new type of radiochromic film to IMRT dose verification. In order to use radiochromic film as a reliable tool to validate our system, the performance of the film was thoroughly tested. A proper and detailed handling procedure was established. The overall estimate of the uncertainty was determined.

The biggest radiochromic product line, which is manufactured by Inter-

national Specialty products Inc. (ISP) is named Gafchromic® film. Some-times radiochromic film is also referred to as Gafchromic film. There is a series of Gafchromic products suitable for different applications. The recent Gafchromic EBT® film is specially designed for application to IMRT QA. The sensitivity and dose range fit IMRT QA the best. Thus, in our research we chose to work with Gafchromic EBT film.

The basic Gafchromic EBT film properties are as follows. The dose range is from 1 cGy to 800 cGy. EBT is ten times more sensitive than the previous generation Gafchromic HS film and MD-55, and is energy independent from the keV range into the MeV range. The uniformity is better than 1.5 %. It has faster and lower post-exposure density growth and can withstand tem-peratures of up to 70℃.

Gafchromic EBT film has two identical active layers sandwiched between surface layers. Two clear polymer layers are on the outside of the two surfaces providing protection. With this configuration, the film could be immersed into water for a relatively long period. However, because the edge is not sealed, water can diffuse into the active layer. But the rate of diffusion is relatively low. Experiment shows that after 24 hours of immersion, water can penetrate as far as 8 mm from the edge. The diffused region can be easily recognized because it turns milky opaque if water molecules have diffused. Cutting could also induce tension at the edge. Reading should be avoided up to several millimeters from the edge. It is also convenient to be able to use ink pen to draw marks on either surface of the film. Marking is necessary to keep track of the orientation of the film.

The tissue equivalence of the new Gafchromic EBT film is better than the old model (Gafchromic HS and Gafchromic MD55). The effective Z is 6.98. This value is closer to the effective Z of water (7.3) than the value for Gafchromic MD-55 ($\sim$6.5). The details of the atomic composition is shown in Table 3.2.

Other properties including post-exposure development, uniformity, and

C	H	O	N	Li	Cl	Zeff
42.3 %	39.7 %	16.2 %	1.1 %	0.3 %	0.3 %	6.98

Table 3.2: Atomic composition and effective atomic number of Gafchromic EBT film

dose rate dependence are discussed in the following sections.

3.2 Film Scanning and Calibration

3.2.1 Scanners

In order to be able to quantitatively analyze the film response, the amount of darkening has to be converted into digital signal. This is usually done by scanning the film using a scanner or measuring the optical density with a densitometer.

Film scanners can be largely categorized into two groups: multiple detector scanners and single detector scanners. The first group includes medical grade scanners such as the Vidar Diagnostic Pro advantage digitizer and high end consumer grade flatbed scanner such as Epson 1000XL. An example of the latter group includes the Welhoffer WP 102 film densitometer and the AZTEK® Premier drum scanner. It is quite obvious that in order to acquire a two dimensional signal array, the single detector scanner has to mechanically move the scanning head in a sweeping pattern across the field of interest, while the multiple detector scanner only has to move the head in one direction (provided the multiple detectors are arranged in a line), and therefore making it faster than the single detector scanner. By sacrificing the time efficiency, the single detector scanner eliminates potential interference across different sources and detectors, and eliminates non-uniformities between detectors. Generally speaking, the quality of the data acquired from single detector scanners is better than multiple detector scanners. However,

in practice, the time consumption is usually intolerable and a multiple detector scanner is the preferred option.

Drum scanners are used in high end photographic scanning. The material to be scanned has to be transparent. The film is attached to a vacuum glass cylinder, which is spinning at a very high speed. A narrow laser beam passes through the film and goes into the vacuum tube, and is converted into electric signal. The spot size is tunable and the scanning speed is relatively high. More importantly, the output quality is very high. However, drum scanners are not commonly used and are extremely expensive. The machine itself is huge and heavy. Also, the way that the film has to be submerged into oil and attached to the drum makes it impractical in a clinical environment.

The Wellhofer WP 102 film scanning densitometer is available in the VCC medical physics department. The light source in this densitometer has a wavelength at 950 nm which is significantly different from the absorption peak of Gafchromic EBT film, which is around 635 nm. Test scanning on Wellhofer WP 102 film densitometer with fully exposed and un-exposed Gafchromic EBT film shows that the densitometer cannot distinguish them. The 950 nm light is not attenuated by the dark blue of the film. Unless we can change the light source of the Wellhofer WP 102 film densitometer, it would not work with the Gafchromic EBT film. Replacement of the light source would require extensive work and the quality of such a modified densitometer has not been tested, so this densitometer has not been considered in this work.

The structure of the Vidar Diagnostic Pro® advantage digitizer is similar to a flatbed scanner. The major difference is that instead of keeping the target still and moving the scanning head across the field, the film actually moves through the scanner in the Vidar scanner design. This could potentially induce variation in the longitudinal direction with a unique pattern[22]. The Vidar scanner is generally believed to have better signal to noise ratio to flatbed scanners due to the fact that it uses LED as the light source. The unique LED light source not only eliminates the necessity of warming up but

also dramatically increases the dynamic range. The primary problem with the Vidar scanner is that the wavelength of the light source does not match the absorption peak of the Gafchromic EBT film, which could result in relatively low sensitivity. In the VCC medical physics department, the Vidar scanner is currently malfunctioning so we could not do any tests on it, but we have some previous data from scanning radiographic film on the Vidar scanner, which can be used as a reference if necessary.

As flatbed scanners may be the most suitable options for clinical film dosimetry, we have chosen to test two models of flatbed scanners available to us. As suggested by the film manufacturer, the flatbed scanner not only works well but also provides several unique advantages. For example, the scanning can be done in RGB mode and the red channel can be extracted to provide the highest contrast, or the information contained in the other two channels could be used to do some additional correction, which is the case for Gafchromic EBT2 film. The two available scanner models at VCC are the Microteck 9800XL and the AGFA Duoscan TMA 1600.

The Microteck scanner is relatively newer than the AGFA scanner, however, with the Microteck scanner we found a severe repeatable fluctuation of measured pixel value in the longitudinal direction. The longitudinal profile of a uniformly exposed film shows a unique "W" shape pattern repeatedly. The amplitude of the fluctuation is relatively high and could dramatically affect the dose measurement. Without being able to fix the scanner we decided to focus efforts on the older AGFA scanner.

Although it is relatively old, the AGFA Duoscan scanner still provides 16 bits per color channel and overall 48 bits per pixel. The configuration is different from most modern scanners in that it has a separate slot with a glass tray to support a transparent target. The scanner is connected to the computer by a SCIS interface. A stand-alone version of software (AGFA FotoLook 3.60.00) is used to provide the software interface for scanning. Figure 3.1 shows the film insert's position on the AGFA Duoscan scanner.

(a)   (b)

Figure 3.1: These photographs show the AGFA Duoscan scanner we use in this project. 3.1(b) explicitly shows the position of the transparent insert used to hold the film.

3.2.2 General settings

When scanning a film, the scanner should be set to RGB mode and with color depth of 48 bits. This gives the red channel a 16 bit color depth, which is equivalent to 65536 steps from black to red. Using 8 bits per channel is strongly not recommended since that could only leave 256 steps in color depth and when converted into dose, the dose resolution is low.

Spatial resolution should be set to 300 dpi. Most modern scanners including the AGFA Duoscan scanner we use, can easily go up to very high spatial resolution for example 1800 dpi. Considering that the dose calculation in most clinical treatment planning systems have a resolution of about 1 pixel per mm, there is no advantage of scanning the film with a much higher resolution. However, the suggested 72 dpi[23] from the manufacturer is not advised. Scanning in low resolution using a scanner with much higher capability could dramatically increase the noise level. This can be explained in the following way. In order to get a low resolution output the scanner can either average the signal from several pixels, or it can simply skip several pixels and pick one particular pixel as a representative. Most scanners will do latter in order to increase the speed of scanning. Since the limiting factor to scanning speed is how fast the head can move, skipping several lines is much faster than scanning each line and doing the average internally. If one scans the film in 72 dpi there is a good chance that the particular pixel will coincidently be a dirt or a scratch, although the physical dimension of that scratch could be much smaller than the pixel it represents. So we determined that the best technique is to scan the film using a moderate resolution and use software to lower the resolution by using a digital filtering method. Median filter is the one used on this step in this project. By doing this, the signal to noise ratio can be maintained. Figures 3.2 demonstrates this effect.

The fluorescent light needs to warm up to keep the light output stable. This means before each scanning session the lamp of the scanner has to be turned on for as least half an hour. The reproducibility of repeated scans

34

(a)   (b)

(c)   (d)
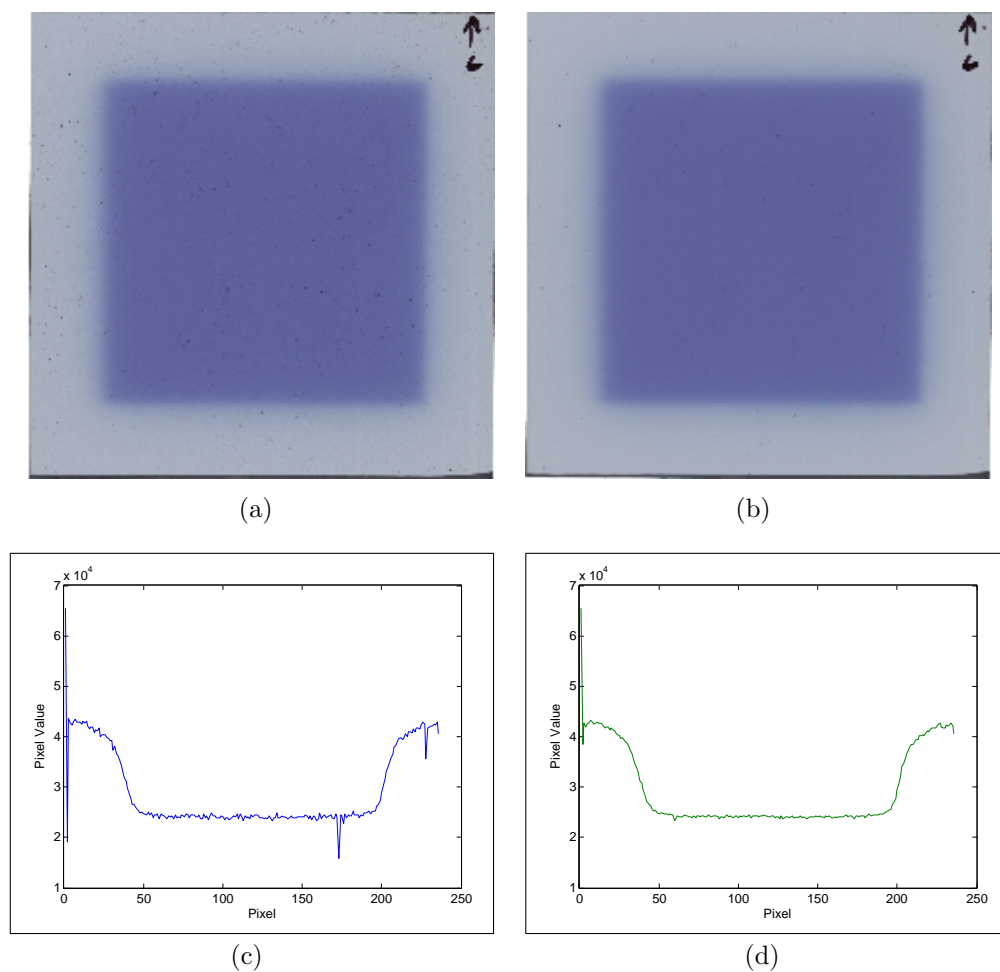
Figure 3.2: Scanned images demonstrating the difference between scanning the film in low resolution mode (100 dpi) 3.2(a) and scanning the film in high resolution mode (300 dpi) and then applying a median filter to adjust the resolution to 100 dpi 3.2(b). The noise level of the first one is significantly higher than the second one. Differences can be more easily distinguished in 3.2(c) and 3.2(d). 3.2(c) and 3.2(d) are horizontal profiles through the image in 3.2(a) and 3.2(b).

is indicated on the profile shown in Figure 3.14. Scanning the film without warming the lamp up could result in poor reliability. Although the absolute amplitude of variation in pixel value seems small, the variation in measured dose could be significant.

Furthermore, the dynamic range should be set to its maximum, and all corrections to the image should be turned off. Scanned images should be saved in TIFF format.

3.2.3   Position and Orientation Dependence

As mentioned by the film manufacturer and many other research groups, film scanners that have a long diffused light source and a CCD detector are susceptible to artifacts that can affect the performance. We shall call this scattering problem. The scattering problem will lead to both position dependence and orientation dependence of the scanned image. Flatbed scanners have a bar shaped light source and normally use fluorescent light. Although these scanners are designed to have some collimation above the CCD detector array that only allows incident photons within a certain angle to enter, calibration is still required to make sure all the detectors produce the same output signal when there is nothing being scanned (or when there is absolutely no attenuation). This procedure is automatically done each time a scan is performed. However, radiographic films and radiochromic films are composed of particles dispersed in a matrix having a different refractive index, and these films will scatter light. As a result, some scattered photons will pass through the collimation system. Even after an internal calibration, if a uniformly irradiated or un-exposed film is scanned, the signal acqiured at the extreme left and right sides will be systematically lower than in the middle. This non-uniform effect is shown in Figures 3.3 and 3.4.

Because this artifact is due to the shape of the light source, its response is related to the position of the film relative to the scanning area. For example, putting a smaller film in a different position within the scanning area will
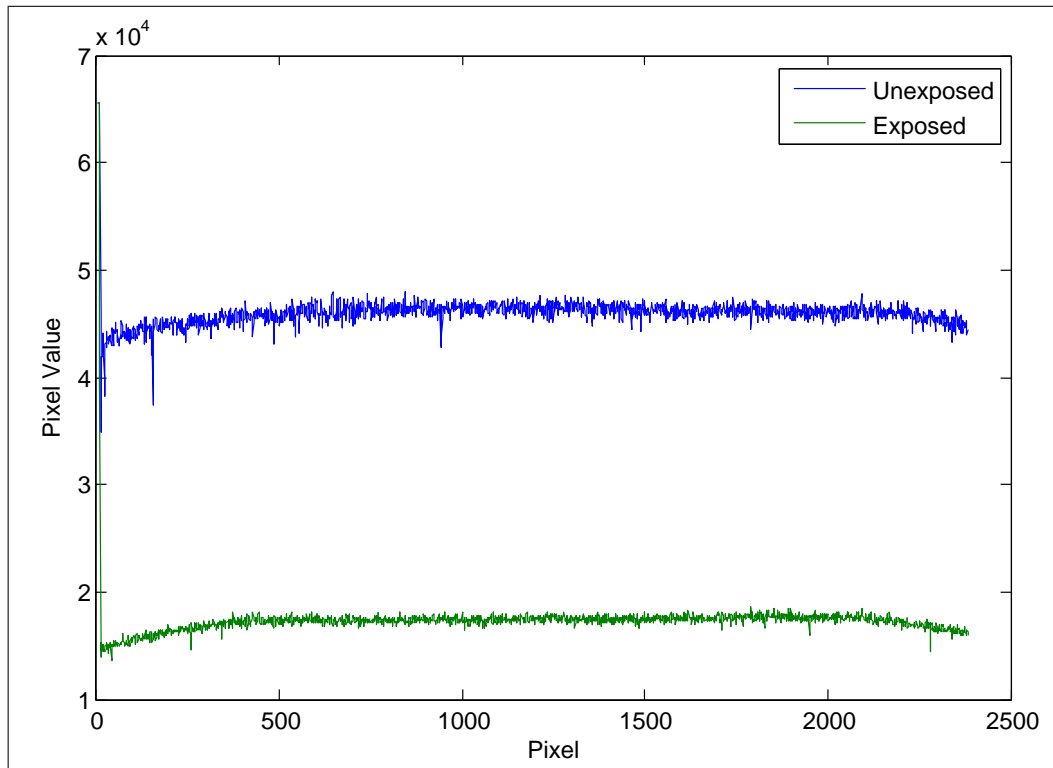
Figure 3.3: These two profiles are taken from scanned images of an un-exposed un-cut piece of film and a uniformly exposed piece of film. Profiles are along the horizontal direction which is perpendicular to the scanning direction. It is obvious that these profiles do not indicate a uniform response cross that direction even though the dose delivered is uniform or zero. At the edge of the field, the pixel value drops significantly for both images.
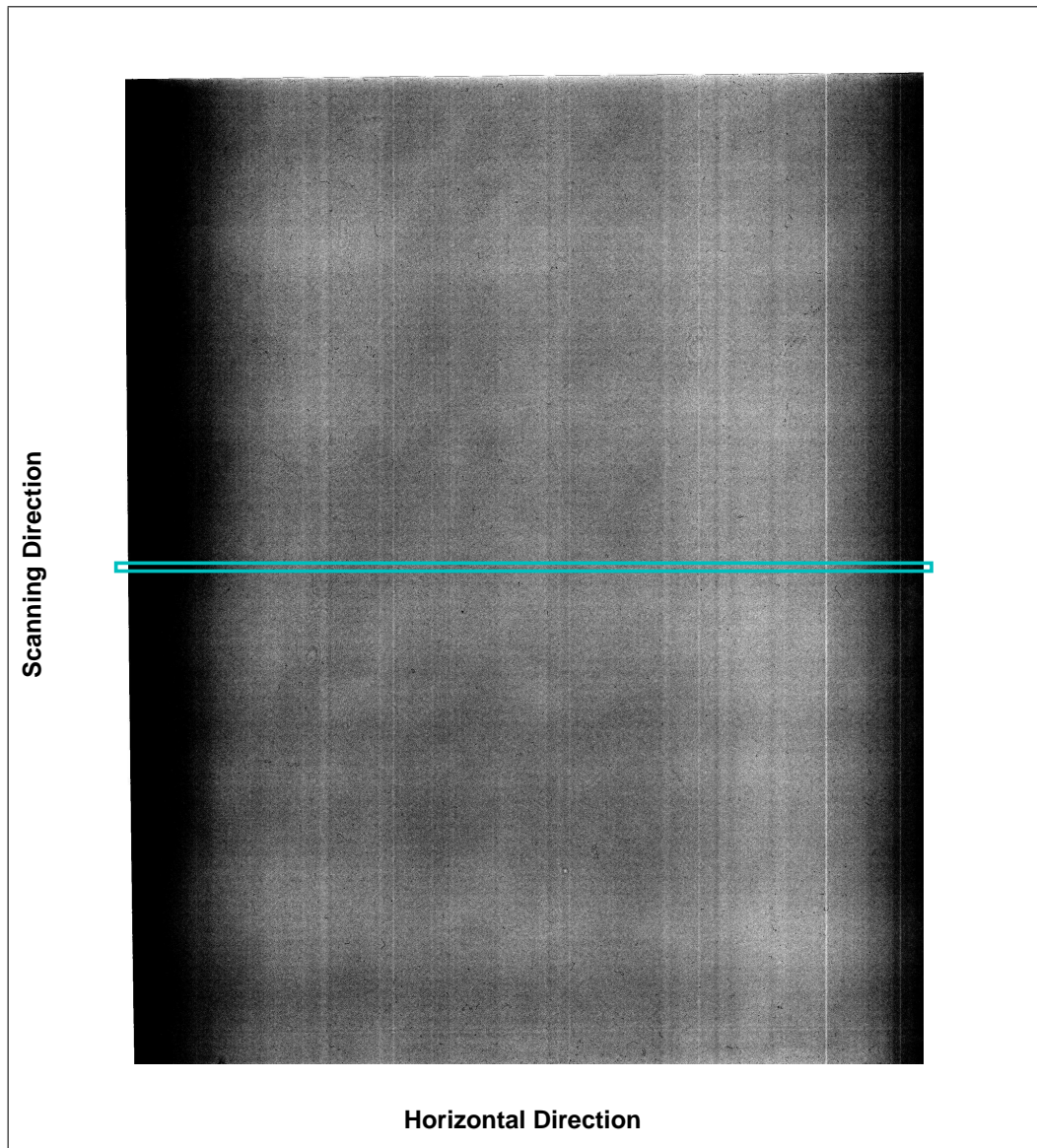
Figure 3.4: This image is taken from the same piece of film corresponding to the second profile in Figure 3.3. The colormap has been adjusted so that the minimum and maximum thresholds are 16500 and 18500 instead of 0 and 65535 by default. The black strips at both left and right side reflect the scattering effect. Those regions lack scattered photons making them significantly lower in pixel value compared with the central region. The light blue line in the center indicates where the profile is taken from Figure 3.3

result in different pixel values. The lateral profile of a uniformly exposed film will be systematically lower in the vicinity of left and right ends of the scanning area.

The manufacturer of EBT film claims that the scattering effect of the film is due to the difference of refractive index between the substrate and the active component and that polymerizations will not change the refractive index. They believe that a correction curve for the scattering artifact will not depend on the dose, thus a universal correction curve can be acquired using an un-exposed film. Many researchers have reached the opposite conclusion that the correction curve does depend on the optical density[24, 25]. Our experiments also verified that correction for the scattering effect indeed depends on the optical density. If we consider this dependence, the correction curve now becomes a two variable function. If the scattering effect is assumed to be only locally dependent, we could practically acquire this two variables relationship and apply it to correct for this artifact[24, 25]. This is indeed how others have dealt with this problem and the reported overall accuracy is still around 4 %. For our measurements, we decided to not correct for this, since our PTV target is small enough that we can put the region of interest onto the central region of scanning area. But efforts are also made to ensure the measurement film and the calibration film are scanned in the central region by building a frame to easily accurately position films with different sizes concentrically. The frames are L shape. The offset for the frame for 17 cm film pieces is 5 cm in the scanning direction and 2.5 cm in the longitudinal direction. The offset for the frame used for 6 cm film pieces is 10.4 cm in the scanning direction and 7.5 cm in the longitudinal direction. The schematic diagram in Figure 3.5 shows the shape of the frame as well as where it was positioned relative to the scanning area and the film.

Both the manufacturer and many research groups have reported that Gafchromic EBT film shows different response if the film is scanned in different directions[23, 24, 26–28]. This has been referred to as the orientation
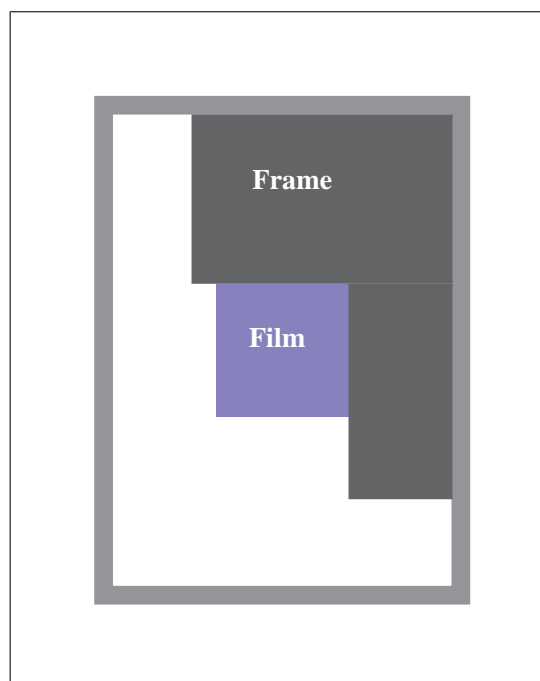
Figure 3.5: This schematic diagram shows the position of the film positioning frame. The grey outer box is the plastic border outside the scanning area. The L shaped dark region is the frame used to localize the film at the center. In actual fact the film is transparent.

dependence of scanning. An explanation provided by the manufacturer and referred to in many articles is that the micro structure of the active component of the Gafchromic EBT film is needle shaped polymers. The orientation of these needle shaped polymers tends to be along a particular direction which depends on how the film is manufactured, in particular, how the protective layer is coated. The manufacturer indicates that the needle like micro structure tends to align with the shorter direction of an un-cut film which is the coating direction[24]. They also suggest that the film should be scanned in an orientation such that the alignment of the micro structure is parallel to the scanning direction. In our experiment, we test this by scanning the same set of films in two different orientations and compare the scanned results. The results show that the same piece of film scanned in two different directions produces a significant difference in pixel value. Profiles taken from each image also show that one profile is approximately 10 % higher pixel value compared to the other. The results are shown in Figure 3.6.

Since pixel values depend on film orientation, calibration has to be acquired such that all pieces are scanned in the same orientation as the measurement film. Although scanning in either portrait or landscape mode is possible, there is a slight difference in the noise level between the two. Scanning in portrait mode gives slightly lower noise, and the scattering effect is less significant than for landscape mode. Hence in our project we choose to scan the film in portrait mode.

3.2.4 Calibration

Film response is represented as pixel value when the film is scanned. However, pixel value is just an intermediate parameter. Ultimately the pixel value is be converted into a dose value for each pixel. Due to the fact that film response for different batches is not expected to be the same, a universal calibration relationship between pixel value and dose does not exist. In order to establish a correlation between film response and dose reading, calibration
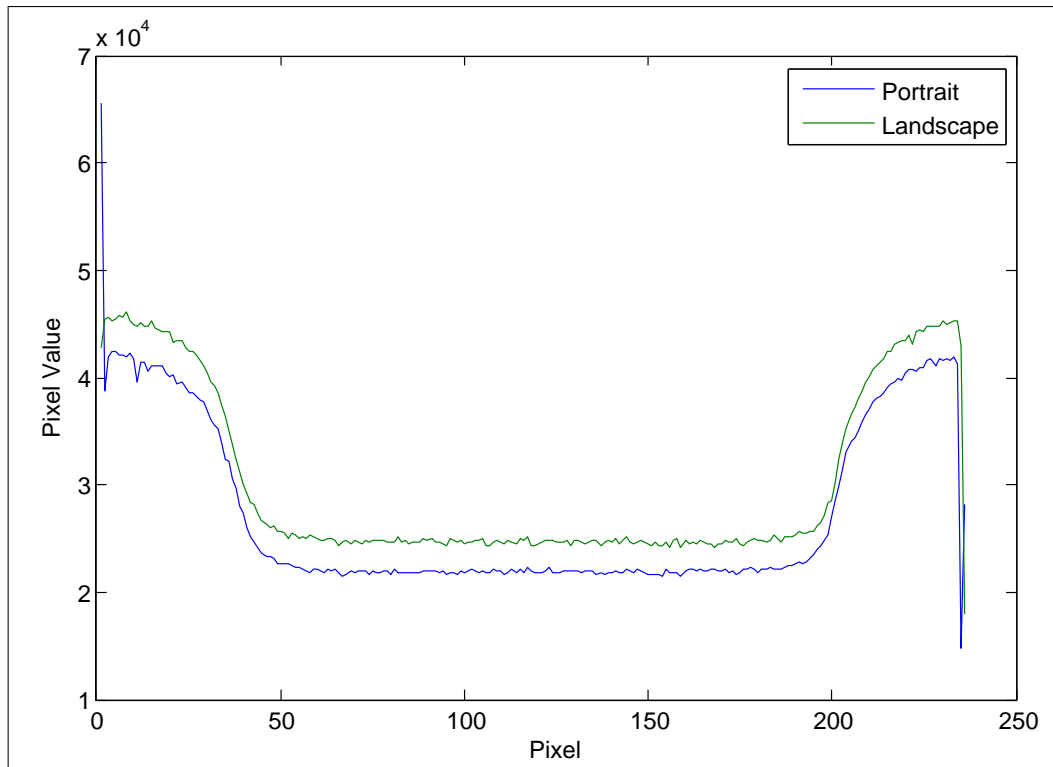
Figure 3.6: Profiles across the same line of the same piece of film (marked c3) scanned in portrait and landscape mode. The green line shows significantly higher pixel value than the other. It appears landscape mode gives a higher pixel value which confirms the hypothesis that landscape mode scatters more light. Portrait mode is the recommended one in this thesis.

irradiation is necessary. The calibration irradiation is performed on a set of small pieces of film under well defined conditions. The dose given to these calibration pieces has to be well known. Calibration pieces of film are from the same batch as the one used in the experimental irradiation, accepting the assumption that pieces of film from the same batch are produced at the same time and thus have much closer dose response. Although post-exposure development for Gafchromic film is reported to be relatively minimal[23], it can contribute up to about 5 % of the overall optical density if the wait time is long enough. To take this into account, the duration between irradiation and scan should be controlled. Either the scan time should be controlled so that the film is only scanned after a certain time post irradiation, or the calibration pieces should be irradiated directly before or after the experimental irradiation and then scanned in the same manner. Requiring that the film always be scanned after exactly a certain time post irradiation is inflexible and inconvenient, therefore we choose to produce calibration pieces each time we use the Gafchromic film. Furthermore, the manufacturer suggests that if the film is used as an absolute dosimeter, calibration pieces should be acquired every time the film is being used[23].

Calibration irradiation can be done in different ways, as long as the dose being delivered is well defined and can be calculated with high certainty. However, for different calibration setups, practical issues affect the outcome. One possible setup is to place the film strip parallel to the beam axis, so that the dose distribution along the center line is essentially a percentage depth dose (PDD) curve. Since PDD data is normally available (either the raw measured data, or from the TPS which is essentially interpolated data from the raw PDD table), by matching it with the dose response along the center line, a correlation between dose and optical density can be acquired[25]. This setup was investigated in this project and several practical drawbacks were discovered. First, the calibration is highly sensitive to geometry matching errors. Any uncertainty in the placement of the film will contribute to error

in the calibration curve. Particularly, if the film is not exactly parallel to the beam axis, a slight rotation can affect the dose distribution. It is challenging to absolutely restrict the film from any random shift or to trace the beam axis based on the irradiation pattern. Secondly, this setup is more vulnerable to noise. Because the dose response keeps changing along the central beam axis, it is not possible to average over this direction. In the perpendicular direction, although it is safe to average over a short distance, it is still not reliable because the dose distribution is not theoretically flat in that direction. Furthermore, a single PDD irradiation spans a limited dose range. To cover the dose range needed for a normal single fraction prescription, several calibration curves should be pieced together. Depending on how the solid water slabs are setup, single calibration curves sometimes suffer from lack of back scattering at the distal end. Together with the positioning uncertainty this usually shows up as a discontinuity when trying to match these curves together. Finally, the parallel setup, is susceptible to fluence perturbation due to the gap between the film and solid water.

Practical experience shows that EBT film together with a flat-bad scanner shows more noise than radiographic film with the Vidar scanner. Without clearly knowing what is the source of this fluctuation and how much it affects the dose measurement, it is recommended to do the calibration irradiation in the most simple, straightforward setup, avoiding any unnecessary potential issue that can compromise the calibration accuracy. Therefore, the calibration pieces for this project are irradiated perpendicular to the beam axis under a square field.

Two identical cube phantoms are used for IMRT measurements. The outer dimensions are 19.5 cm × 19.5 cm × 19.5 cm. The phantoms are shown in Figure 3.7. One of the phantoms is designed to work with films. The film is held at the central slice through the geometric isocenter, which is at a depth of 9.2 cm. Figure 3.8 shows the internal structure of this phantom and how the film is held inside of it. Both calibration irradiation
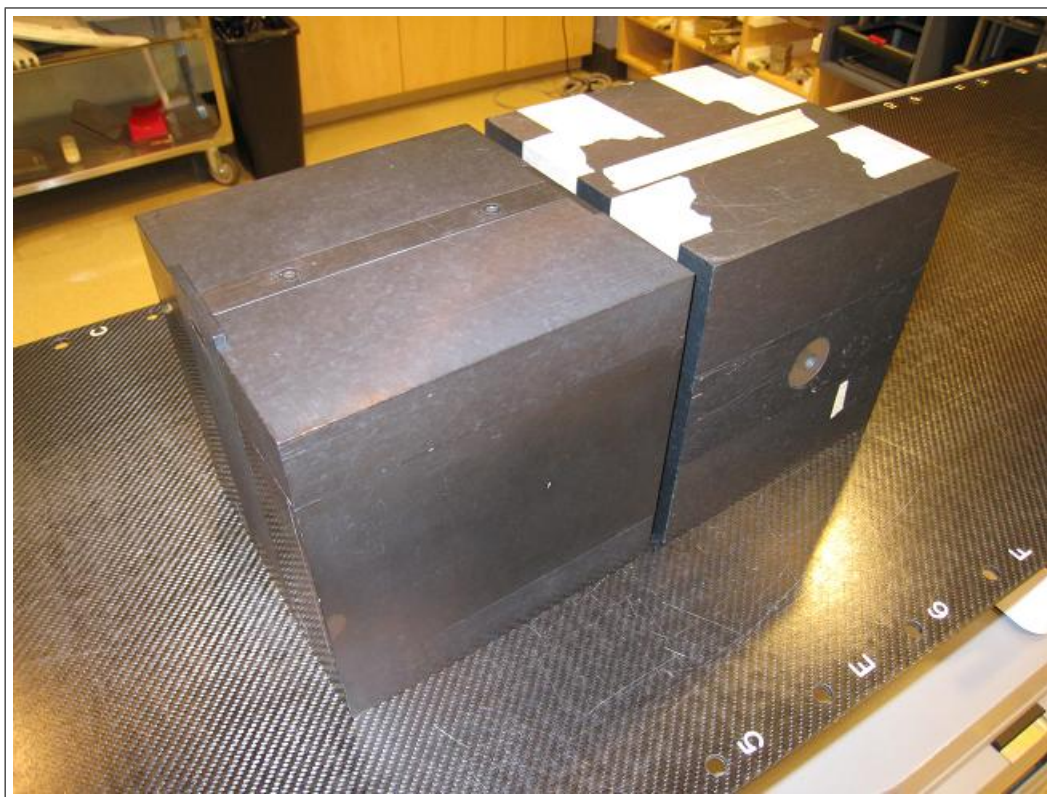
Figure 3.7: Two cube phantoms used in this project. Both of them have the same outer dimensions. The left one is designed for film dosimetry.

Figure 3.8: Part of the film cube phantom is opened showing the internal structure.

film ID	Monitor Unit (MU)	Dose (cGy)
c2	0	0
a1	50	34.48
a2	100	68.97
a3	150	103.45
b1	200	137.93
b2	250	172.41
b3	300	206.90
c1	350	241.38
c3	450	310.34
d1	550	379.31
d2	700	482.76
d3	800	551.72

Table 3.3: Monitor units and calculated dose for calibration exposures

and measurement irradiation are done at this depth. The film piece used for dose measurement is cut to 17 cm by 17 cm, while the calibration pieces are 6 cm by 6 cm. When they were irradiated they were both positioned at the center of the phantom. The irradiation of both calibration and measurement films is done at 100 cm SAD. For calibration, the field size is set to 4.2 cm by 4.2 cm with m3 micro collimator opening also set to 4.2 cm by 4.2 cm at isocenter. The monitor units delivered can be found in Table 3.3. The actual dose given is calculated using iPlan treatment planning software in conformal treatment mode. The highest dose given is up to 551.7 cGy, which is sufficient for IMRT commissioning purposes. Matlab code is used to create the calibration curve and convert the measured optical density distribution to dose. The scanned file is saved as tagged image file format (.tif). Matlab can directly read the file into a three dimensional matrix. Matrix elements are 16 bit integers. The three dimensions correspond to three color channels in the order of red, green and blue. A roughly 1 cm by 1 cm square region in the center of each calibration piece is sampled pixel by pixel. The average pixel value is used as a representative value for each piece. The dose delivered to

each piece can be calculated based on the monitor units given, so that a pixel value to dose calibration curve can be acquired. Figure 3.9 shows the pixel value calibration curve. A fourth order polynomial fit to the measurement data is used as the calibration curve. The curve fits the measurement data well except for the zero dose point.

Another way used by many groups is to convert the pixel value to optical density according to equation 3.1. Because the maximum possible reading without any attenuation is always internally calibrated to 65535 in 16 bit mode by the scanner, 65535 is always used as I_0.

$$OD \quad = \quad -\log_{10} \frac{I}{I_0} \qquad (3.1)$$

$$OD_{net} \quad = \quad OD - OD_0 \qquad (3.2)$$

Net optical density is calculated using Equation 3.2. Net optical density describes the change in attenuation due to exposure, where

$$OD_0$$

represents the optical density of unexposed film. We have tried both calibration methods and the results show negligible difference except for the extremely low dose regions. The results are shown in Figures 3.11 and 3.12. The discrepancy is mainly due to interpolation between the zero dose point and the first non-zero dose point. This discrepancy is believed to have no significant clinical importance because the peripheral region of the IMRT field is of relatively low importance. However, we still chose to perform film analyze using the optical density technique due to this effect.
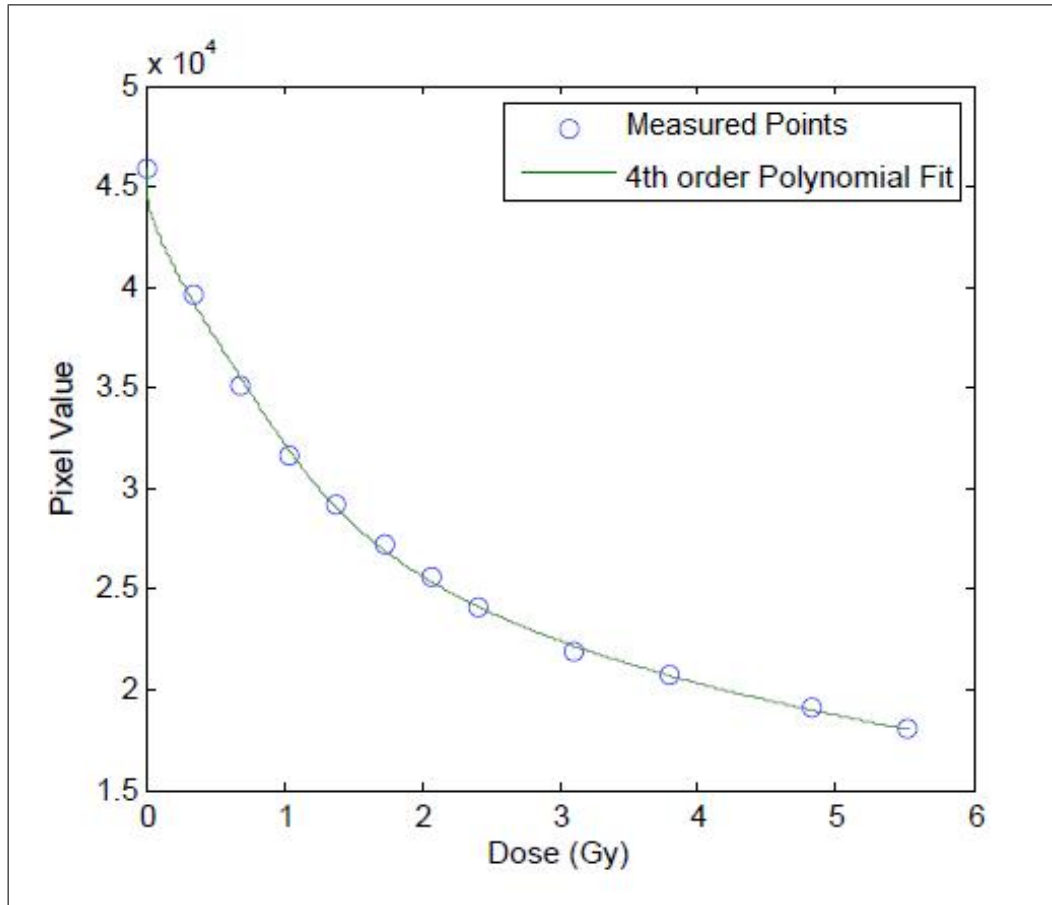
Figure 3.9: This is the pixel value to dose calibration curve. The green line represents the 4th order polynomial fit of the experimental data. The curve fits with the original data well except for the zero dose point. This introduces a discrepancy at the low dose end between pixel value calibration and optical density calibration. Uncertainty of each point is caused by the non-uniformity of the film and is approximately 500 for each point. The y error bars for each point are approximately the same size as the circle symbols.
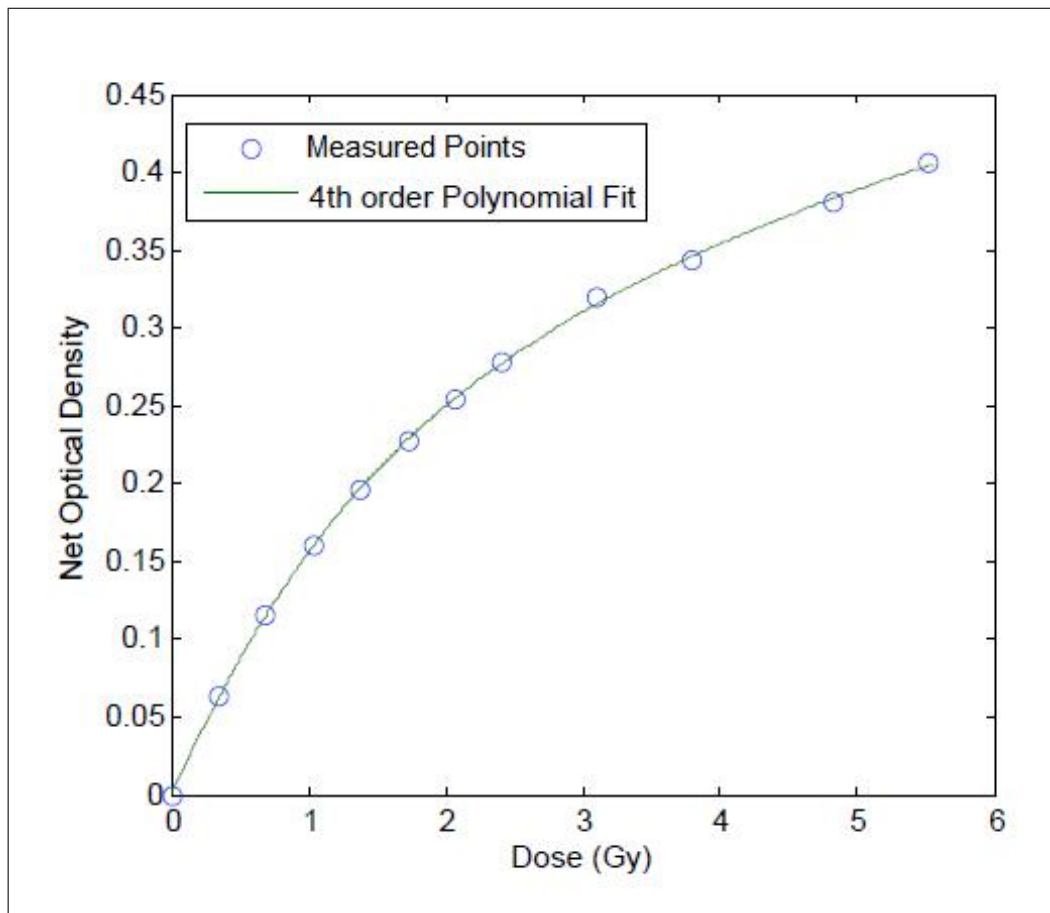
Figure 3.10: Net optical density calibration curve
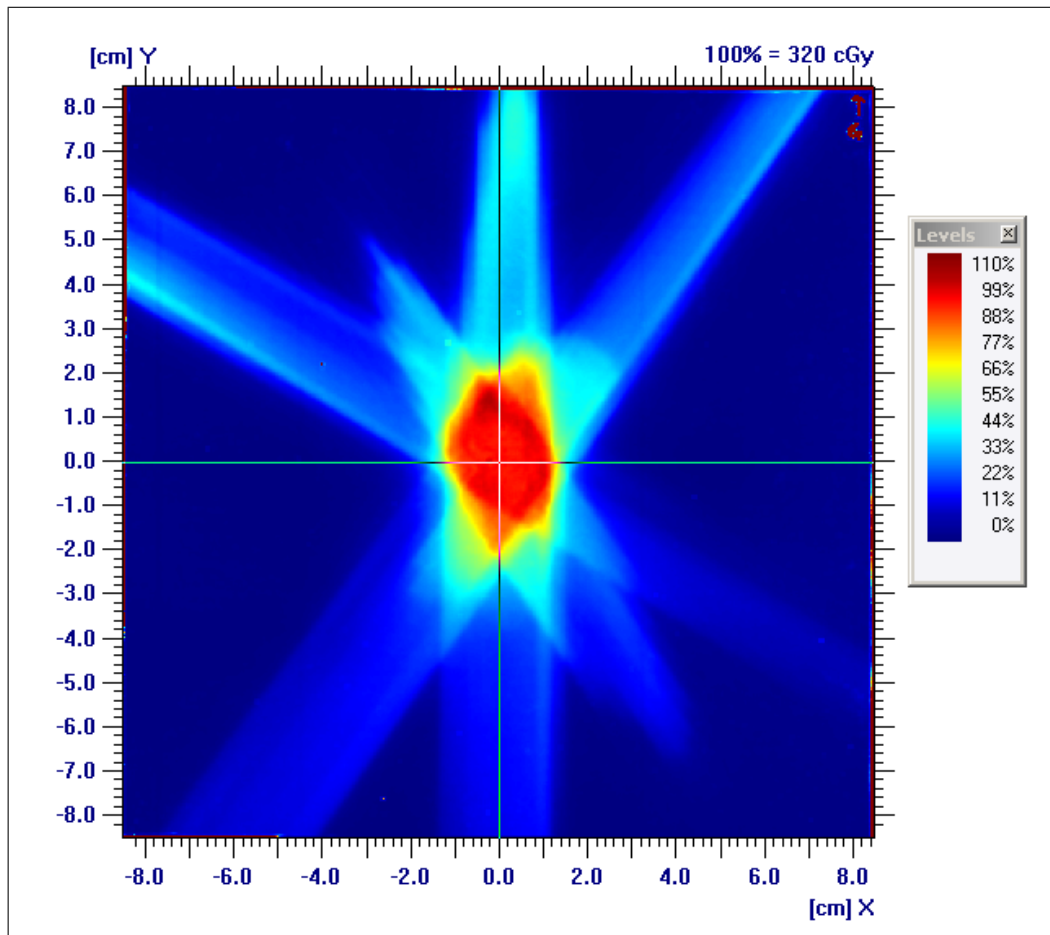
Figure 3.11: Comparison between pixel value and optical density calibration techniques. This image indicates the calculated dose distribution and the position of the x profile shown in Figure 3.12.
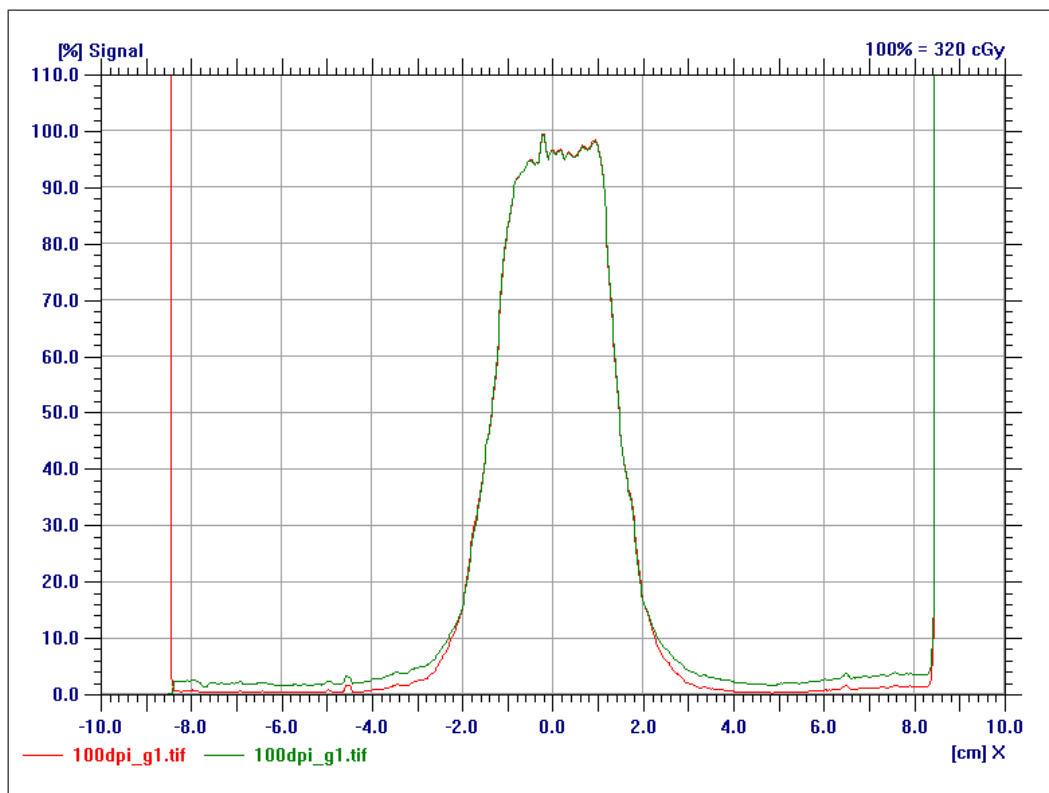
Figure 3.12: In this graph, the red curve is calculated using pixel value calibration while the green curve is calculated using the optical density calibration. Both of them are based on the same data set. The comparison indicates that the discrepancy is only significant at the low dose end.

3.3 Performance of Gafchromic EBT Film

3.3.1 Post-exposure Development

Post-exposure development is measured by scanning the same piece of film sequentially at different times after exposure. Films are scanned three times in each session and an average pixel value was plotted against the post exposure time. Result are shown in Figure 3.13. The field size was 10 cm by 10 cm. Depth of solid water build up is 10 cm. The pixel value is a calculated average over a 2.5 cm by 2.5 cm square central region. The dose was 200 cGy and was delivered using a 100 SAD setup. The majority of post-exposure development occurs in the first couple of hours, after which the rate of change is very small. So, we suggest that the irradiated film should be stored at least overnight before being scanned and if possible scanning of the measurement film and calibration film should always be done together following the same order used in irradiation. This is the method applied to all film scanning in our project.

The manufacturer claims that post-exposure development contributes less than 5 % of the overall darkness change. Their data suggests post-exposure density growth is not dose dependent. Our experiments show that post-exposure development contributes about 2 % of the optical density for a post exposure time of 15 hours.

There is a concern about day-light sensitivity. The manufacturer claims the film can be exposed to office light for several hours without developing noticeable density change. However, if exposed to sunlight or similar high intensity light environment, the density change can be much greater. We have not done any experiments to test this effect. However, our practice is to shorten such unnecessary exposure time. After the film is cut, it is always put back into a light-proof envelope. Unused films are always kept in a light-proof environment.

There is also concern about the density being affected by the scanning
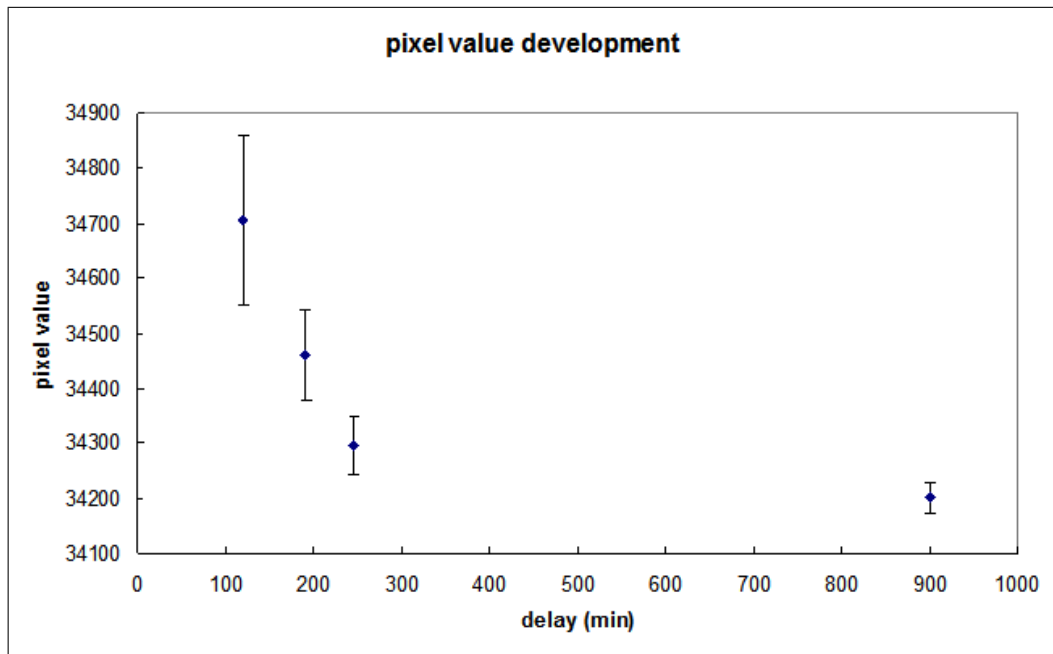
Figure 3.13: This graph shows the pixel values acquired at different post-exposure times of a single piece of film. The initial pixel value 34700 corresponds to 0.276 in optical density, while the last data point corresponds to 0.282. The difference (0.006) is approximately 2 % of the value of last data point, which corresponds to maximum development.

process because the light intensity of the scanner appears to be higher than room light. However, we have not found a report on this issue in any publication. We tested the reproducibility of consecutive scans to see if the darkness can be affected noticeably. The result is shown in Figure 3.14. There is no noticeable darkness change between the two scans. We conclude that the influence of scanning on the optical density is negligible. This result also in-
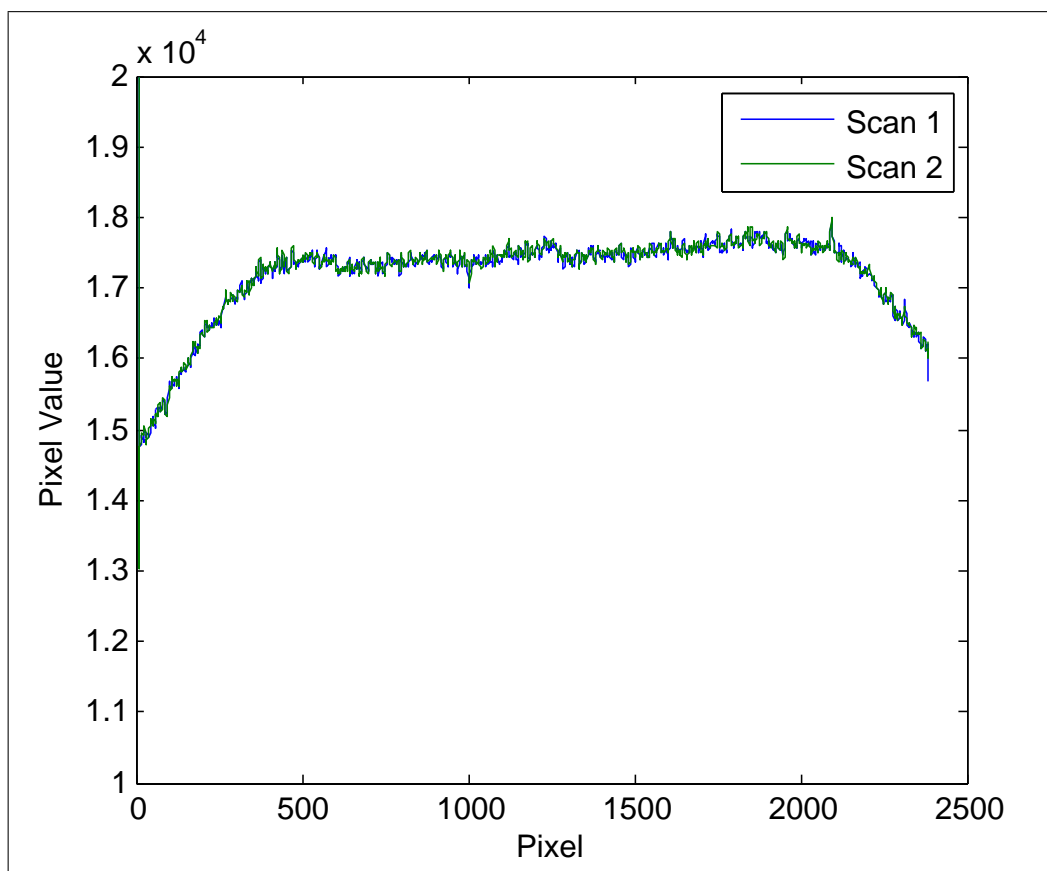
Figure 3.14: This graph shows the profile of consecutive scans of the same piece of film. The film is exposed to a uniform square field. The film is scanned at 300 dpi. A 5 by 5 Wiener filter is used to reduce the noise. There is no obvious difference between those two curves.

dicates that the scanned result is highly reproducible in consecutive scans in

the short term, if the film is not taken out of the scanner and placed again. Introducing a delay between scans or removing the film from the scanner and placing it could lead to darkness development between scans, changes in alignment, change of distribution of the dirt on the film and the sensitivity fluctuation of scanners.

3.3.2 Uniformity

The intrinsic uniformity of a single sheet of film is declared to be better than 0.8 % by the manufacturer. They also claim that the scanning variation contributes to 0.4 % and the total variation within a single sheet can be up to 1.2 % in total. The sheet to sheet variation is reported to be less than 1.5 % by the manufacturer[29]. The optical density variation is believed to be primarily due to the variation of the film's active layer thickness[30]. This variation is detected in our experiments. Figure 3.4 explicitly shows this variation. The graph shows the variation in red channel pixel value. By default, the pixel value range is from 0 to 65535, with correlates with 16 bit gray scale. On this scale, the image appears uniform to the human eyes. However the pixel value is not the same over the entire region. If the color window is adjusted to from 16500 to 18500, bright and dark bands will be visible. However, the source of this variation is not clear. It could be the intrinsic variation within the film, or it may be caused by the scanner. To determine the source of this variation, the same piece of film is scanned a second time with the film shifted by a small amount in the scanning direction. In Figure 3.15, profiles along the scanning direction are plotted. Here we see that the trend of variation appears to be the same for both profiles except that one profile is shifted relative to the other, which confirms that variation shifts with the shift in film position. This is evidence that the variation is caused by the film not the scanner. The amplitude of the variation in this example is at most 500 in pixel value which corresponds to a variation in pixel value around 3 % of the mean pixel value. It is more important to
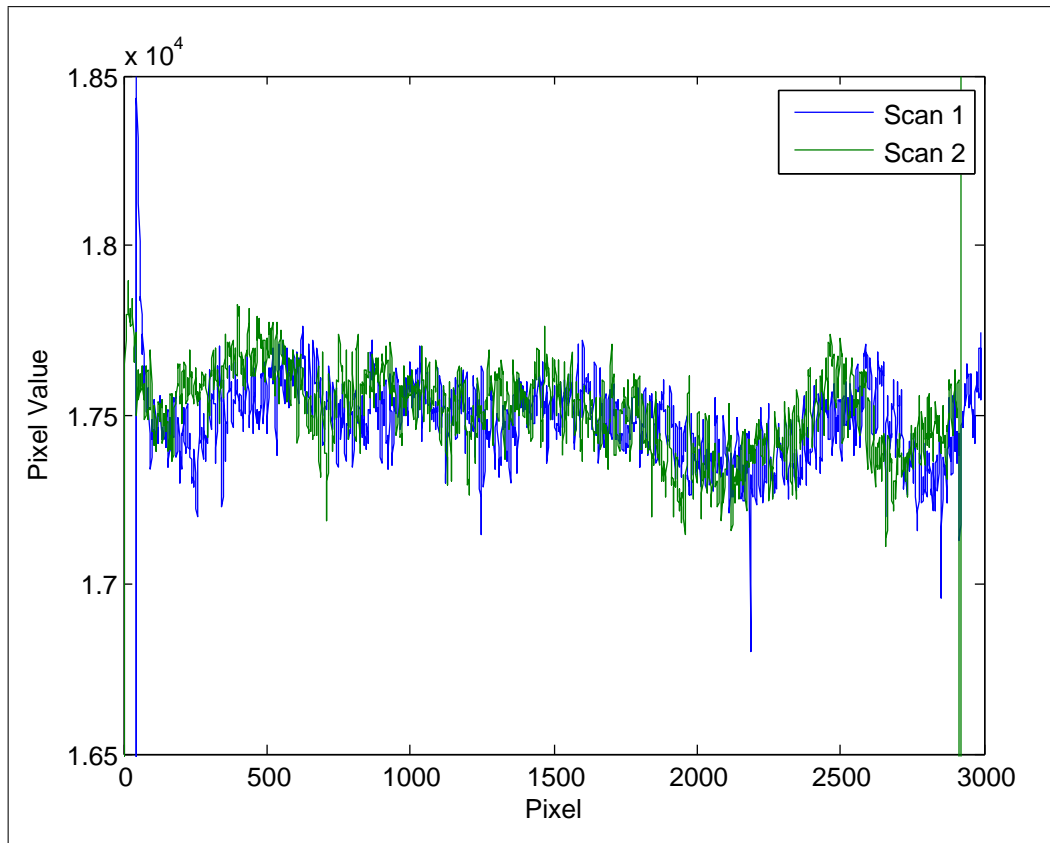
Figure 3.15: Longitudinal profiles of consecutive scans of the same piece of film is show in this graph. The film is shifted on purpose between the scans. The green profiles clearly is shifted towards left relative to the blue profile, which confirms that the variation is caused by the film itself not the scanner.

convert this variation in pixel value amplitude to variation in dose reading. This, however, highly depends on how much dose is given, due to the fact that the calibration curve is non linear and the derivative of the calibration curve depends on dose itself. In this example, it is at the high dose end of the calibration curve, the variation in dose will be greater than 3 %. Thus the intrinsic variation in film optical density is the major factor limiting the accuracy of applying the Gafchromic EBT film for dosimetric purposes. This problem is acknowledged by the manufacturer. A new product named Gafchromic EBT2 film has been introduced to address this problem. Details of the new Gafchromic EBT2 product are discussed in Section 7.1.

3.3.3 Dose Rate Dependence

Dose rate dependence of Gafchromic EBT film is theoretically a concern for the purpose of verifying IMRT treatment, because the dose rate is not constant during delivery. Rink *et al* have investigated the dose rate dependence of Gafchromic EBT film for real-time changes in optical density[31]. They claim that a statistically significant difference between change of optical density of films exposed at different dose rates occurs within approximately one order of magnitude change in the dose rate. The percent standard deviation of the change of optical density values using dose rate from 16 cGy/min to 520 cGy/min was <4.5 %. It is important to note the fact that this dependence is for real-time optical density change, with is different from the situation in our project, where the film is stored at least over night to allow the post-exposure density to fully developed. The post-exposure density development could contribute to as much as 2 % from 100 min to 900 min post exposure in our experiments. The rate of change of optical density is much higher in the first 100 min post irradiation indicated by extrapolation of the experimental data. It is understandable that read time dose rate dependence is related to the post-exposure darkness development. However, the did not test the dose rate dependence for non real-time reading. Although

the manufacturer declare the dose rate dependence is negligible, this remains a potential cause for uncertainty in dose reading.

3.3.4 Overall Accuracy

The overall accuracy of the film dosimetry system was tested by comparing the dose distribution acquired using the film with calculation results. This accuracy test accounted for the performance of film, the scanner, the codes and the procedure we use. Six pieces of film were irradiated with square fields under a 100 SAD setup condition. The dose value was picked up in a small square around the isocenter and the average value was used as the measured dose value for each piece. In order to exclude any influence of the TPS calculation error, the setup of the measurement irradiation was the same as the setup used to expose the calibration pieces, with field size of 4.2 cm by 4.2 cm and SAD of 100 cm. Therefore the same MU to dose ratio was used for both the calibration calculation and dose calculation for the measurement pieces. This ratio, if inaccurate, would affect the calculation of both the calibration pieces and the measurement pieces in the same way and would cancel out. Hence, this test excludes any TPS calculation errors.

Among the six pieces of film, three were given 500 MU. The other three are given 250 MU, 700 MU and 100 MU respectively. The same Matlab code was used to convert the film response to dose and the dose distribution was evaluated using OmniPro I'mRT® software. Figure 3.16 shows how the region of interest was chosen. The data are listed in Table 3.4. They show that for well defined square fields the film measurement yields up to 2.5 % error in dose.

To determine the reason for the discrepancies, an additional experiment was done to test the consistency among different pieces of film. Three calibration sets, each containing 12 pieces of film and all acquired in the same way, were rescanned in one session. The calibration curves were recalculated based on the new data and a set of optical densities from one of them was fit

Film ID	MU	Calc. Dose (cGy)	Measured Dose (cGy)	Diff. (%)
E1	500	344.8	342.3	-0.73
E2	500	344.8	342.8	-0.58
E3	500	344.8	350.7	1.71
F1	250	172.4	169.4	-1.74
F2	700	482.8	495.0	2.53
F3	100	69.0	70.8	2.61

Table 3.4: Results of the overall accuracy testm
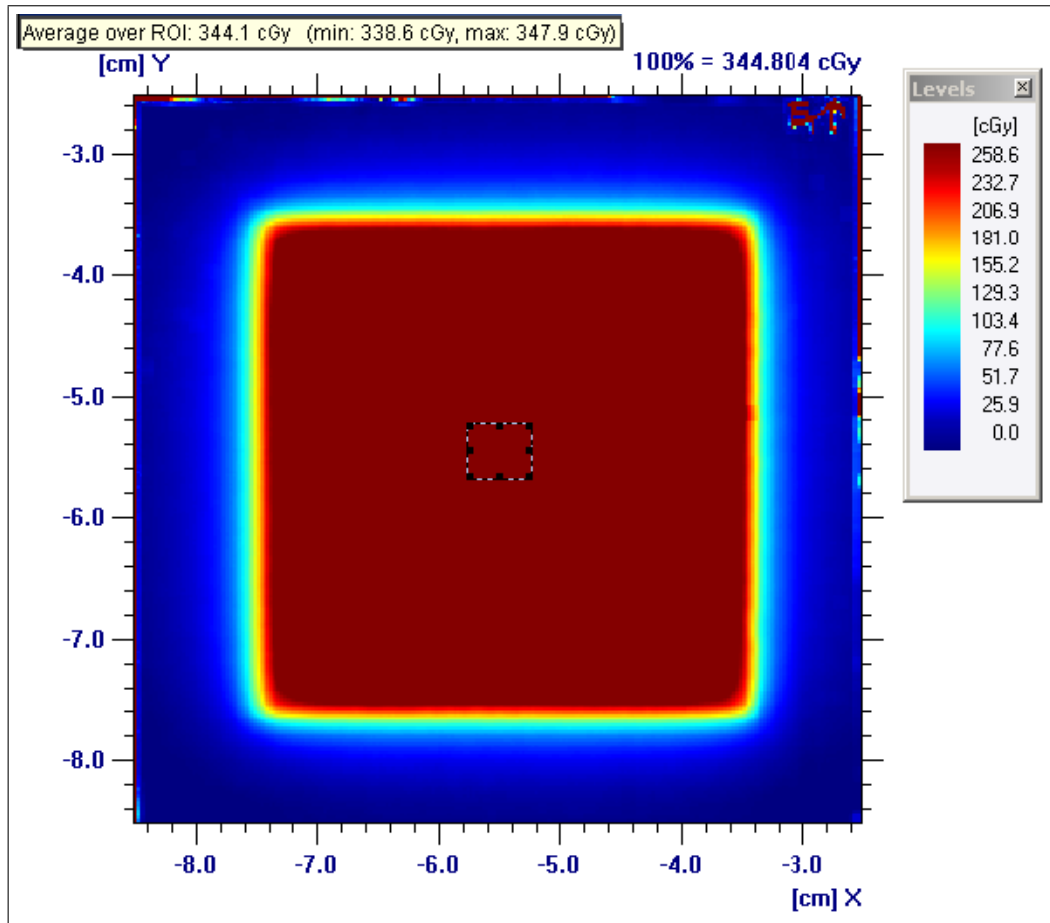
Figure 3.16: The region of interest for the film data listed in Table 3.4 is shown here.

through all three calibration curves. Calculated dose values were compared. Figure 3.17 shows the three calibration curves. The Table 3.5 shows the dose
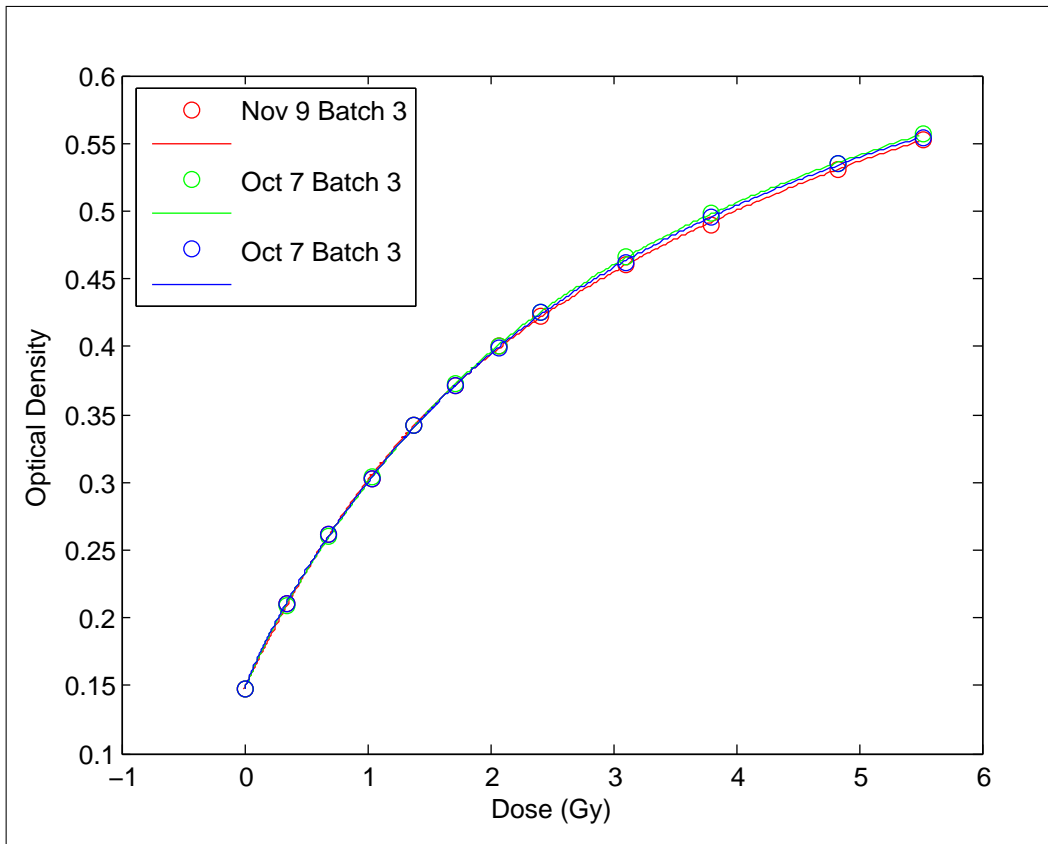
Figure 3.17: Three calibration curves scanned and generated in one session

values calculated using three different calibration curves. The percentage differences are listed. The discrepancies were up to 2.5 %, which is the evidence that the discrepancies found in Table 3.4 are primarily caused by the variation in film response difference from piece to piece. This difference is expected to be similar to the variation across a single piece of film, although the magnitude of the non uniformity within single pieces may be smaller. This non uniformity effect contributes at most 2.5 % to the overall discrepancies in our experimental results. It is this non uniformity effect that the

manufacturer intents to address with EBT2® film.

Dose by Original Calibration (Gy)	Dose by Cali. 2 (Gy)	Dose by Cali. 3 (Gy)	Diff. of Cali. 2 (%)	Diff. of Cali. 3 (%)
0.000	-0.004	-0.005	N/A	N/A
0.345	0.353	0.347	2.317	0.725
0.690	0.694	0.678	0.623	-1.734
1.034	1.018	1.034	-1.575	-0.027
1.379	1.376	1.373	-0.235	-0.469
1.724	1.718	1.739	-0.354	0.844
2.069	2.075	2.096	0.305	1.307
2.414	2.471	2.419	2.374	0.222
3.103	3.130	3.183	0.862	2.560
3.793	3.885	3.841	2.429	1.252
4.828	4.960	4.846	2.737	0.382
5.517	5.569	5.604	0.930	1.564

Table 3.5: Inter-piece variation of film calibration

Chapter 4

Treatment Planning and Dose Verification

A radiotherapy treatment system consists of a planning system and a delivery system. The treatment planning system applied in this work is the iPlan® treatment planning software. The delivery system consists of a Varian linear accelerator and a BrainLAB m3 high-resolution multi-leaf collimator. The treatment planning system generates the IMRT treatment plan, which is essentially an optimized leaf sequence file, based on the dose prescription to the PTV and the dose deposition constraints on the critical organs close to the PTV. The plan is then transferred through the central information system to the Linac and MLC control consoles. The control consoles control the leaf motion as well as the dose rate during the treatment delivery. Before the system can be clinically used, the treatment system has to be commissioned to ensure that the planning system can correctly calculate dose distributions based on the leaf sequence files, as well as to ensure that treatment can be delivered according to the treatment plan within the tolerance level. It is clear that dose verification is an essential part of the commissioning process. The first section of this chapter focuses on the treatment planning system. It explains the typical work flow for generating a stereotactic treatment plan and how the dose verification works from the software end. The second section introduces the delivery system. Localization and immobilization devices as well as the m3 micro MLC are discussed because they are directly related to the dose delivery. The last section explains the methods and materials used in dose verification. It includes detailed information about phantom structure,

MLC performance tests, ion chamber measurement and film dosimetry.

4.1 iPlan Treatment Planning Software

The iPlan treatment planning software is a multi-purpose planning system developed by BrainLAB. It can generate treatment plans for different kinds of techniques. The reason we choose it as the planning system for our project is that the m3 high-resolution multi-leaf collimator used in this project is a product from the same company. Thus the iPlan treatment planning software and the m3 MLC should be highly compatible. Moreover, the m3 MLC has already been commissioned for static application for clinical use in iPlan. IPlan has some unique features compared with the Eclipse treatment planning system. To give a clear picture, a brief introduction of the planning work flow using the iPlan system is given in the following sections. A flow chart of a typical treatment planning procedure using the iPlan system is shown in Figure 4.1.

4.1.1 PatXfer

The user interface of the iPlan treatment planning system has a step by step guided style. Although different tasks are done using different modules of the system, the user interface features of these modules are all similar so that users can easily master all of them. A typical treatment plan using the iPlan system starts with importing CT, MRI or PET images into the planning system. This is done using PatXfer, a module of the iPlan software package.

4.1.2 iPlan Image

After the patient CT data set and MR data set are imported into the iPlan system, the next step is to deal with the issues of image analysis such as setting up the coordinates, image fusion and contouring the organs and PTV.
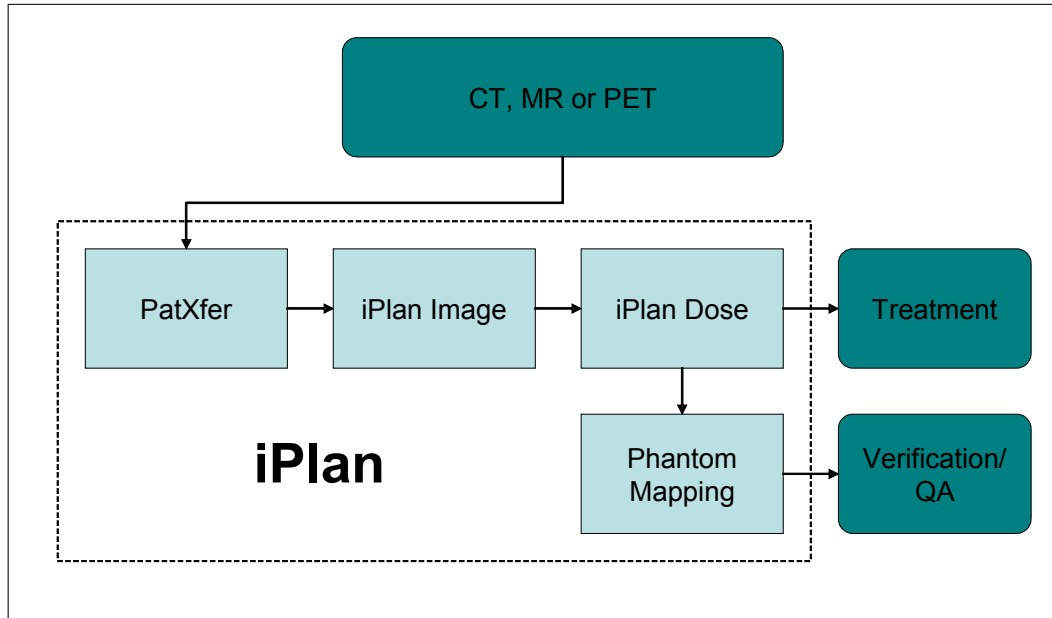
Figure 4.1: The flow chart of iPlan

This is done in iPlan Image. The software will guide the user through the typical work sequence.

For stereotactic treatment a rigid coordinate system is setup based on the CT scan. The CT scan of the patient's head is acquired with a specially designed reference box fixed to the head, so that the box has a fixed spatial relationship with the patient's anatomy. There are two Aluminum rods embedded on each surface of this box which can be detected on the CT scan and represented as six dots on each slice. The software detects the position of these six markers and uses the distance between each pair to determine the relative position of each slice to the reference coordinate system. This coordinate system is used throughout the remaining process of treatment planning and delivery, serving as a basis for accurate spatial positioning which is the essential difference from non-stereotactic treatment techniques. Figure 4.2 shows a screen capture of this step.

MR images are acquired since they provide better soft tissue contrast
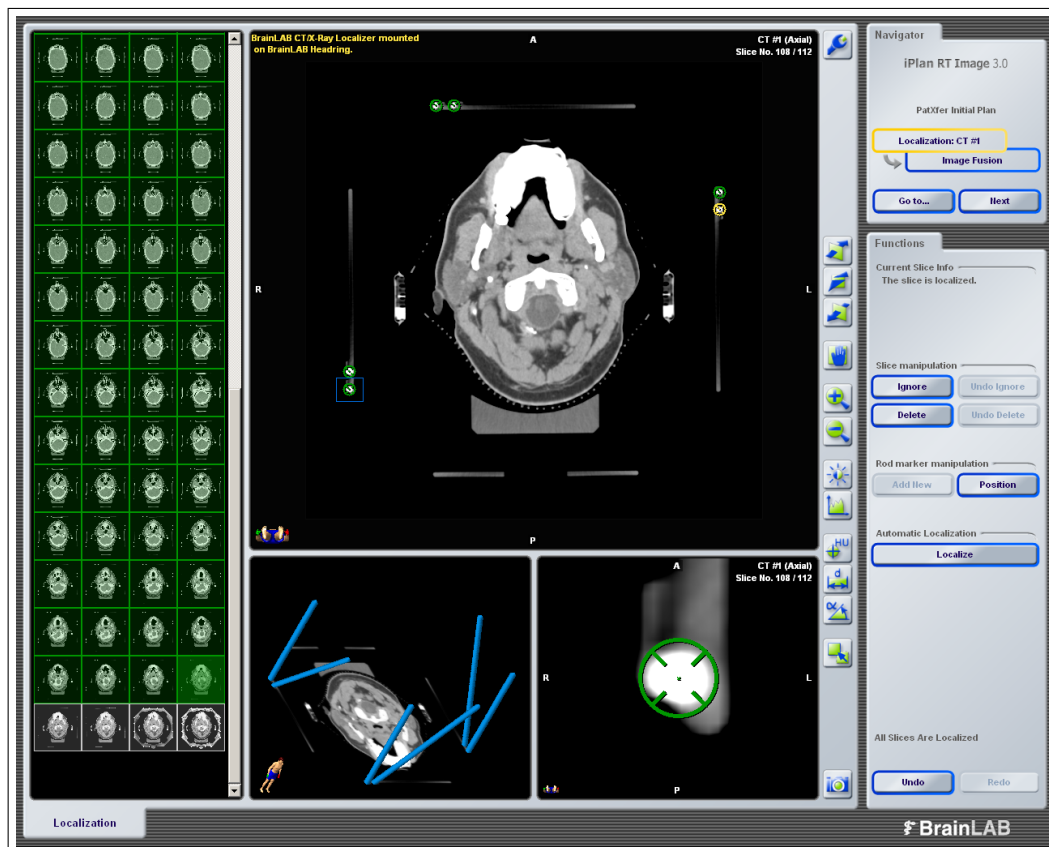
Figure 4.2: A screen capture of the iPlan image recognizing the markers on the reference box which is used to determine the relative position of each slice to the coordinate system

compared with CT. The MR data set has to be fused with the CT data set before it can be used to help with contouring critical organs and PTV. For iPlan, image fusion is done automatically based on the least square algorithm using the intensities of both images. The fusion result is checked and if not satisfactory, users can manually adjust the fusion.

The next step is to contour the critical organs as well as the tumor volume. For intracranial treatment, the critical organs include the eyes, the brainstem, the medulla oblongata, the optic tracts, the optic nerves and the optic chiasm. The contouring of these structures is automatically done on the MR images using an anatomic atlas. Tumor target is manually contoured by the oncologist. The PTV is grown from the gross target volume (GTV) by a certain margin, usually 2 mm. If there is no overlap between the PTV and any other critical structure, the next step is to proceed with treatment planning. Sometimes the PTV region does overlap with a nearby critical structure. Because the algorithm for beam optimization requires the overlapping volume to be treated differently, the user must then use the Boolean operation function to separate the overlapping part from the critical organs. For example, in the situation that the brainstem overlaps with the PTV, two new volumes have to be generated: one named brainstem 1 referring to the overlapping part, the other named brainstem 2 referring to the non-overlapping part. During IMRT planning brainstem 1 will be assigned a lower priority (which in iPlan is called 'guardian number'), so that treatment planning software assures the tumor control of this volume as the first priority. The Figure 4.3 shows how the OAR is separated using Boolean operation. Figure 4.4 shows the screen shot of the iPlan image after the OAR and PTV are contoured.

4.1.3   iPlan Dose

The iPlan dose module is the core of this planning system. The inverse optimization and dose calculation is performed in this module. The work flow
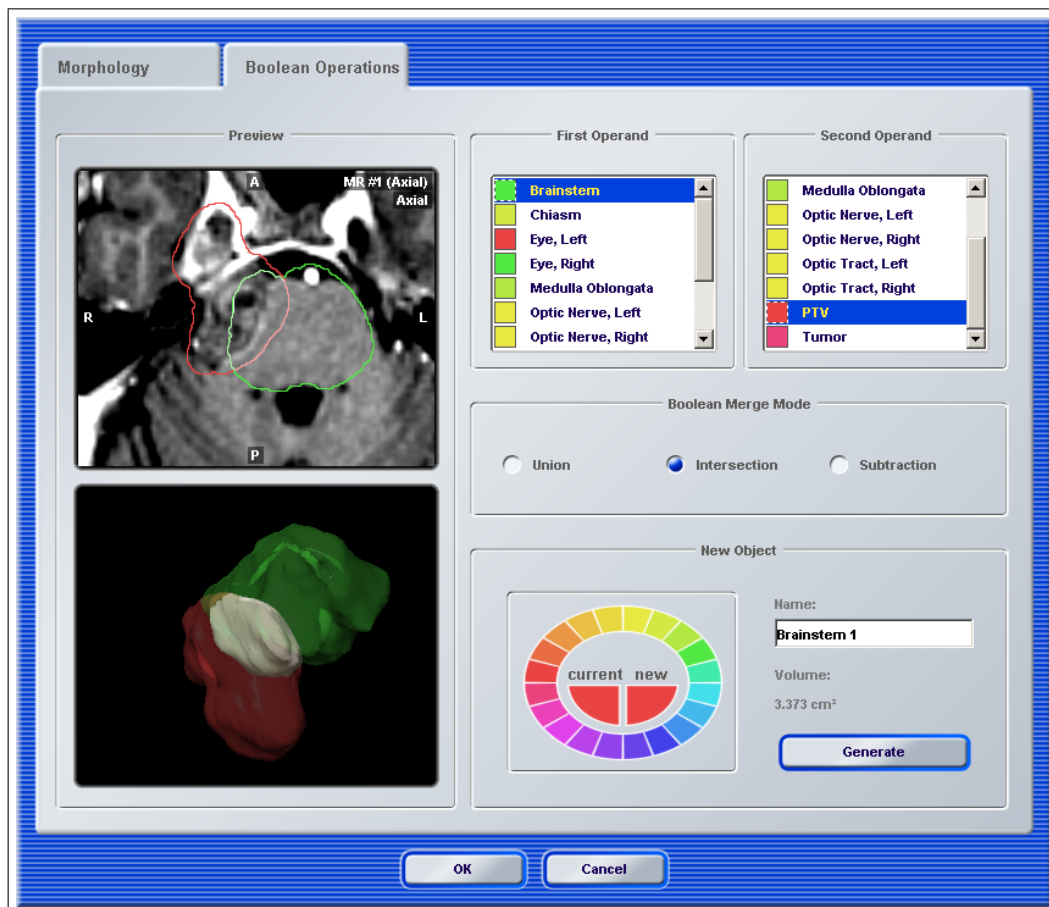
Figure 4.3: Screen capture of the Boolean operation interface.
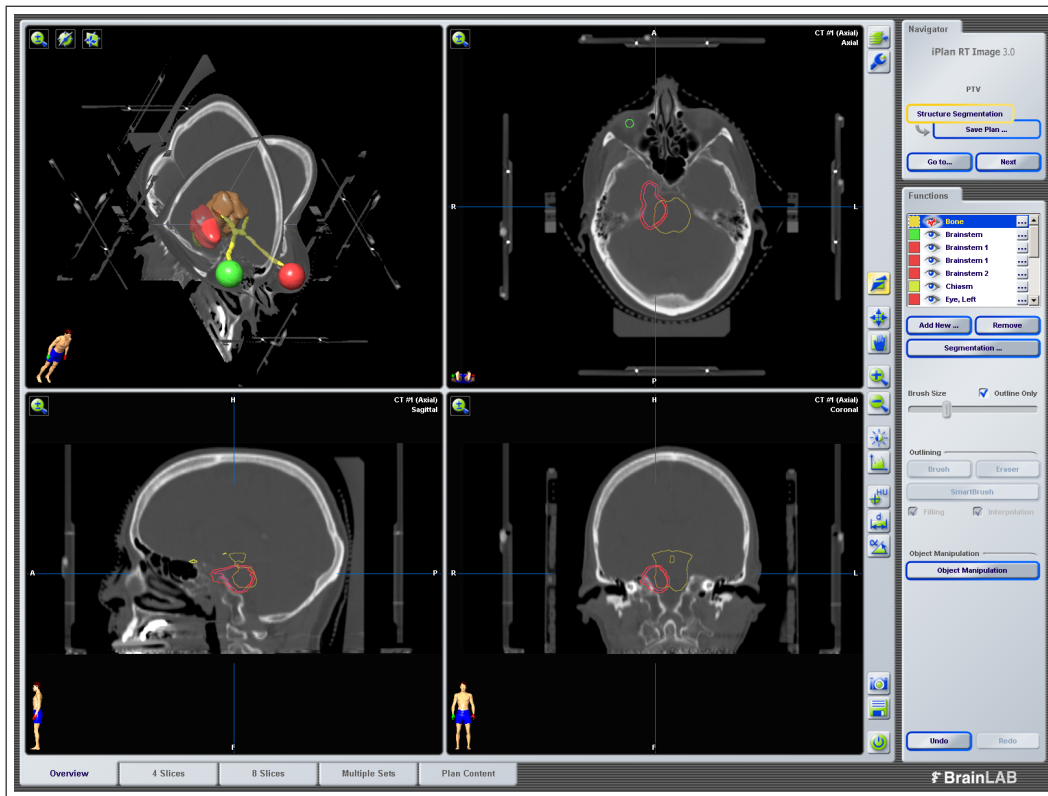
Figure 4.4: Screen capture of the iPlan image after the objects are contoured.

starts with locating the isocenter, which is typically taken as the geometric center of the PTV. Then, treatment beams are associated with the isocenter. The treatment technique can be either conformal, IMRT or arcs. The number of beams, beam angles and couch angles have to be specified and entered by the planner. The treatment planning system will calculate leaf position for conformal treatment, or it will generate the leaf sequence file for IMRT treatment. To be able to optimize the leaf sequence file and calculate the dose distribution correctly, the proper machine data set has to be chosen. These machine data files are created based on measured data. The measured data include PDD, RDF and the nominal linac output for a specific set of conditions. The machine data files are energy specific and machine specific, although it is possible that several similar machines share the same data file if the difference among them is not significant. There is a debate on whether the IMRT beam arrangement should be coplanar. Body IMRT treatments are usually coplanar based on the fact that there is not much room for the couch to rotate without colliding with the gantry. But for intra-cranial treatment, since the target is located at the end of the couch and is held by a narrower stage than the couch itself, the available couch angle range is much larger. The advantage of using non-coplanar setup is to avoid primary beam passing through the eyes or other critical organs.

The next step is beam optimization. This is when the program uses dose volume constraints set by the user to determine optimal modulation for each beam. Users have to first specify the grid size, which is the spatial resolution used in the dose calculation. Smaller grid size gives higher accuracy but obviously costs more in calculation resources. It is advised that the grid size should be bigger than the pencil beam algorithm beamlet size. The dose prescription to the PTV and critical structure dose constraints can be specified at this point. Both prescription and constraints are defined on dose volume histograms (DVH). BrainLAB suggests that the PTV dose constraint should be set on the 50 % volume level, because the actual DVH curve

70

always shows an S shape, setting the constraint on 50 % volume is a good compromise to balance the cold spot and hot spot. However, at the VCC the standard is to cover the PTV with the 90 % isodose surface. Practically, we move the constraint point closer to the high volume side to force the result to give better dose coverage by compromising the hot spot dose. Figure 4.5 explains this problem.

The optimization generates four different plans including: PTV only, OAR low, OAR medium and OAR high. As their names indicate, each plan spares the OAR to different degrees. Usually, considering an acceptable dose coverage and reasonable OAR sparing, OAR low or OAR medium are good candidates. If none of these plans is acceptable, the user can go back to modify the OAR constraint and dose prescription to hopefully get a better result. This optimization process is iteration based and time consuming. Only one of the four plans can be chosen and saved for future access.

4.1.4   Phantom Mapping

After the plan is completed a number of verification tests need to be made before the plan is ready for treating the patient. The dose distribution can be exported by just clicking the 'dose export' button. However, for the purpose of a phantom test, since the phantom has a completely different shape from the patient, the dose distribution from the original beam setup is different from the original calculation. The planning system should be able to re-calculate the dose based on a phantom shape so that this can be used to compare with film measurement or ion chamber measurement. The iPlan phantom mapping module allows the user to map any existing IMRT treatment plan onto a phantom and calculate the dose distribution. The user must be careful to specify the isocenter to the right position of the phantom. For fractionated treatment, the total dose or MU is transferred. The program will ask for the number of fractions in order to calculate the dose distribution for a single fraction. If the user wants to modify the number of
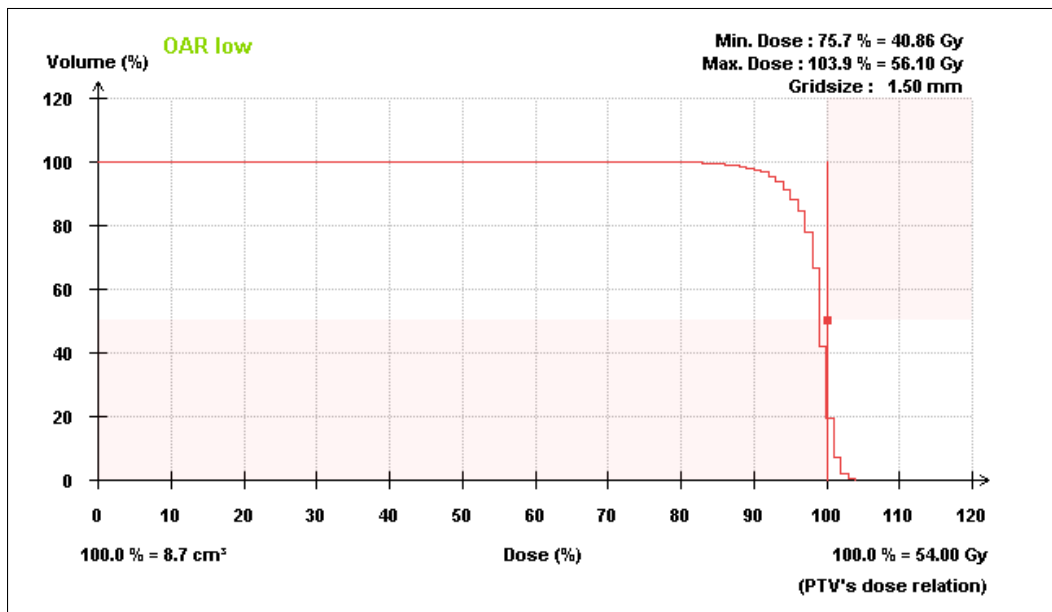
(a)
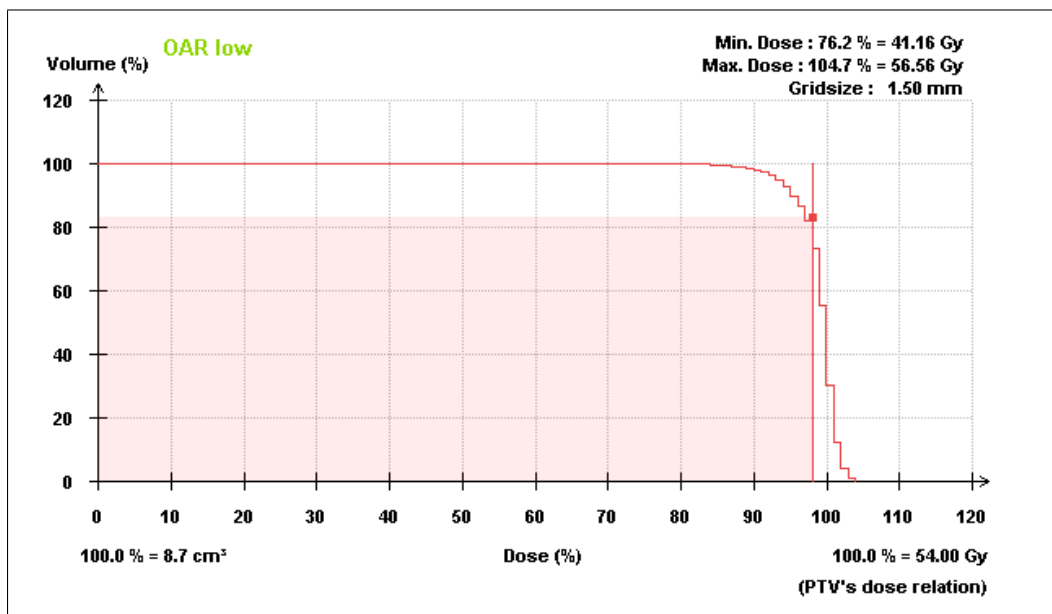
(b)

Figure 4.5: Different constraint points on the DVH affecting the 90 % dose coverage

fractions, they can multiply the prescription by an arbitrary factor. Finally, the dose distribution is exported so that the calculated dose distribution can be compared to the measurement.

The coordinate system used in phantom mapping is determined by the coordinate system associated with the CT data of the phantom, in this case, a cube phantom. The film plane position relative to this coordinate system does not vary in these experiments. To get the dose distribution of the film plane of a 17 cm × 17 cm square area with a 1 pt/mm resolution, the range should be L: -83.63, R: 86.37, step: 1.0; F: -59.4, H: 110.6, step: 1.0; A: 5.82. This range is symmetric relative to the geometric center of the phantom. This is how the film data is registered with the measurement data.

4.2 Stereotactic IMRT Delivery System

4.2.1 Localization and Immobilization

Extra-cranial or body IMRT treatment has limited spatial positioning accuracy, because of the conventional localization and immobilization technique applied. For body treatment, typical localization and immobilization devices include thermoplastic masks and vacuum molded bags. The vacuum molded bag is placed between the patient and the linac couch, while the thermoplastic is placed over the patients' body. Both devices' shape can be fixed to maintain the consistency of the patient's position. If the thermoplastic mask is not tight enough, the patient can still move a little bit within the mask. Often the mask does not fit the patient perfectly, so there is an intrinsic freedom of movement. Figure 4.6 compares the thermoplastic masks used in conventional IMRT and stereotactic treatment. Moreover, unlike the intra-cranial environment, the relative position of the anatomy is more likely to change for body treatment. Tumor target may shrink or migrate in between fractions. Breathing motion can also dramatically change the target position for some cases. All these factors contribute to the positioning inaccuracy of

(a)

(b)

Figure 4.6: The mask in Sub-figure 4.6(a) is the mask used in conventional IMRT treatment. The mask is soft and not tight enough to fully restrict the patient's movement. The mask in Sub-figure 4.6(b) is the one used in stereotactic treatment. It is more rigid and can restrict the movement of the jaw.

body IMRT treatment. Hence, body IMRT treatment is suitable for relatively large targets. The Varian Millennium MLC is used in these cases with a minimum leaf width of 5 mm projected at 100 cm SAD.

For intra-cranial treatment, stereotactic radiosurgery is used to help increase the positioning accuracy. Traditional stereotactic radiosurgery uses an invasive head frame to restrain the patient's motion. For the IMRT application, an alternative of using an immobilization mask is a much better candidate. Compared to the mask used in body IMRT this stereotactic immobilization mask is more rigid and has a bite block attached to it. The small amount of movement within the mask is measured by taking two X-ray photos from two different directions and matching the CT data to these photos. Furthermore, the position is also monitored using infra-red markers on the patient in real time to maintain the accuracy. This frame-less SRS/SRT system can achieve comparable spatial accuracy to the technique using the frame system. The BrainLAB m3 MLC has a 3 mm minimum leaf width projected at 100 cm SAD surface, which provides higher spatial resolution than the Varian Millennium MLC[2, 6]. The combination of stereotactic and IMRT technique will benefit relatively smaller intra-cranial lesions compared to the normal size that will benefit from conventional IMRT[6–10].

4.2.2 BrainLAB m3 Micro MLC

As discussed in Chapter 2.3.2, the MLC is an essential component of the IMRT technique. The BrainLAB m3 micro multi-leaf collimator, as the name indicates, is designed to define a high resolution treatment field. For stereotactic treatments, a steep dose fall-off is required to protect normal tissue and, in particular, critical structures from high doses. Stereotactic single fraction treatment should meet special requirements of dose gradient steepness which have been defined by the AAPM. For single fraction radiosurgery, the recommended limit for dose gradient in the beam penumbra (from 80 % to 20 %) should be greater than or equal to 60 %/3 mm[32]. The steepness of

the dose gradient in radiosurgery is a function of beam geometry and beam penumbra. The 5 mm width of the Varian Millennium MLC cannot guarantee that in all cases the requirement of 60 %/3 mm can be met. The m3 with its 3 mm-wide leaves has an effective penumbra of less than 3 mm for all SRS field sizes and meets all SRS requirements[2, 6].

Since the development of the m3 was a joint project between BrainLAB and Varian, the m3 is designed based upon the architecture of a standard Varian Millennium MLC to be fully compatible with Varian linacs. Figure 4.7 is a photograph of the BrainLAB m3 MLC. The M3 has 52 tungsten leaves (26 pairs), which move along a plane that is perpendicular to the beam central axis. Unlike the Varian Millennium MLC that has a minimum leaf width of 5 mm at isocenter, the m3 has minimum leaf width of 3 mm around isocenter. Details of leaf specification can be found in Table 4.1.

Number of leaves	26 Pairs
Leaf width (at isocenter)	14×3.0 mm
	6×4.5 mm
	6×5.5 mm
Maximum field size	9.8 cm $\times$ 9.8 cm
Maximum leaf over-travel	5 cm
Clearance from isocenter	31 cm
Maximum leaf speed	1.5 cm/s
Weight	30 kg

Table 4.1: Specifications of BrainLAB m3 micro multi-leaf collimator

Except for leaf width and leaf number, the most distinct difference is tongue and groove design and the leaf tip shape. A more complicated 'tongue and groove' leaf cross-section was necessary to allow drive shafts to be inserted into each leaf. Adjacent leaves have this shaft inserted at vertical increments to permit optimum positioning of each leaf's driving motor. Leaf tips are milled to three angled straight edges to cover the whole range that the leaves can travel. Compared to Varian Millennium MLC this angle is

Figure 4.7: This is a photograph of the BrainLAB m3 micro MLC. This device is attached to the gantry head when in use. The square window in the center is where the beam passes through. Noticeably the maximum field size is only 10 cm by 10 cm defined at 100 cm distance. The leaves can be seen on the right edge inside of the window.

much smaller, about 3°, due to the fact the maximum field opening is only 9.8 cm by 9.8 cm.

4.3   Dose Verification

4.3.1   Phantom

Two phantoms are constructed for the purpose of dose verification. Both
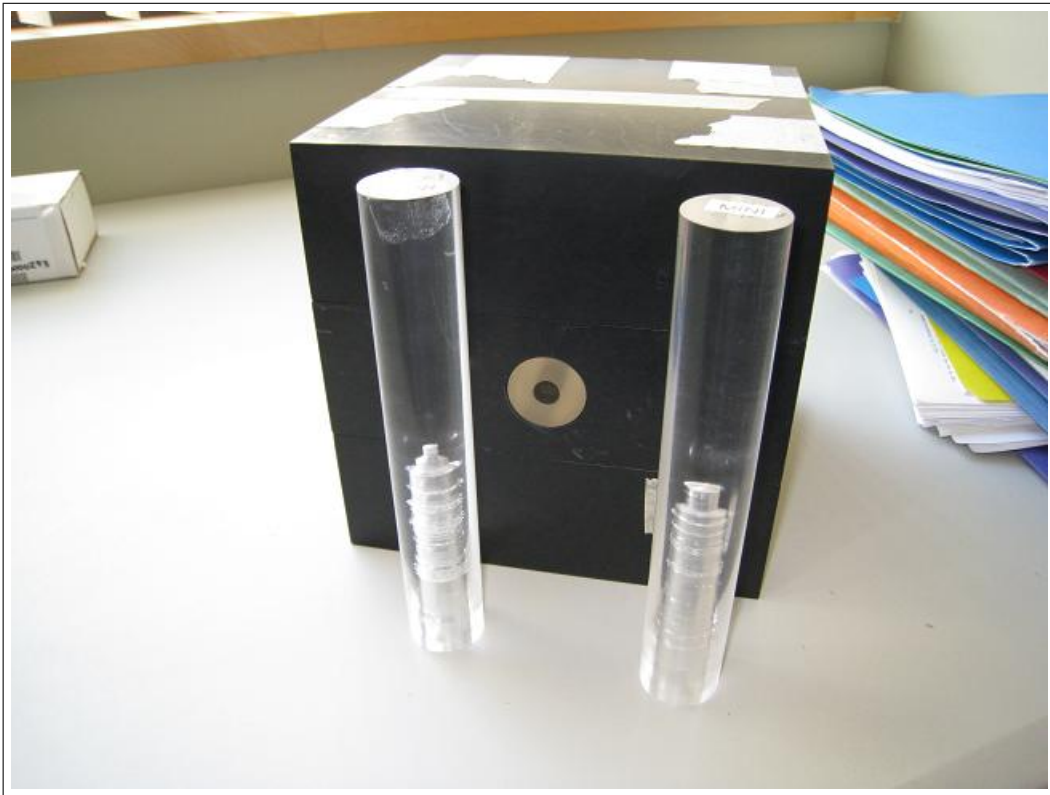
Figure 4.8: This figure shows both the ion chamber cube phantom and the interchangeable inserts. Notice the different internal structure of the inserts. They were designed to fit for different types of ion chambers. The location of the chamber tip is supposed to be at the geometric center of the cube phantom.

of them are plastic cubes with dimension of roughly 18.5 cm by 18.5 cm by 18.5 cm. The outer dimensions of both phantoms are identical, while the inner structure is different. One of them has a cylindrical hole which fits cylindrical inserts that in turn fit different types of chambers (The two most frequently used chambers are a 0.01 cc chamber and a 0.1 cc chamber). Figure 4.8 shows both cube phantoms and the interchangeable inserts. The chamber's sensitive volume is located at the geometric center of the phantom if the chamber is fully inserted into the proper insert. The other phantom is for film dosimetry. It was originally designed to contain traditional radiographic film requiring it to be light proof. The cube has a shell with thickness of 5 mm. Four identical slabs are placed inside the shell of the cube. The film is supposed to be located between the second and the third slabs. The slabs are tightly fit so that the air gap in between the slabs is small. Rotating the phantom will not cause significant movement of the slabs within the phantom. Figure 4.9 illuminates the internal structure described above. The material of which the phantom is made is polystyrene. The effective atomic number is 5.74. This phantom can contain a piece of film with a maximum size of 17 cm by 17 cm. For smaller size, four pieces of tape are pasted on top of the second slab forming a double line cross shape to restrict the small piece of film inside of it. This is also shown in Figure 4.9. The overall uncertainty of film positioning is less than 1 mm in both longitudinal and lateral directions.

To simulate the clinical treatment setup, the stereotactic head rest is modified to support the phantom. Figure 4.10 shows how the head stage assembly is used to hold the phantom. Two plastic bars are pasted on two adjacent edges of the plastic plate on the head rest. Pushing the phantom against this corner will assure the position of the geometric center of the phantom is at a reproducible location. By switching between the two phantoms, ion chamber measurement and film dosimetry experiments can be performed in the same configuration. Ignoring minor difference between the two phantoms, the ion
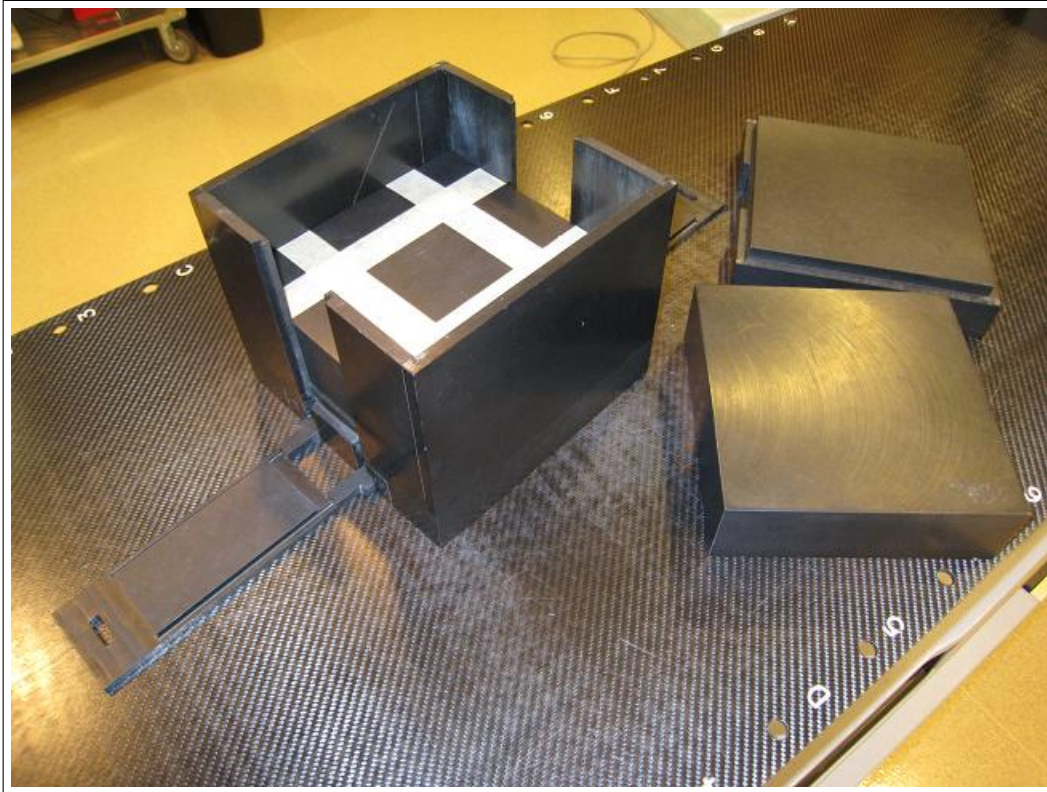
Figure 4.9: This photograph shows the internal structure of the film dosimetry phantom. The surface with tape on it is located at the central depth. The total area of that surface is 17 cm by 17 cm. When 6 cm by 6 cm pieces are used, they were restricted at the center by the cross of the tape.
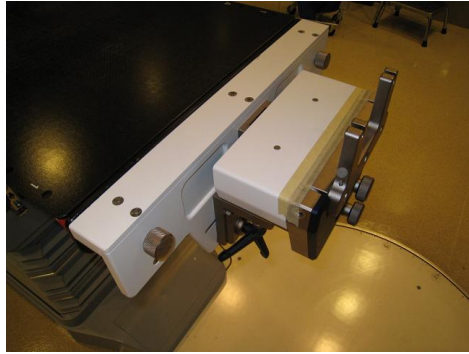
(a)
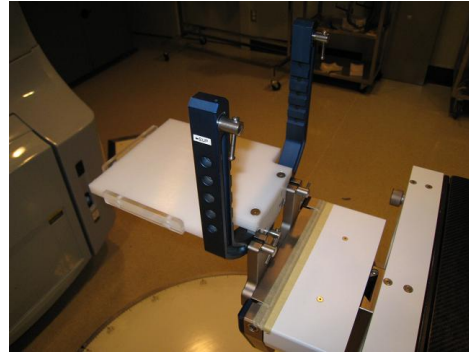
(b)
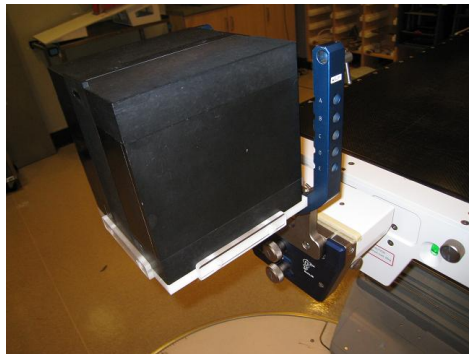
(c)
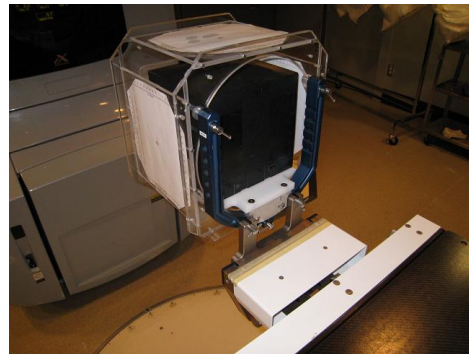
(d)

Figure 4.10: These photographs indicate how the stereotactic head stage is attached to the linac couch and how the cube phantom is held on it. 4.10(a) shows how the adjustable stage is mounted on the linac couch. 4.10(b) shows how a modified plastic plate design for the phantom is connected on the stage. 4.10(c) shows how the cube phantom is located on the plate. 4.10(d) shows how the reference box is connected to this assembly and used to help align the geometric center of the box to the isocenter.

chamber reading corresponds to the center point of the film. .

4.3.2   MLC performance Tests

MLC is the component that most likely could affect the accuracy of beam delivery. Therefore, MLC performance tests have to be performed prior to dose verification. MLC performance tests for this project involve three parts: static MLC positioning test, dynamic MLC statistic test and the effective leaf gap test. These three tests focus on different aspects of MLC performance. The first one inspects the absolute leaf positioning accuracy for static beam delivery; the second one measures the dynamic response of the MLC. The last one insures that the TPS correctly models the distance between actual leaf tip position and the divergence line of the beam edge.

Static MLC Positioning Test

Because the m3 micro MLC is currently used in clinical treatment, the static MLC positioning test is routinely performed during the monthly QA on it. A set of MLC patterns include three simple rectangular openings with sizes of 2, 5 and 9 cm, and a special pattern called "Multiport" is used. The actual MLC position is detected using EPID. A small amount of dose is delivered with each pattern of MLC. Edge position of each MLC leaf is measured on the EPID acquired image and is compared with the planned position. The whole measurement is repeated for four times at different gantry positions (0, 90, 180, 270°) in order to take the effect of gravity into account. Sample data of the 5 cm by 10 cm pattern at 0° gantry position is shown in Table 4.2. Figure 4.11 illuminate the data in Table 4.2. The last column of Table 4.2 represents the actual distance between opposite leaves which is supposed to be around 50 mm. The tolerance level is set such that the discrepancy should be less than 1 mm. Maintenance is performed when the discrepancy is larger than 2 mm. Since this static MLC positioning test is part of the

	Lbank (mm)	Diff (mm)	Lbank (mm)	Diff (mm)	Sum (mm)
Leaf 01	25.2	0.2	25.0	0.0	50.2
Leaf 02	25.0	0.0	25.1	0.1	50.1
Leaf 03	25.1	0.1	25.2	0.2	50.2
Leaf 04	25.0	0.0	25.2	0.2	50.2
Leaf 05	25.4	0.4	25.3	0.3	50.7
Leaf 06	25.1	0.1	25.2	0.2	50.3
Leaf 07	25.1	0.1	25.2	0.2	50.3
Leaf 08	25.1	0.1	25.2	0.2	50.4
Leaf 09	25.1	0.1	25.3	0.3	50.4
Leaf 10	25.1	0.1	25.3	0.3	50.4
Leaf 11	25.1	0.1	25.3	0.3	50.4
Leaf 12	24.8	-0.2	25.3	0.3	50.1
Leaf 13	25.2	0.2	25.3	0.3	50.5
Leaf 14	24.8	-0.2	25.4	0.4	50.2
Leaf 15	24.8	-0.2	25.5	0.5	50.2
Leaf 16	25.2	0.2	25.4	0.4	50.6
Leaf 17	25.2	0.2	25.4	0.4	50.6
Leaf 18	24.9	-0.1	25.4	0.4	50.3
Leaf 19	24.9	-0.1	25.4	0.4	50.3
Leaf 20	24.9	-0.1	25.4	0.4	50.3
Leaf 21	24.9	-0.1	25.5	0.5	50.4
Leaf 22	24.9	-0.1	25.5	0.5	50.4
Leaf 23	24.9	-0.1	25.5	0.5	50.4
Leaf 24	24.6	-0.4	25.4	0.4	50.0
Leaf 25	24.6	-0.4	25.5	0.5	50.1
Leaf 26	24.7	-0.3	25.4	0.4	50.1

Table 4.2: Results of the statistic MLC position test for the m3 MLC. The data was taken on Aug 26, 2009. The gap size was 5 cm. Gantry angle was 0°. All distance are measured at 100 cm SAD.
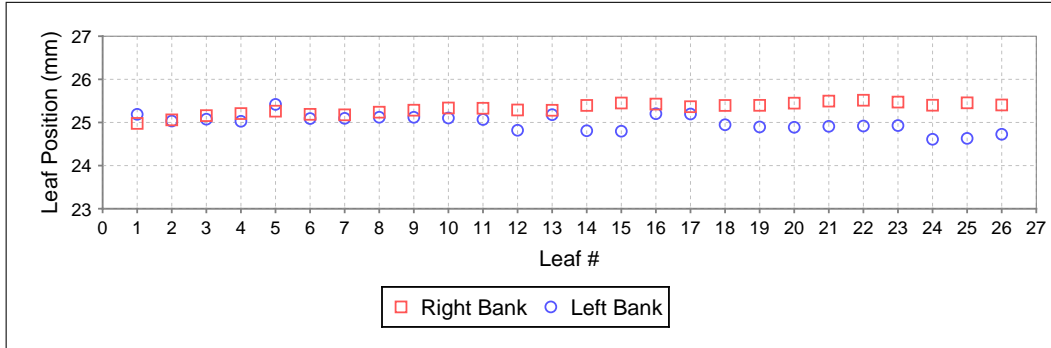
Figure 4.11: Static leaf position QA test results

routine monthly QA, there is a large amount of historical data available. All these data suggest that the average discrepancy is within the tolerance level. Occasionally, discrepancies can reach around 1 mm, but they are always well below 2 mm.

Dynamic Log files Statistical Analysis

The m3 micro MLC creates a log file after each dynamic beam delivery. This log file is called Dynalog file. The dynalog file contains information about the states of all leaves recorded at each approximately 50 ms interval throughout the beam delivery. The format of the Dynalog file is illustrated in Table 4.3. The number on the very top-left corner is the tolerance level. The unit associated with this number is MLC driving motor counts. This number defines the tolerable discrepancy between the actual leaf position and where the leaf should be. If the discrepancy goes beyond this value, a beam hold-off signal will be triggered. Starting from the next entry, the first column is called dose fraction index, which ranges from 0 to approximately 25000. The dose index reflects the dose fraction of each entry. The second column is the previous segment number. The MLC works as follows. In the DVA file (leaf sequence file), which defines the leaf movement over the delivery time, leaf position is predefined at certain points in time. These predefined points

84

A										
↓										
200										
B	C	D	E	F	G	H	I	J	K	L
↓	↓	↓	↓	↓	↓	↓	↓	↓	↓	↓
0	0	0	1	0	25	-3070	-3069	-3070	-3070	⋯
13	0	1	1	0	25	-3070	-3069	-3070	-3070	⋯
69	1	1	0	25	832	-3070	-3069	-3070	-3070	⋯
69	1	1	0	25	832	-3070	-3069	-3070	-3070	⋯
⋮										
24990	30	1	1	24167	25000	-3070	-3069	-3070	-3070	⋯

M ← (pointing to the 24990 row, representing a completed field delivery)

Key	Description
A	Plan tolerance
B	Current dose fraction. Range is from 0 (0 %) to 25000 (100 %)
C	Previous segment number
D	Beam Hold- Off state
E	Beam ON state
F	Previous segment's dose index (out of 25000)
G	Next segment's dose index (out of 25000)
H	Leaf A1 interpolated plan position
I	Leaf A1 actual position
J	Leaf A1 plan position for previous dose index
K	Leaf A1 plan position for next dose index
L	Represents the repeating data for other leaves
M	Represents a completed field delivery

Table 4.3: Dynalog file format

are called control points. The period in between two adjacent control points is called a segment, during which the leaf position is linearly interpolated. Usually, for one beam delivery, the number of segments is approximately 30. The third column is the beam hold-off state, if a beam hold-off signal is issued, the entry will record as 1 for this column. The forth column is the beam-on state. Theoretically, the beam on state and the beam hold-off state should be opposite. In reality, there is a one entry lag of the beam-on state relative to the beam hold-off state. The fifth and sixth column represents the previous and next control points' dose indices. From the next column on, the columns contain the information for each leaf. Four columns as a group are for each leaf. The first one represents where the leaf should be base on interpolated data from the control points. The second one represents where the leaf actually is. The third and the forth columns are the leaf position of previous and next control points.

Because the actual Dynalog file is too long to be presented here, only statistical results are shown. The detailed discussion of the statistical analysis of Dynalog file is continued in Section 5.1.1.

Effective Leaf Gap Test

BrainLAB refers to the effective leaf gap test as the "Measurement of dynamic leaf shift". The dynamic leaf shift describes an effective leaf shift due to the leaf end design. BrainLAB provides a standard procedure to measure the dynamic leaf shift which is essentially an ion chamber dose measurement of sliding windows with different widths. The determined dynamic leaf shift is to be entered into the beam profile file at the "Radiologic Field/Leaf shift dynamic" field of the iPlan system. The following steps are the detailed procedure provided by BrainLAB:

- Use a large detector (ionization chamber) and position it in the water phantom in such a way, that the detector axis is perpendicular to the leaf direction. Set the water sur-

face level to an SSD = 980 mm and adjust the detector at isocenter (depth = 20 mm).

- Set the jaws to form a square field of 100×100 mm^2.

- Set the dose rate of the LINAC to 300 MU/min and deliver 300 MU for each field.

- Successively irradiate the dynamic mMLC file "M3_1.d01", "M3_5.d01", . . . ,"M3_100.d01" (gap sizes: 1, 5, 10, 20, 50, 100 mm) and note the dose values.

- Close the mMLC and measure the leakage dose using the same setting as above (asymmetric gap setting; intra-leaf gap should be 50 mm off the isocenter).

- Set the mMLC to a square field of 100×100 mm^2 and measure the open field dose using the same setting as above.

- The measured dose D can approximately be describe by a linear function $D - D_{leak} = b(gap + 2\delta) = b \cdot gap + a$, where gap is the nominal gap width (1, 5, . . . , 100 mm), D_{leak} is the measured mMLC leakage and δ is the effective dynamic shift per leaf. After determination of a and b by linear regression, δ is calculated by $\delta = a/2b$.

The results of this dynamic shift measurement can be found in Section 5.1.2.

4.3.3   Ion Chamber Measurement

The ion chamber measurement is one of the most important parts of the dose verification, mostly because of its proven reliability. Film dosimetry is usually used as a relative dosimetry method; therefore a reference point is required and often measured by the ion chamber. Even if other dosimetry methods are intended to be used as absolute dosimetry methods it is always a good idea to cross check the data with ion chamber measurement, which is

of extreme importance if the reliability of these dosimetry methods are still under investigation.

The ion chamber used in this project is a NAC009 TRIAX miniature ionization chamber. The chamber and the cable are shown in Figure 4.12. The electrometer used is a Victoreen Model 530 precision electrometer. A Varian linac is used to irradiate the phantom and is referred as Unit 2 in Vancouver Cancer Center.

<div align="center">(a)   (b)</div>
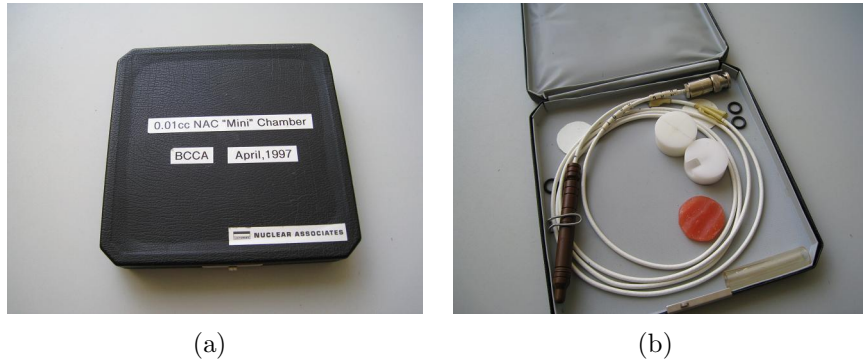
Figure 4.12: These photographs show the mini chamber used in this project.

Because the ion chamber is not calibrated for absolute dosimetry, any measurement using this ion chamber is relative. A calibration measurement is performed under a 10 cm by 10 cm field size at depth of 5 cm in solid water. In order to be more efficient and check the machine output and ambient condition variation, a consistency measurement is also performed just before any clinical dose verification using the cube phantom. Details of this procedure are described in Section 3.2.4.

Because most of the stereotactic treatment plans use a non-coplanar beam arrangement, it was also important to establish whether a significant angular dependence exists for ion chamber in the cube phantom.

A cylindrical phantom was built for this purpose. The schematic diagram of the cylindrical phantom is shown in Figure 4.13. The cylinder is 9 inch high and with a diameter of 20.8 cm. A cylindrical hole is drilled from the
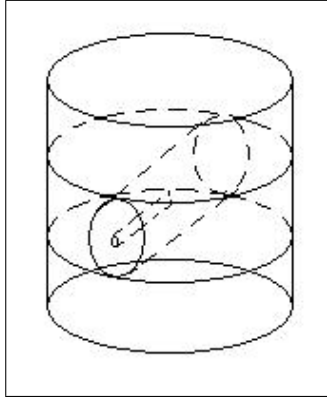
Figure 4.13: Schematic diagram of the cylindrical phantom.

center of the side so that the same insert of the cube phantom can be fitted into this cylinder, holding the ion chamber at the geometric center. The cylinder is build with acrylic resin which is the same material used to build the insert. During the experiment, the cylindrical phantom is sitting on the couch in a way that the ion chamber axis is along the couch axis. Linac gantry is rotated to 90° or 270° so that the beam is coming from the side of the phantom. By rotating the couch, the beam incident angle with respect to the ion chamber axis is changed. The convention used in defining the ion chamber angle is shown in Figure 4.14. A square field is delivered for every 15° increment. Two field sizes are used. The results are presented as the ratio of the ion chamber reading at a given angle, normalized to the reading for the perpendicular case and are shown in Table 4.4 and Table 4.5. Figure 4.15 and Figure 4.16 are graphical representations of the data in Table 4.4 and Table 4.5. In general, the ion chamber sensitivity increases when the incident direction approaches the ion chamber axis. The amplitude of variation is at most 1.5 %. The detailed relationship relative to the angle is different for the two field sizes and there is a relatively large uncertainty in the shape of the curve. The relatively large uncertainty in the angular dependence curve is likely due to gantry sag and wobble in couch rotation axis. These data are not suitable for correcting IMRT verification measurements, but do
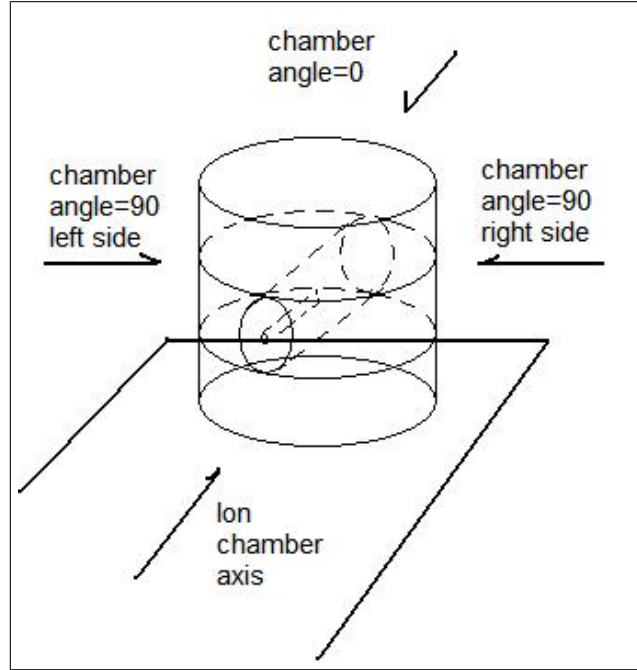
Figure 4.14: Schematic diagram showing the convention used in the definition of chamber angle

Angle	Left side rdg. (nC)	Left side ratio	Right side rdg. (nC)	Right side ratio	Average ratio
90	-0.3924	1.0000	-0.3872	1.0000	1.0000
75	-0.3937	1.0033	-0.3878	1.0015	1.0024
60	-0.3937	1.0033	-0.3890	1.0046	1.0040
45	-0.3944	1.0051	-0.3899	1.0070	1.0060
30	-0.3952	1.0071	-0.3924	1.0134	1.0103
15	-0.3940	1.0041	-0.3904	1.0083	1.0062
0	-0.3950	1.0066	-0.3964	1.0238	1.0152

Table 4.4: Ion chamber reading of a 4.2 cm by 4.2 cm square field with different incident angle relative to the ion chamber axis. 200 MU is delivered per each field.

Angle	Left side rdg. (nC)	Left side ratio	Right side rdg. (nC)	Right side ratio	Average ratio
90	-0.3164	1.0000	-0.2965	1.0000	1.0000
75	-0.3137	0.9915	-0.2974	1.0030	0.9973
60	-0.3180	1.0051	-0.2979	1.0047	1.0049
45	-0.3188	1.0076	-0.2984	1.0064	1.0070
30	-0.3198	1.0107	-0.2991	1.0088	1.0098
15	-0.3199	1.0111	-0.2995	1.0101	1.0106
0	-0.3222	1.0183	-0.3010	1.0152	1.0168

Table 4.5: Ion chamber reading of a 1.2 cm by 1.2 cm square field with different incoming direction relative to the ion chamber axis. 200 MU is delivered per each field.

establish the magnitude of the directional dependence of the ion chamber measurements. The stem irradiation theory predicts that when irradiate the ion chamber along the long axis, more volume of the ion chamber stem will be irradiated and will contribute to the collected charge. This theory supports the result that approximating the ion chamber axis yields larger readings. It is also expected that different field sizes or field shapes would yield different curves. For IMRT dose verification, field sizes do dynamically change and the cumulative dose is the average of several beams coming from different angles. So, that the expected effect should be even smaller than the 1.5 % we acquired.
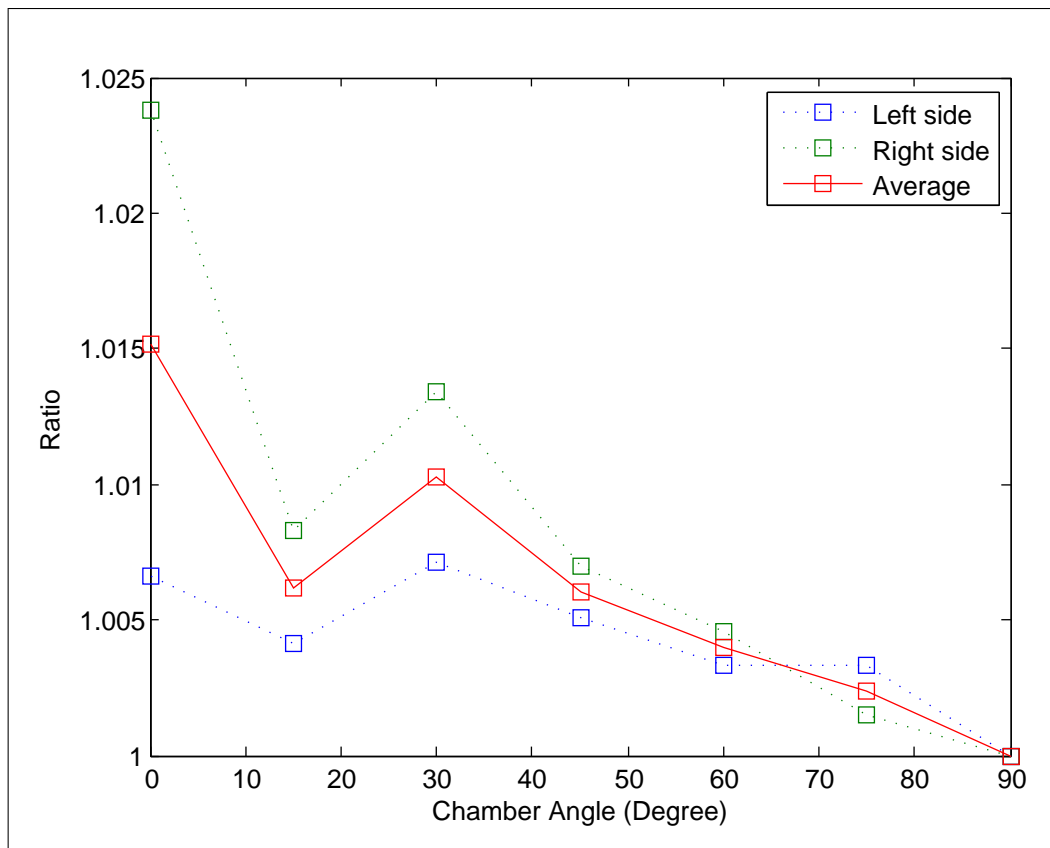
Figure 4.15: Plot of the ion chamber angular dependence (4.2 cm)
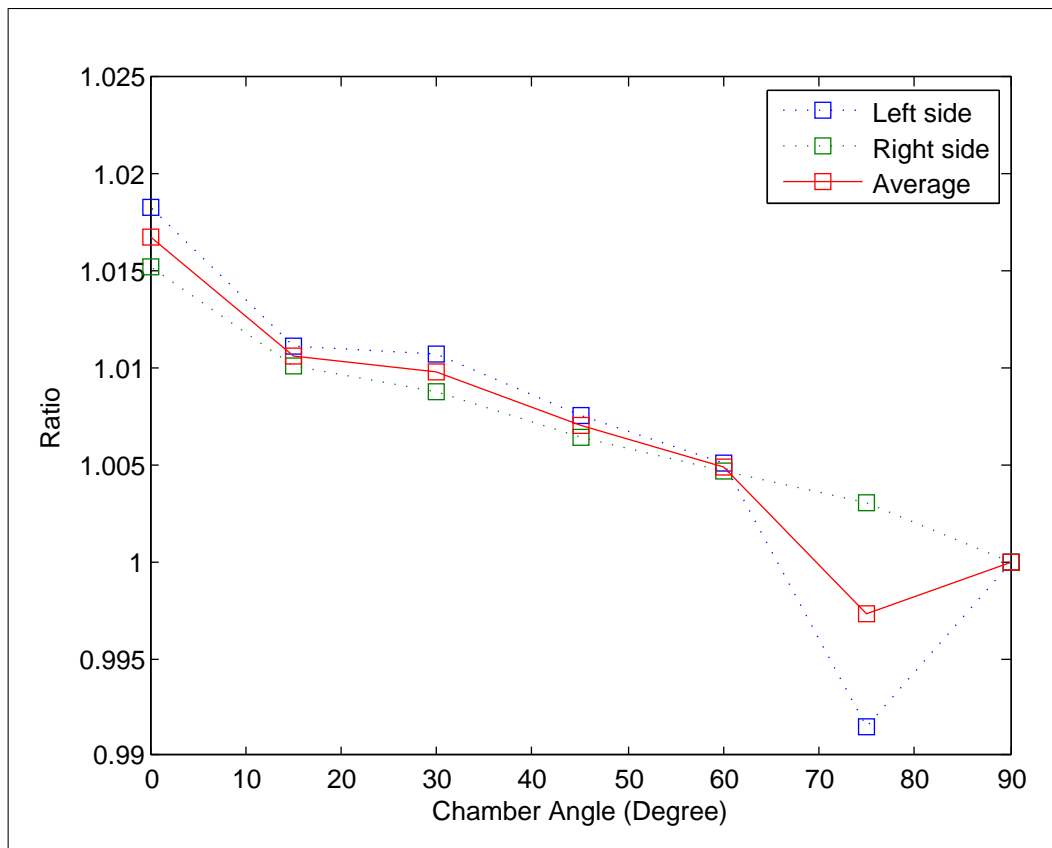
Figure 4.16: Plot of the ion chamber angular dependence (1.2 cm)

Chapter 5

Results and Discussion

This chapter contains results and discussion of the MLC performance tests, ion chamber measurements and film dosimetry measurements described in previous chapters. MLC performance tests are presented in the first section. Because these experiments assess the general performance of the most critical component of the delivery hardware, the results of these tests assist with the determination of reasonable expectations for dose verification of clinical cases. After the MLC performance tests, the results and discussion of ion chamber measurements are presented in the section 5.1.1. Ion chamber calibration is discussed first, followed by ion chamber dose verification of three clinical cases. The third section contains the dose verification data for film dosimetry for the same clinical cases.

5.1   MLC Performance Tests

5.1.1   Dynamic MLC Dynalog Statistical Analysis

As previously introduced in Section 4.3.2, the statistical analysis of the Dynalog file of one particular beam of an IMRT treatment is presented in Table 5.1 and Table 5.2 as an example.   The tolerance level for MLC leaf position is 200 motor counts. The analysis only includes those entries for which the beam state is on. Sometimes a particular leaf may have to travel a relatively long distance to reach the designated position required by the leaf sequence files. This usually happens at control points where a relatively sudden change of the leaf position may be required. Under such a condition, the leaf usually

	Max. of $|\Delta|$	Ave. of $|\Delta|$	Std. of $|\Delta|$	Num. exceeding the threshold
Leaf 01	1	1	0	0
Leaf 02	1	1	0	0
Leaf 03	1	1	0	0
Leaf 04	1	1	0	0
Leaf 05	1	1	0	0
Leaf 06	1	1	0	0
Leaf 07	1	1	0	0
Leaf 08	547	5.1176	46.8149	1
Leaf 09	592	21.2721	77.0172	4
Leaf 10	302	11.7868	42.8664	3
Leaf 11	744	31.4412	96.4892	7
Leaf 12	770	32.0735	102.0655	5
Leaf 13	795	8.0882	68.5996	1
Leaf 14	815	9.4191	71.3447	1
Leaf 15	815	9.6912	71.6380	1
Leaf 16	798	8.8750	69.5089	1
Leaf 17	753	6.6324	64.4779	1
Leaf 18	649	5.8750	55.5605	1
Leaf 19	1	1	0	0
Leaf 20	1	1	0	0
Leaf 21	1	1	0	0
Leaf 22	1	1	0	0
Leaf 23	1	1	0	0
Leaf 24	1	1	0	0
Leaf 25	1	1	0	0
Leaf 26	1	1	0	0

Table 5.1: This is the statistical analysis of the bank A Dynalog file. The data is considered only when the beam is on. The first column is the maximum discrepancy between the planned leaf position and the actual leaf position. The second column is the average of the discrepancy. The third column is the mean. The last column is the number of entries, of which the discrepancy exceeds the tolerance.

	Max. of $|\Delta|$	Ave. of $|\Delta|$	Std. of $|\Delta|$	Num. exceeding the threshold
Leaf 01	1	1	0	0
Leaf 02	1	1	0	0
Leaf 03	1	1	0	0
Leaf 04	1	1	0	0
Leaf 05	1	1	0	0
Leaf 06	1	1	0	0
Leaf 07	1	1	0	0
Leaf 08	481	4.5294	41.1597	1
Leaf 09	398	14.7868	61.5429	4
Leaf 10	124	4.1250	17.0609	0
Leaf 11	443	30.5735	86.8110	7
Leaf 12	507	31.1324	90.8176	6
Leaf 13	254	2.8603	21.6946	1
Leaf 14	252	2.8456	21.5231	1
Leaf 15	252	2.8456	21.5231	1
Leaf 16	277	3.0294	23.6668	1
Leaf 17	329	3.4118	28.1258	1
Leaf 18	375	3.7500	32.0702	1
Leaf 19	1	1	0	0
Leaf 20	1	1	0	0
Leaf 21	1	1	0	0
Leaf 22	1	1	0	0
Leaf 23	1	1	0	0
Leaf 24	1	1	0	0
Leaf 25	1	1	0	0
Leaf 26	1	1	0	0

Table 5.2: This is the statistical analysis of the bank B Dynalog file of the same field as in Table 5.1.

needs more than 50 ms to reach the designated point and thus triggers a series of beam-hold off signal. Because the beam is off during such hold-off the discrepancy during that period does not have any clinical significance. Note that the first entry of these beam hold-off series is recorded, because of the lag time between beam hold-off and beam off state.

As mentioned in the paragraph above, a discrepancy that is large enough to trigger a beam hold-off is in most cases triggered at the control points. The number of the beam hold-off series triggered for each leaf is listed in the last column of each table. In this column the number for each leaf is under 10 and the sum of them is up to approximately 30. Noticeably the average discrepancy listed in the second column is well under 200 motor counts.

The nominal dose rate is 300 MU/min which corresponds to 5 MU/s. So for each entry, which corresponds to approximately 50 ms, approximately 0.25 MU is given. This is the estimated MU leakage due to the lag in beam response, as one entry is the lag time. Considering the number of beam hold-off series triggered may be up to 30, the upper limit of the MU leakage during a single beam is estimated to be 7.5 MU. The total MU given in a single beam is approximately 200 MU, the worst estimated discrepancy caused by this lag is 3.75 %. In practice, it is observed that when the beam hold-off is removed, there is still a one entry lag before the beam is turned on. So this effect is largely cancelled. The 3.75 % is therefore an upper limit.

5.1.2   Effective Leaf Gap Tests

Table 5.3 summarizes the results of the effective leaf gap test. The manufacturer provides a calculation sheet to calculate the dynamic leaf shift parameter which is then input into the planning system. The number obtained for this measurement is 0.29 mm, which is the same as the number acquired during the acceptance and obviously the zero difference is within the tolerance of 0.01 mm[6]. This indicates the effective leaf gap parameter is stable and accurate.

Doserate (MU/min)		300
Total Dose		300
Field width (cm)		10
Leaf speed (cm/min)		20
MLC Leakage		0.019367
MLC file	Gap size (mm)	Measured ionization signal (nC)
M3_1.D01	1	1.5598
M3_5.D01	5	2.692
M3_10.D01	10	4.121
M3_20.D01	20	6.953
M3_50.D01	50	15.448
M3_100.D01	100	29.61
Static Field	Square Size	Measured ionization signal (nC)
Open Field	100x100	57.76
Closed Field (Leakage)	0x0	1.1186
Dynamic leaf shift (mm)	0.29	

Table 5.3: Dynamic leaf shift measurements

5.2   Ion Chamber Measurement

5.2.1   Calibration

In order to establish absolute dose for validation of treatment plans, cross calibration of the ion chamber in the phantom used to validate the TPS calculation is performed by delivery of a known dose to the phantom. The ion chamber reading per unit dose is then established. The reference dose condition at VCC is that under a 10 cm by 10 cm field at SAD 100 cm, if 1 MU is delivered 1 cGy dose will be given at d_{max} in water. For the cross calibration, solid water is used and 200 MU is delivered. The ion chamber is set up at depth of 5 cm. (Detailed information is listed in Table 5.4.)   Using

Phantom	Solid water
SAD	100 cm
Depth	5 cm
Field size	10 cm $\times$ 10 cm
Millennium MLC	Retracted
m3 MLC opening	Off
Linac energy	6 MV
Dose rate	300 MU/min
Monitor unit	200MU
Ave. elec. rdg.	-0.5723 nC

Table 5.4: Ion chamber cross calibration data measured in solid water phantom (Sept. 15 2009)

the TMR data for depth of 5 cm, the dose given to the solid water phantom at the isocenter can be calculated in following way.

$$
\begin{aligned}
Dose \quad &= \quad MU \times TMR(depth = 5, 10 \times 10) & (5.1) \\
&= \quad 200 \times 0.915 & (5.2) \\
&= \quad 183(cGy) & (5.3)
\end{aligned}
$$

Phantom	Cube phantom
SAD	100 cm
Depth	~9.2 cm
Field size	4.2 cm × 4.2 cm
Millennium MLC	Retracted
m3 MLC opening	4.2 cm × 4.2 cm
Linac energy	6 MV
Dose rate	300 MU/min
Monitor unit	200MU
Ave. elec. rdg.	-0.4310 nC

Table 5.5: Ion chamber cross calibration data measured in cube phantom (Sept. 15 2009)

Since the electrometer reading acquired is -0.5723 nC, the dose to electrometer reading relationship for this ion chamber is determined.

$$Dose/E.Rdg. = 183cGy/(-0.5723nC) = -319.8cGy/nC \qquad (5.4)$$

This dose to electrometer reading ratio is essentially based on the assumption that the dose delivered at the reference condition is accurate. However, the linac output does vary about 1 % on a daily basis. Therefore, we cannot guarantee that this dose to electrometer reading ratio is correct in terms of absolute dosimetry.

During the calibration, the same field (Detailed information of the beam setup is listed in Table 5.5.) is also delivered to the cube phantom. The electrometer reading acquired is -0.4310 nC. Using the dose to electrometer reading ratio acquired above, the dose at the isocenter of the cube phantom can be calculated.

$$
\begin{aligned}
Dose &= -319.8cGy/nC \times -0.4310nC & (5.5) \\
&= 137.8cGy & (5.6)
\end{aligned}
$$

Therefore the monitor unit to dose ratio for the cube phantom under this

field setup condition is,

$$MU/dose = 200MU/137.8cGy = 1.451MU/cGy \qquad (5.7)$$

Compared to the TPS calculated result that by delivering 145 MU, 100 cGy will be given to the isocenter, this measurement agrees with the prediction within 0.1 %. This monitor unit to dose relationship holds when the linac output is stable. Since the linac output drifts on a daily basis, the MU to dose ratio changes accordingly. A consistency verification is performed prior to the dose measurement for clinical cases, during which this MU to dose ratio may change. However, the purpose of the dose verification of these clinical cases is to compare the measured dose (under the commissioned delivery condition) with the TPS predicted value. Machine output drift should thus be excluded. For this purpose, the monitor unit to dose ratio is fixed at the value we measured during the cross calibration as 1.451 MU/cGy.

5.2.2   Verification of IMRT Cases

Ion chamber dose verification of three clinical IMRT cases is described in this subsection. The detailed information is listed for Case One only and for the other two cases only the final results are shown. A cube phantom is used for the measurements of clinical cases as well as the dose calibration, and dose calibration of the ion chamber is performed as described in previous paragraphs. In order to test the machine output consistency a square field is delivered to the cube phantom.

Case One

The first case is based on a previously treated right sided meningioma. The original treatment is a seven beam stereotactic technique. For the purpose of this study, the case was replanned using stereotactic IMRT technique retaining the original seven beam angle arrangement. The treatment plan

was optimized by the iPlan treatment planning software. In the original plan, a dose of 1.60 cGy per fraction was prescribed and optimized to the isocenter. In order to be consistent with the film dosimetry measurement, twice the dose was delivered for dose validation. In other words, 3.20 Gy was delivered to the phantom. Detailed beam parameters for Case One are listed in Table 5.6. From the result of the previous subsection, the MU

Phantom	Cube phantom
SAD	100 cm
MLC name	BrainLAB m3
Linac energy	6 mV
Dose rate	300 MU/min
Leaf sequencing	Dynamic
TaG optimization	on
Isocenter dose	3.20 Gy
x1	20.0 mm
x2	20.0 mm
y1	28.0 mm
y2	29.0 mm

Name	Table angle	Gantry angle	Coll. angle	Depth equiv. (mm)	Dose to isoc. (cGy)	MU	Ave. elec. rdg. (nC)
Beam 1	90	20	90	91.8	1	34	-0.0021
Beam 2	90	100	90	88.1	66	190	-0.1921
Beam 3	90	130	90	111.0	54	142	-0.1624
Beam 4	55	60	90	120.9	57	166	-0.1678
Beam 5	55	95	90	106.0	45	156	-0.1381
Beam 6	330	275	90	98.6	38	156	-0.1155
Beam 7	305	250	90	112.0	60	204	-0.1687
Total					320	1048	-0.9467

Table 5.6: Ion chamber measurement of stereotactic IMRT plan (Case One)

to dose relationship is measured as 1.451 MU/cGy and is assumed to be fixed. During the consistency test on the same day of verifying Case One,

the electrometer reading acquired is -0.3101 nC. Also, because 145 MU is delivered, the dose given to the isocenter of cube phantom is,

$$Dose = 145MU \div 1.451MU/cGy = 99.93cGy \qquad (5.8)$$

Therefore the dose to electrometer reading relationship for this day is,

$$Dose/E.Rdg. = 99.93cGy/-0.3101nC = -322.3cGy/nC \qquad (5.9)$$

Comparing to the value acquired during calibration, which is -319.8cGy/nC, the difference is 0.78 %. This discrepancy includes machine output variation and is within the tolerance.

The total acumulated eletrometer reading for this stereotactic IMRT treatment plan is -0.9467 nC, the total dose delivered to the isocenter is,

$$Dose = -322.3cGy/nC \times -0.9467nC = 305.1cGy \qquad (5.10)$$

The TPS calculation results showed that the dose delivered to the isocenter should be 311 cGy. So, the discrepancy is -1.9 % for this case. For individual fields, the calculated and measured dose is listed in Table 5.7. Chamber angle is also calculated and listed as the last column of this table. The chamber angle is defined as the acute angle between the incident beam axis and the ion chamber axis. The chamber angle effect is discussed in 4.3.3.

Although a mini ion chamber was used for the dose measurement, the averaging effect over a finite volume could contribute to the discrepancies. To illustrate how significant the averaging effect could be, profiles along three perpendicular directions of Case One are plotted in Figure 5.1, Figure 5.2 and Figure 5.3. Off all the figures the blue vertical line indicates where the ion chamber measurement is. The profiles indicate that for two directions, there is no significant dose gradient. For the other direction, dose gradient is noticeable. Considering the fact that the stereotactic IMRT is supposed

Beam ID	C. Dose (cGy)	M. Dose (cGy)	Differenc. (%)	Chamber Angle (°)
Beam 1	1	0.6	-32.3	70.0
Beam 2	62	61.9	-0.1	10.0
Beam 3	53	52.3	-1.2	40.0
Beam 4	55	54.0	-1.7	44.8
Beam 5	44	44.5	1.2	35.3
Beam 6	37	37.2	0.6	60.1
Beam 7	59	54.3	-7.8	39.7

Table 5.7: Dose comparison for individual fields (Case One)

to be used in situations that the target volume has a irregular shape, the presence of dose gradients around the isocenter is to be expected.

Case Two

The second case is based on a previously treated right trigeminal schwannoma. This patient was originally treated with an eight beam stereotactic treatment. For the purpose of this study, the case was re-planned using stereotactic IMRT technique retaining the original beam angle arrangement. Similar to the first case, twice the dose is delivered in order to be consistent with film dosimetry measurement. 3.21 Gy is delivered to the isocenter. The consistency test indicated that the variation in dose due to ambient conditions is 0.41 %, which is within the tolerance level. The cumulative dose measured is 318.2 cGy, compared with the TPS calculated result of 321 cGy, the discrepancy is -0.9 %. The comparison for individual fields is listed in Table 5.8.

Case Three

The third case is based on a previously treated pituitary adenoma. The patient was previously treated with a seven beam stereotactic treatment. The case was re-planned using stereotactic IMRT technique and retaining the
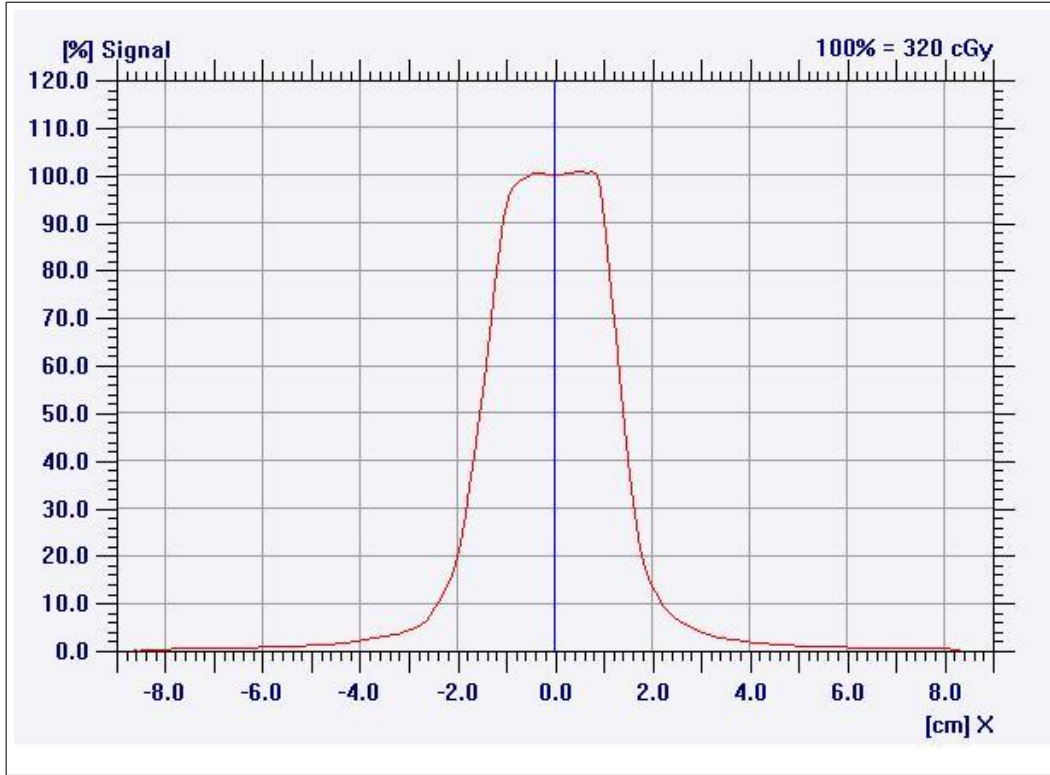
Figure 5.1: Dose profile in L-R direction of Case One

Name	Table angle	Gantry angle	Coll. angle	Depth equiv. (mm)	Dose to isoc. (cGy)	MU	Ave. elec. rdg. (nC)
Beam 1	47	50	90	132.3	46	174	-0.1614
Beam 2	47	84	90	118.3	23	140	-0.0590
Beam 3	47	117	90	130.9	10	124	-0.0365
Beam 4	350	222	90	138.2	72	158	-0.2214
Beam 5	350	305	90	105.6	21	144	-0.0696
Beam 6	310	240	90	129.9	78	174	-0.2373
Beam 7	310	310	90	133.5	12	160	-0.0415
Beam 8	300	275	90	97.4	66	154	-0.1644
Total					321	1228	-0.9911

Table 5.8: Ion chamber measurement of stereotactic IMRT plan (Case Two)
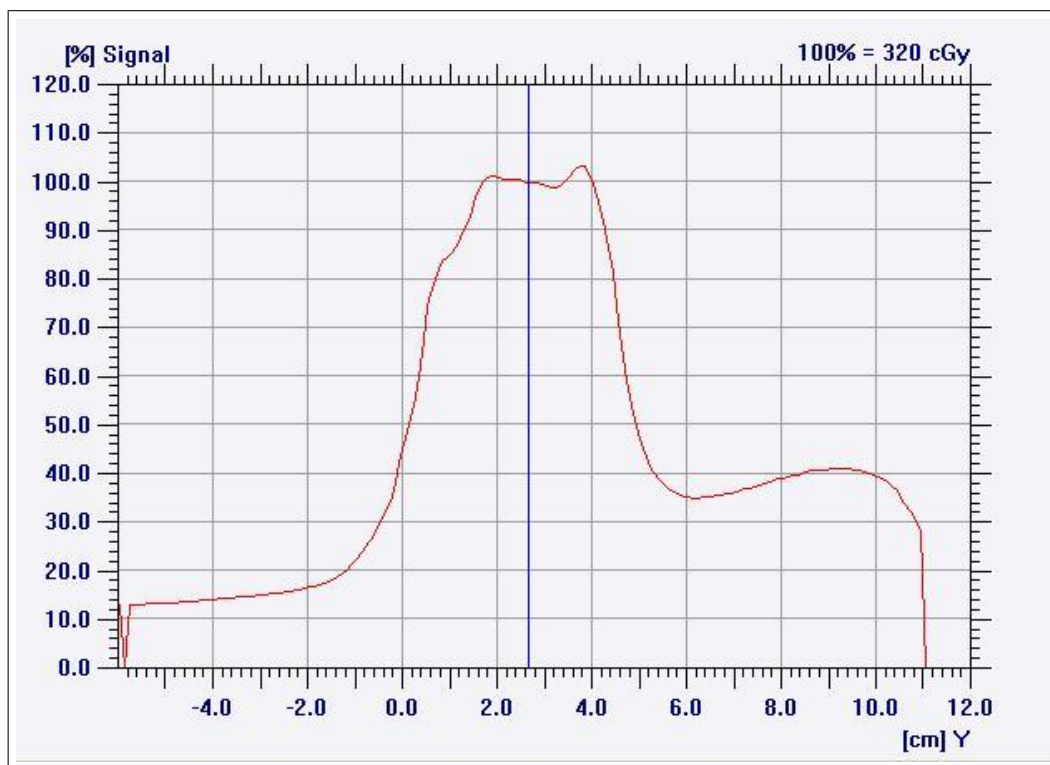
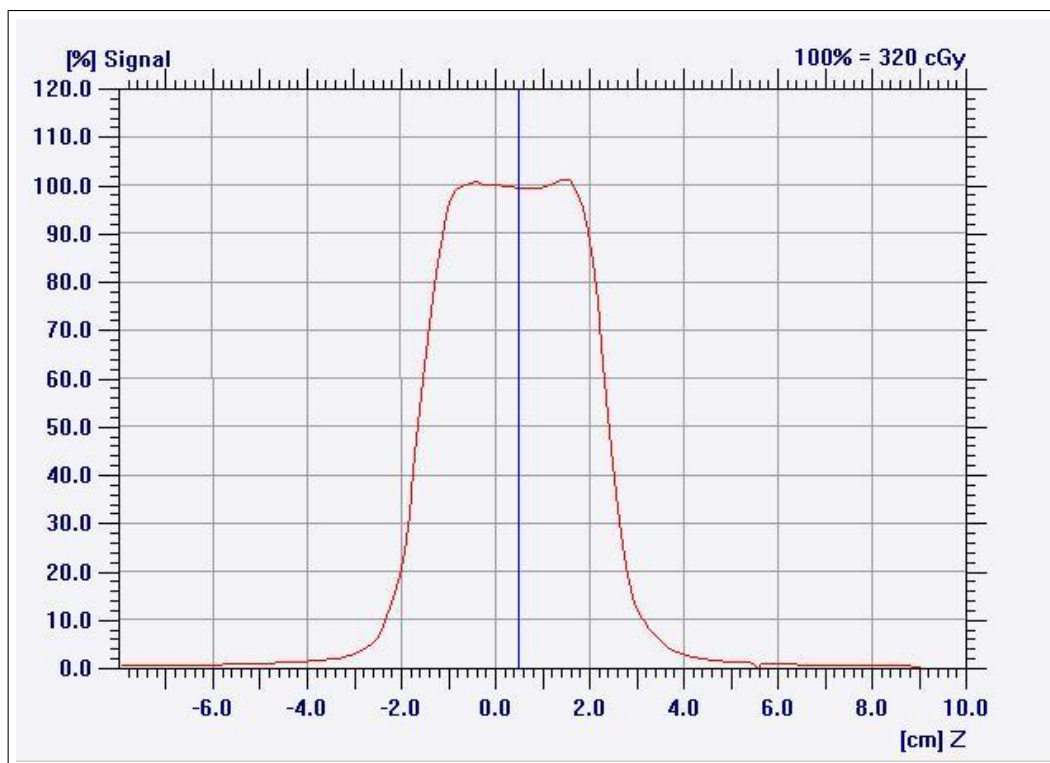Figure 5.2: Dose profile in F-H direction of Case One

Figure 5.3: Dose profile in A-P direction of Case One

same beam angle arrangement. 1.66 Gy is prescribed to the isocenter per fraction. During the consistency test, the variation in dose rate due to ambient conditions is measured to be 0.66 %, which is within the 1 % tolerance level. The cumulative dose measured is 167.0 cGy, compared with the TPS calculated result of 166 cGy, the discrepancy is 0.6 %. The comparison for individual fields can be found in Table 5.9.

Name	Table angle	Gantry angle	Coll. angle	Depth equiv. (mm)	Dose to isoc. (cGy)	MU	Ave. elec. rdg. (nC)
Beam 1	60	85	90	99.4	25	64	-0.0776
Beam 2	45	120	90	137.7	21	70	-0.0641
Beam 3	10	75	90	92.6	26	61	-0.0798
Beam 4	350	290	90	93.6	25	64	-0.0785
Beam 5	270	330	90	100.4	25	57	-0.0777
Beam 6	310	240	90	129.9	22	62	-0.0688
Beam 7	310	320	90	112.4	24	58	-0.0722
Total					166	436	-0.5187

Table 5.9: Ion chamber measurement of stereotactic IMRT plan (Case Three)

For the three cases measured, the ion chamber measurement and the TPS calculation of the total dose to the isocenter agreed within 1.9 %, which is within standard clinical tolerance. However, the discrepancy for individual fields can be quite large. The reasons for this are as yet undetermined. Angular dependence of the ion chamber has been ruled out (See Subsection 4.3.3). Noticeably, the third case has significantly smaller discrepancy for individual fields compared with the second case. The distinguishing property of the third case is that the shape of the treated volume is close to a sphere and relatively regular. In Case Three, the individual fields are not heavily modulated and the dose from each field is similar. This may be an indication that the larger discrepancy for the individual fields in Case Two is related to a high degree of intensity modulation, which leads to a relatively high dose gradient for individual fields in the vicinity of the measurement point. A

slight shift of the chamber position could result a fairly large dose discrepancy on a field-by-field basis. However, the net effect could be quite small, when the dose from all fields is taken together[33–35].

5.3   Film Dosimetry

All films were calibrated and analyzed using the techniques described in Section 3.2.4. A film calibration was done for each case. The order of the cases is the same as in the ion chamber measurement.

5.3.1   Case One

Figure 5.4 shows the TPS calculated dose distribution for this case, with which the measured dose distribution is to be compared with. For this case the calculated dose to the isocenter is 320 cGy. Figure 5.5 shows the isodose line comparison between the two datasets. In general, the isodose lines show good agreement except for the 100 % isodose line. The measured film dose in the center region is systematically lower than the TPS calculated dose. This is clearly seen in Figure 5.6 which shows the profile comparison along the y-direction. Only the central area shows a noticeable discrepancy which is roughly 5 %. Figure 5.7 shows the 2D dose difference map. A cold spot is found in the central area, while some hot spots are found in high dose gradient areas. It is noted that the ion chamber measurement in the central area reported -1.9 % lower dose than the TPS calculated result. Figure 5.8 shows the results of 2D Gamma test for this case. The 2D Gamma test[36] is a frequently used test incorporating both the distance to agreement and dose difference between two dose distributions. Thus the 2D Gamma test works well in both high dose gradient regions and low dose gradient regions[36].
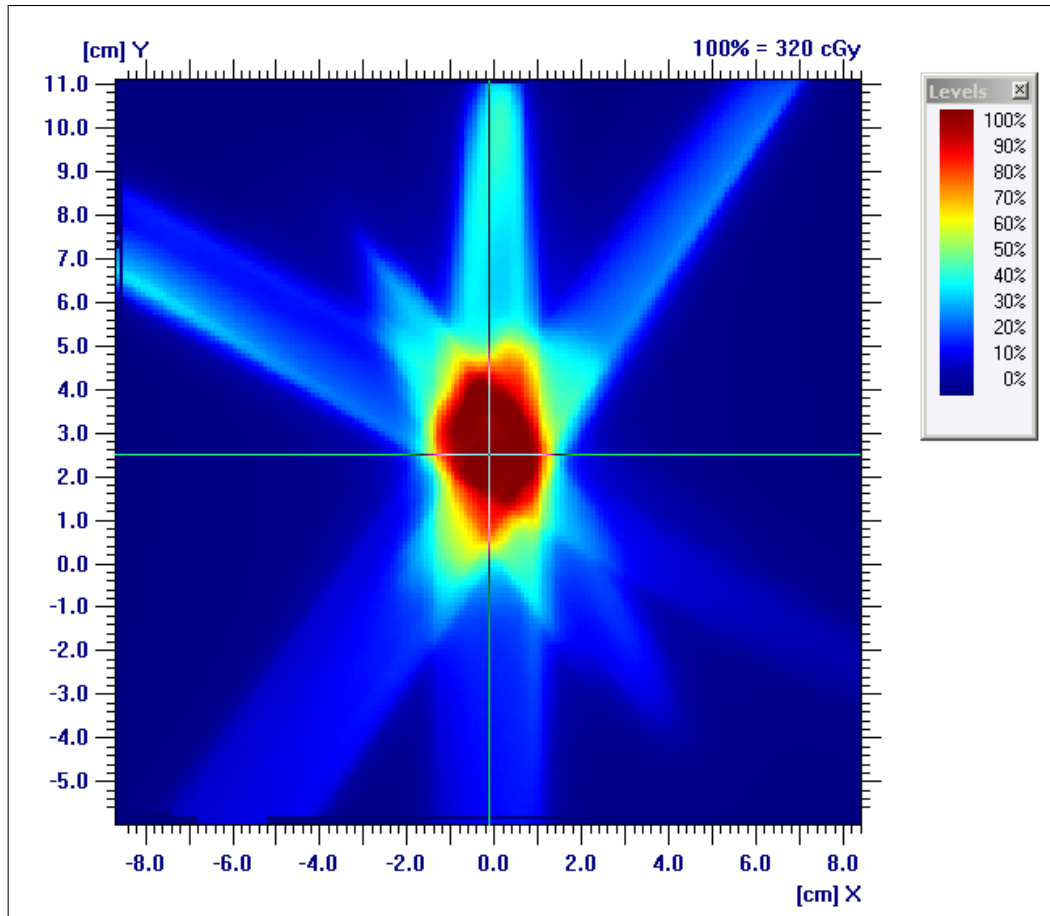
Figure 5.4: The calculated dose distribution of Case One (Coronal plane)
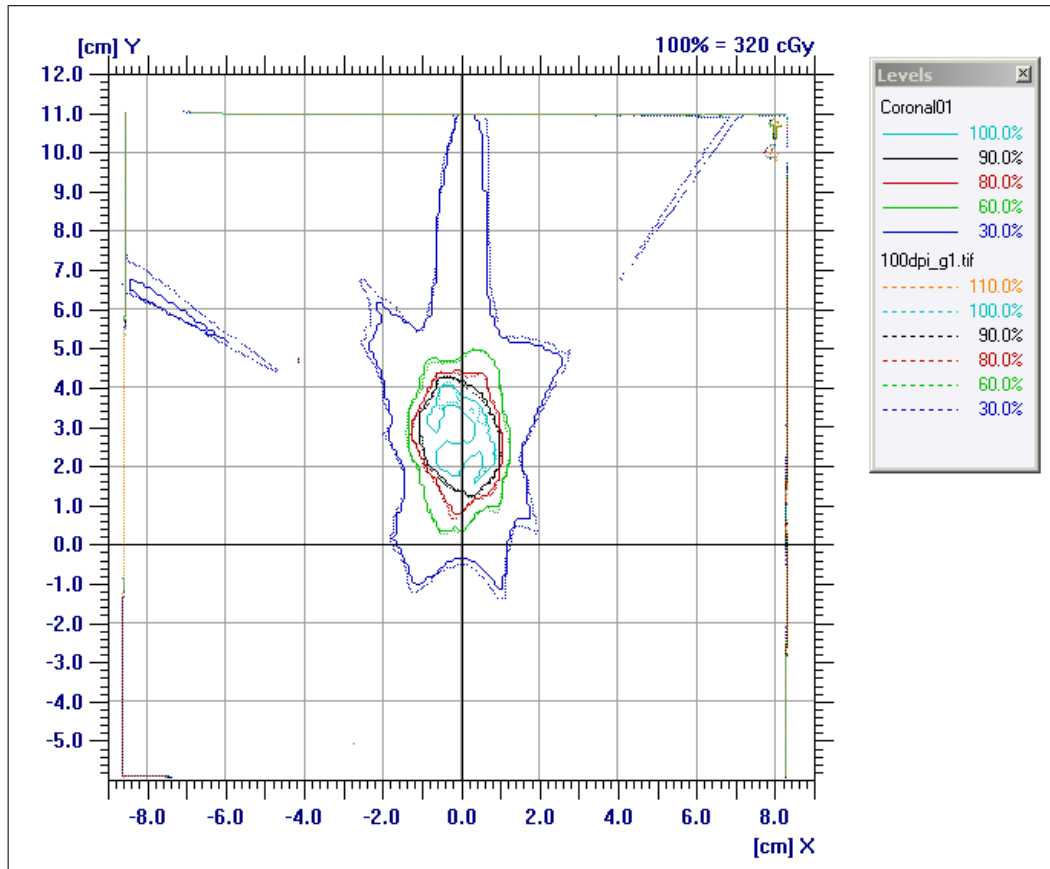
Figure 5.5: The isodose line comparison of Case One. The solid lines are for the TPS calculation. The dash lines are for the film measurement. (Coronal plane)
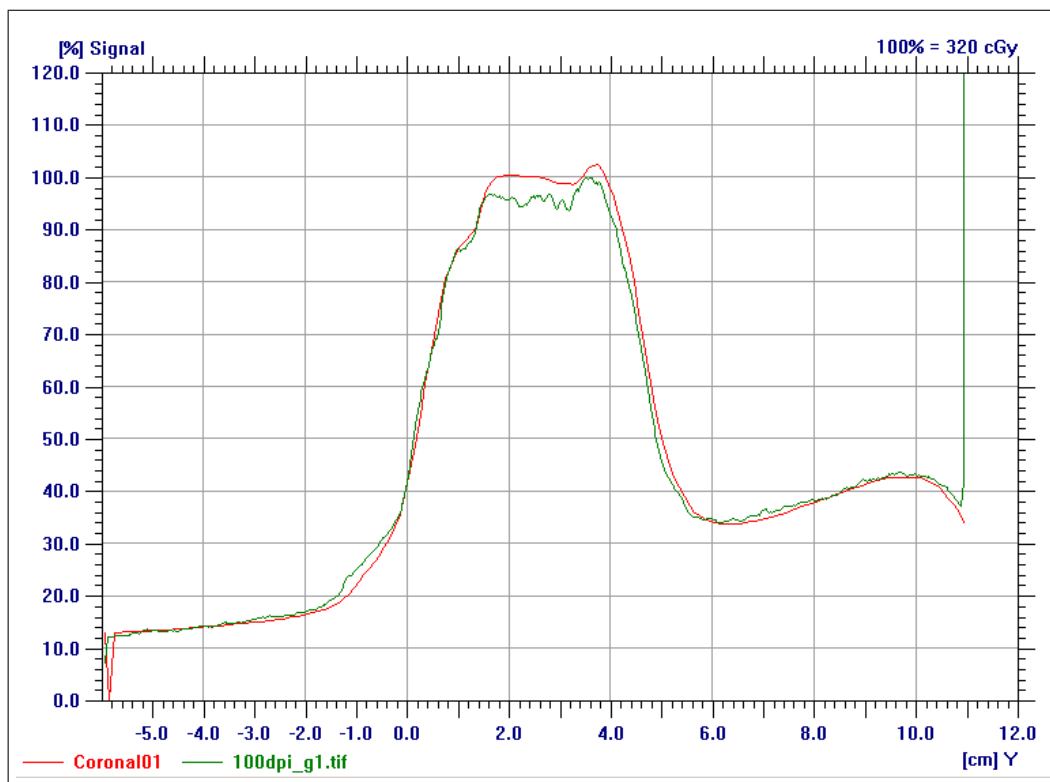
Figure 5.6: The y-profile comparison of Case One. The red line is for the TPS calculation. The green line is for the film measurement. (Coronal plane)
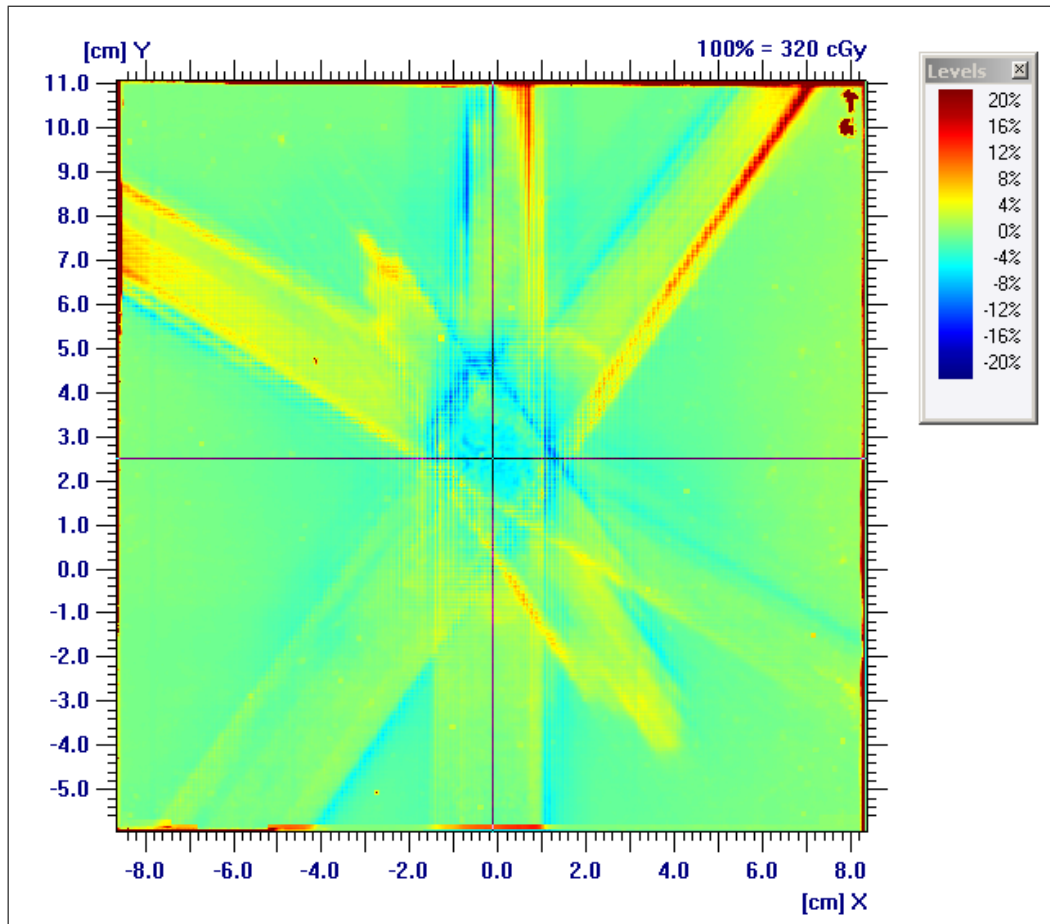
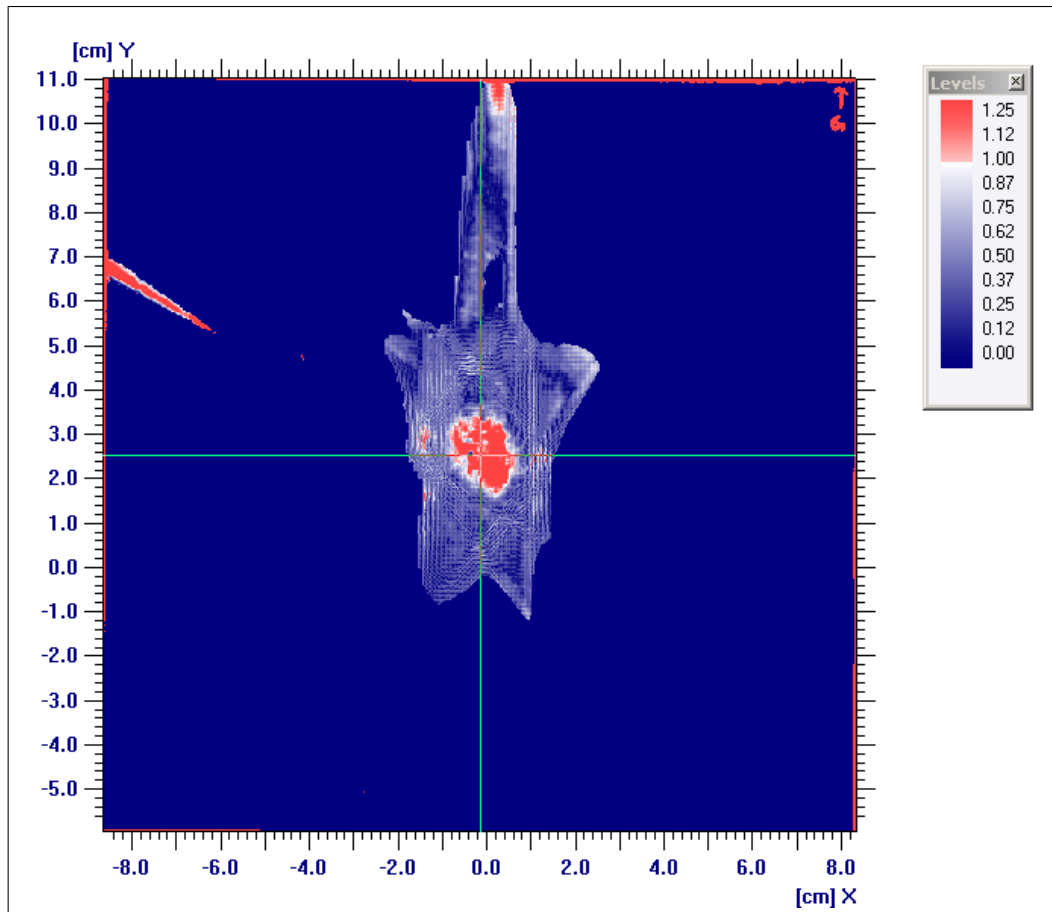Figure 5.7: The 2D dose difference map of Case One (Coronal plane)

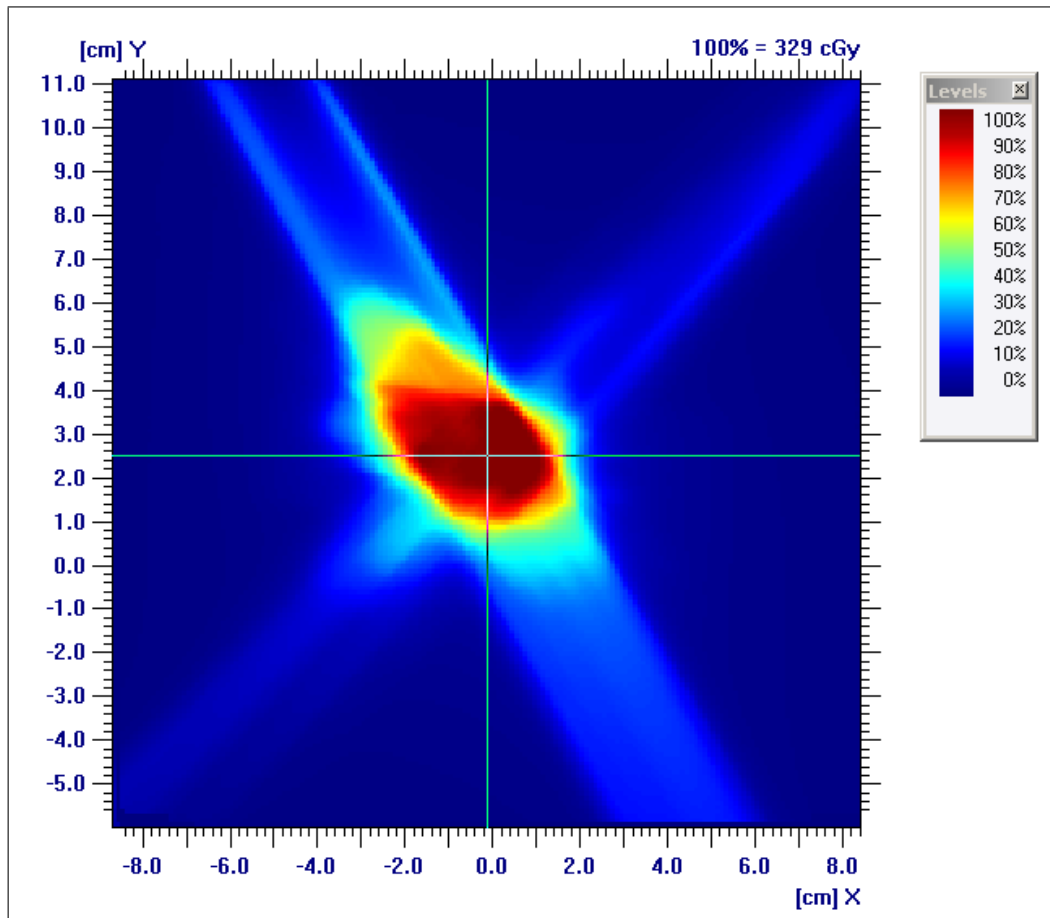Figure 5.8: The 2D Gamma test with 3 mm and 3 % criteria of Case One (Coronal plane)

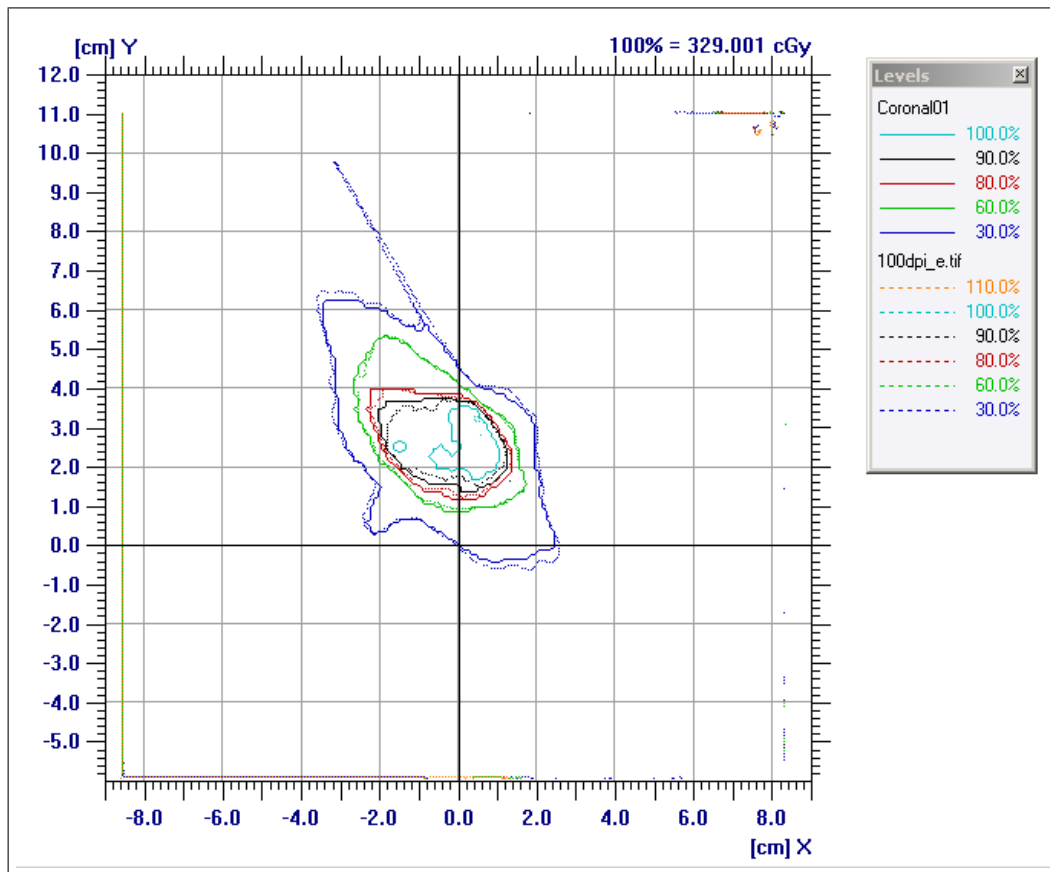Figure 5.9: The calculated dose distribution of Case Two (Coronal plane)

Figure 5.10: The isodose line comparison of Case Two. The solid lines are for the TPS calculation. The dash lines are for the film measurement. (Coronal plane)
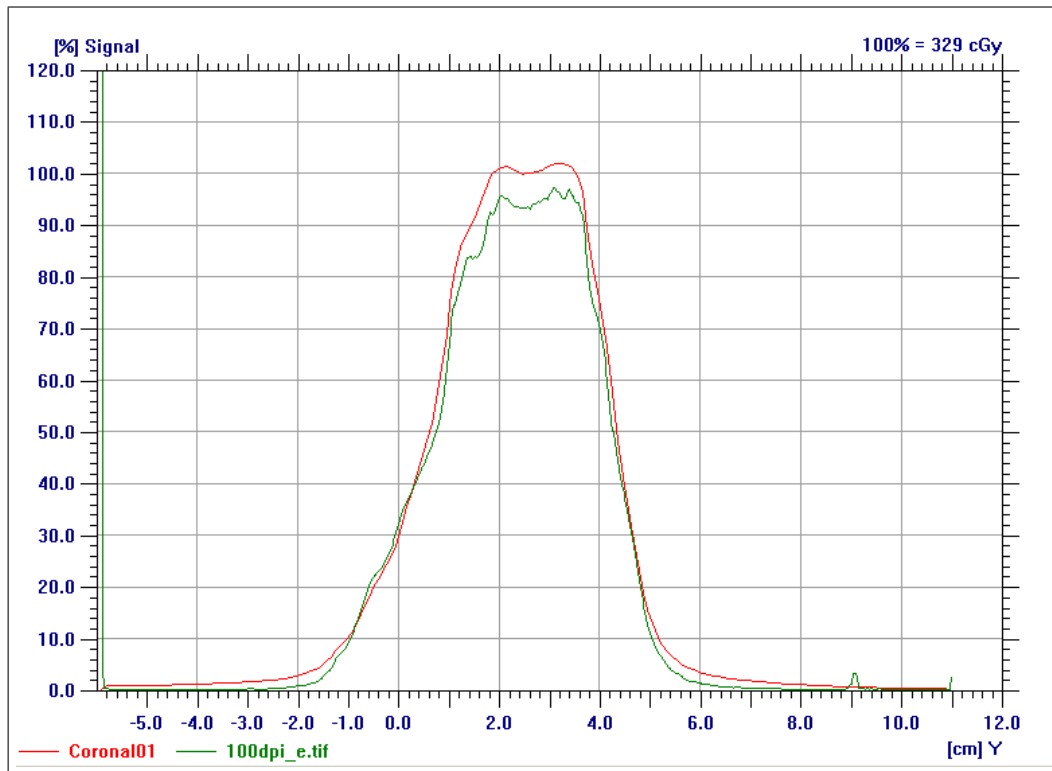
Figure 5.11: The y-profile comparison of Case Two. The red line is for the TPS calculation. The green line is for the film measurement. (Coronal plane)
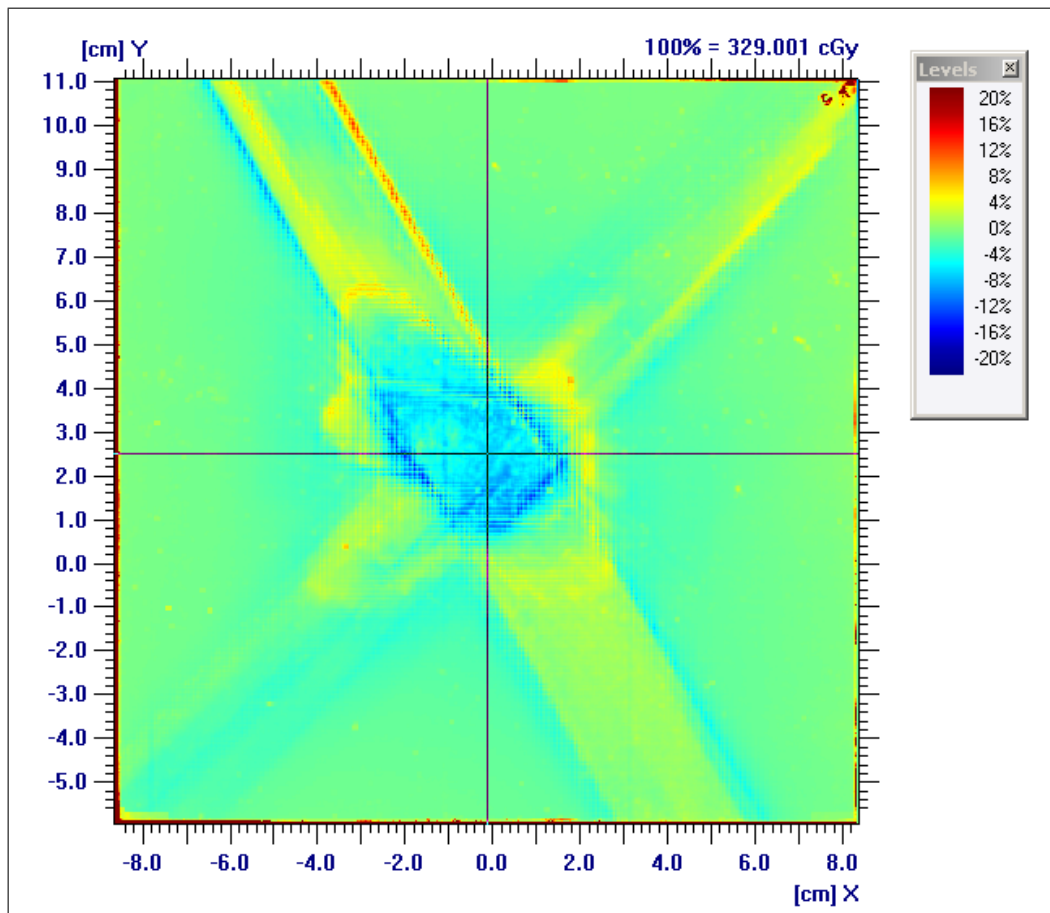
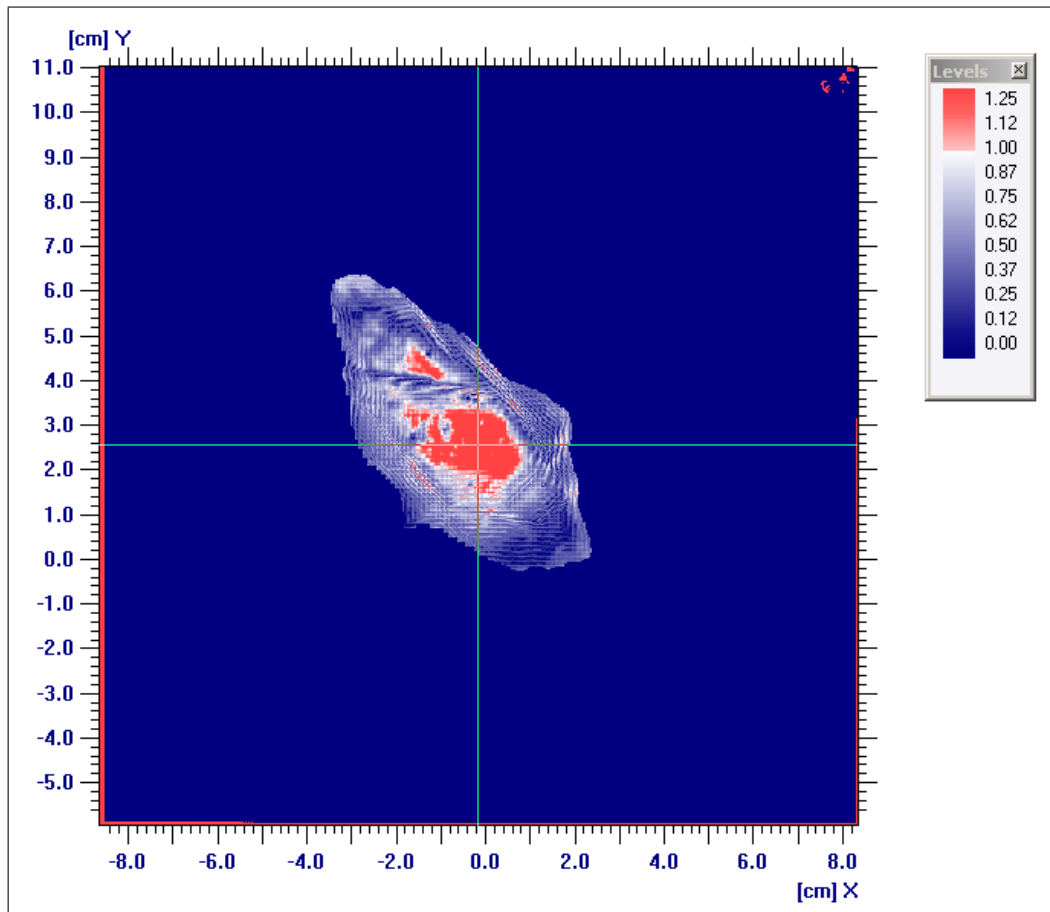Figure 5.12: The 2D dose difference map of Case Two (Coronal plan)

Figure 5.13: The 2D Gamma test with 3 mm and 3 % criteria of Case Two (Coronal plane)

5.3.2 Case Two

Figure 5.9 shows the calculated dose distribution for Case Two. The TPS calculated dose to the isocenter is 329 cGy. Figure 5.10 shows the comparison between isodose lines from the TPS and film measurement. Figure 5.11 is the profile comparison along the y-direction. Figure 5.12 is the 2D dose difference map. The discrepancy found in the region near the isocenter is about 6 % lower as measured by film, compared with the TPS calculated result. For comparison the ion chamber measurement was -0.9 % lower than TPS in this region. Figure 5.13 shows the 2D Gamma test of this case.

5.3.3 Case Three

Figure 5.14 shows the calculated dose distribution for Case Three. The calculated dose to the isocenter is 168 cGy. Figure 5.15 is the isodose line comparison. Figure 5.16 is the profile comparison along the y-direction. Figure 5.17 is the 2D dose difference map. The discrepancy found in the isocenter dose is about 3 % lower compared with TPS. In comparison, the dose measured with ion chamber was 0.6 % higher than the TPS calculation. Figure 5.18 shows the 2D Gamma test of this case.

In general, the film dosimetry results for the three cases show the same trend. The measured doses for the central region are all systematically lower than the calculated doses. The discrepancy is up to approximately 6 to 8 %, which is significant and beyond our expectation based on ion chamber results. This discrepancy is significantly larger than the uncertainty that had been ascribed to the film thickness variation described in Chapter 3, Section 3.3.4, which is expected to be approximately 2.5 %. The same phantom was used to verify the dose distribution for the static square field. Also the same procedure was used to scan the film and calibrate the film. Thus, theoretically, the additional discrepancy is not caused by either the phantom or the handling procedure. There is a concern that this additional discrepancy is
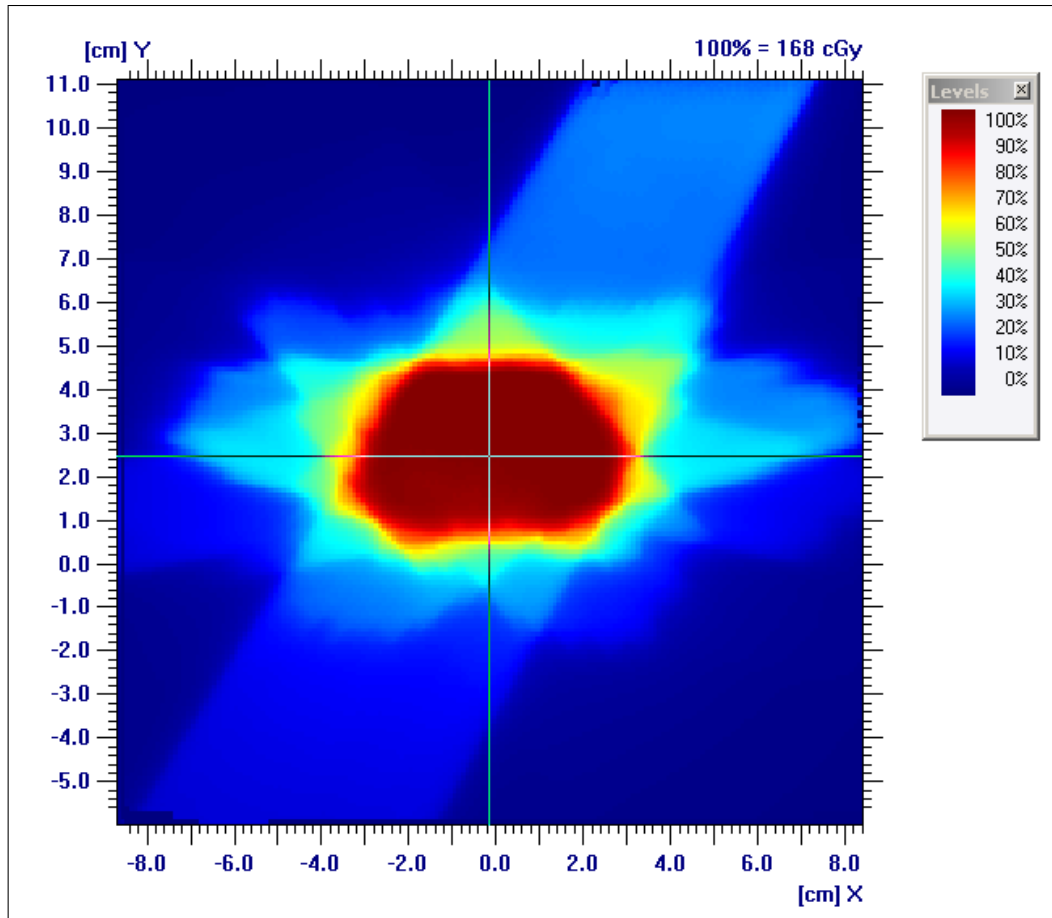
Figure 5.14: The calculated dose distribution of Case Three (Coronal plan)
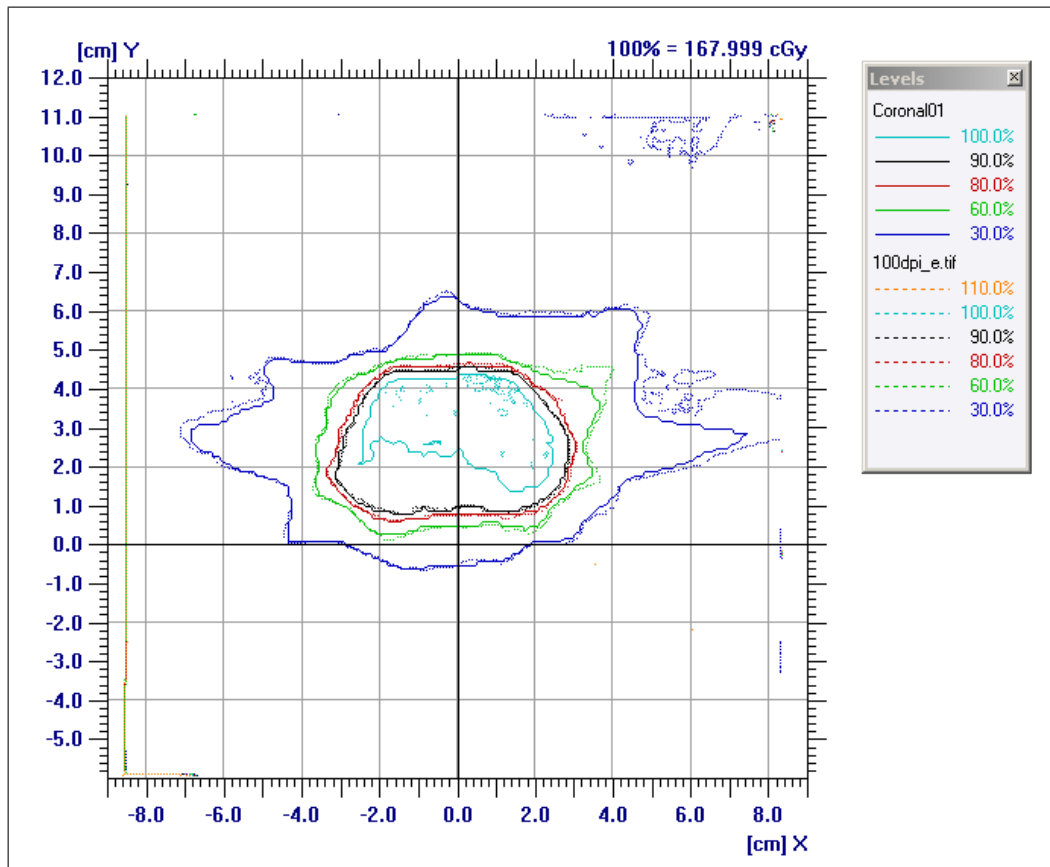
Figure 5.15: The isodose line comparison of Case Three. The solid lines are for the TPS calculation. The dash lines are for the film measurement. (Coronal plane)

Figure 5.16: The y-profile comparison of Case Three. The red line is for the TPS calculation. The green line is for the film measurement. (Coronal plane)

Figure 5.17: The 2D dose difference map of Case Three (Coronal plan)

Figure 5.18: The 2D GAMMA test with 3 mm and 3 % criteria of Case Three (Coronal plane)

due to the uncertainty of film positioning, however, in terms of the three dimensional dose distribution, the accumulated dose is fairly smooth around the isocenter, because the isocenter is within the PTV and the shape of the PTV is not highly irregular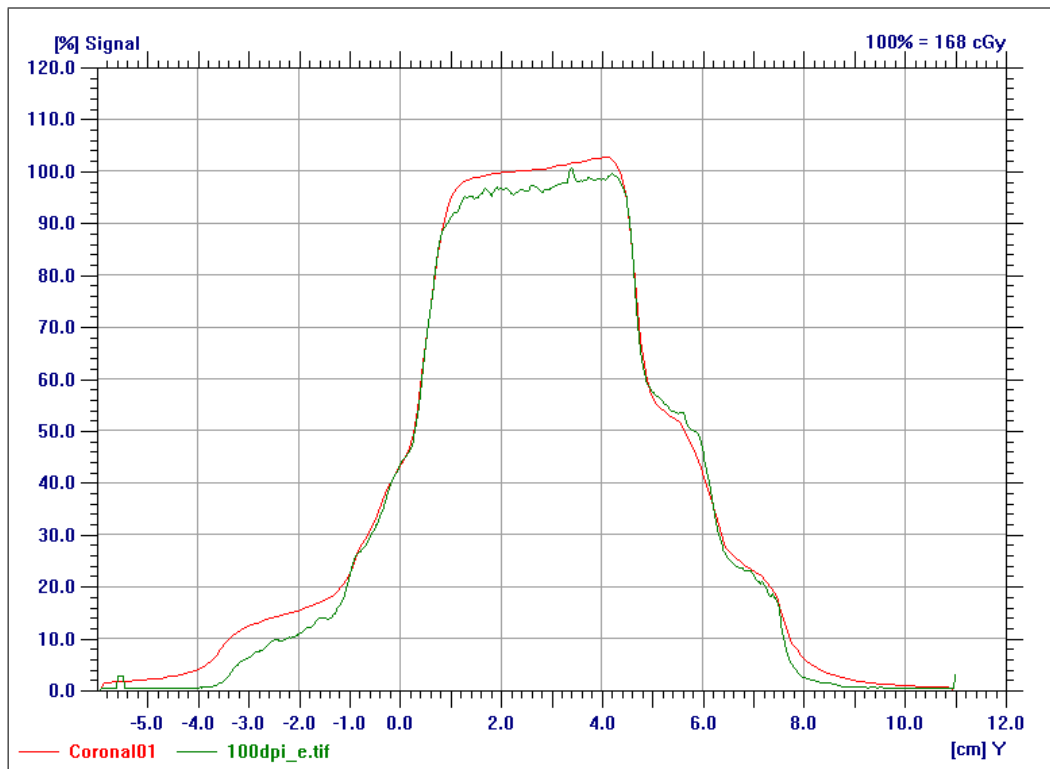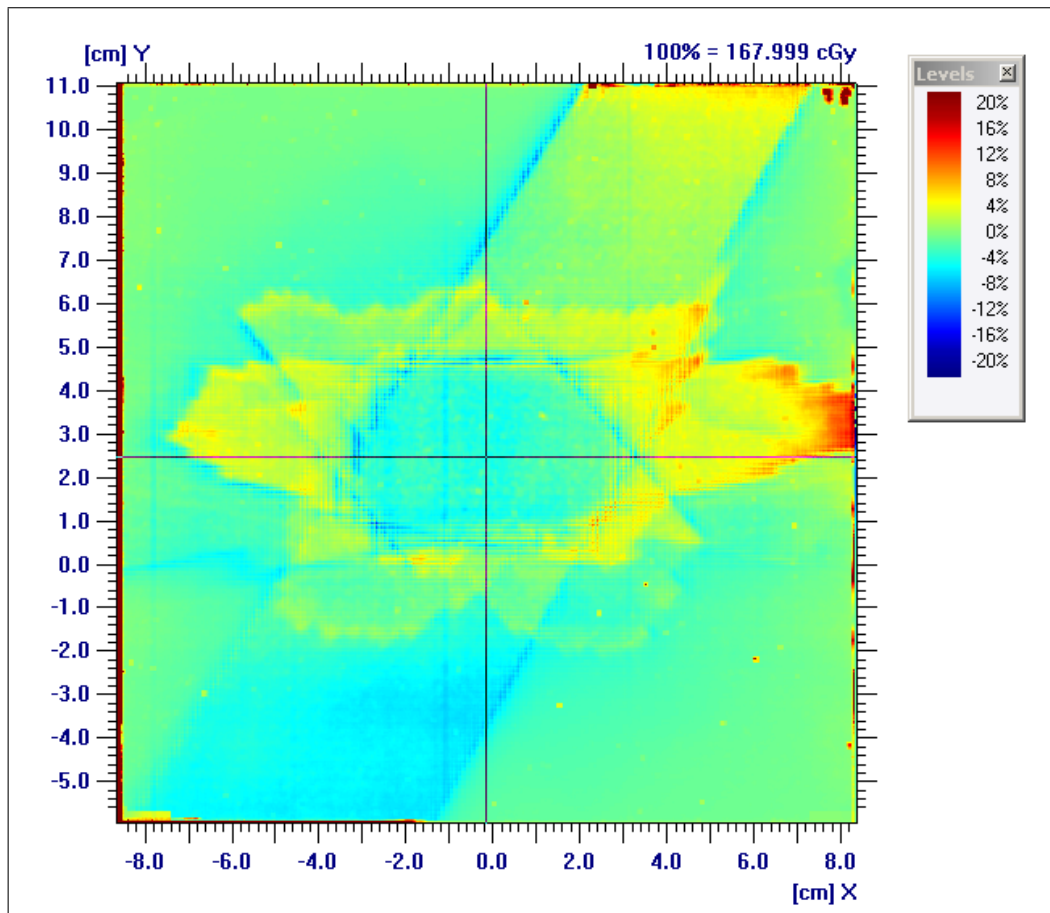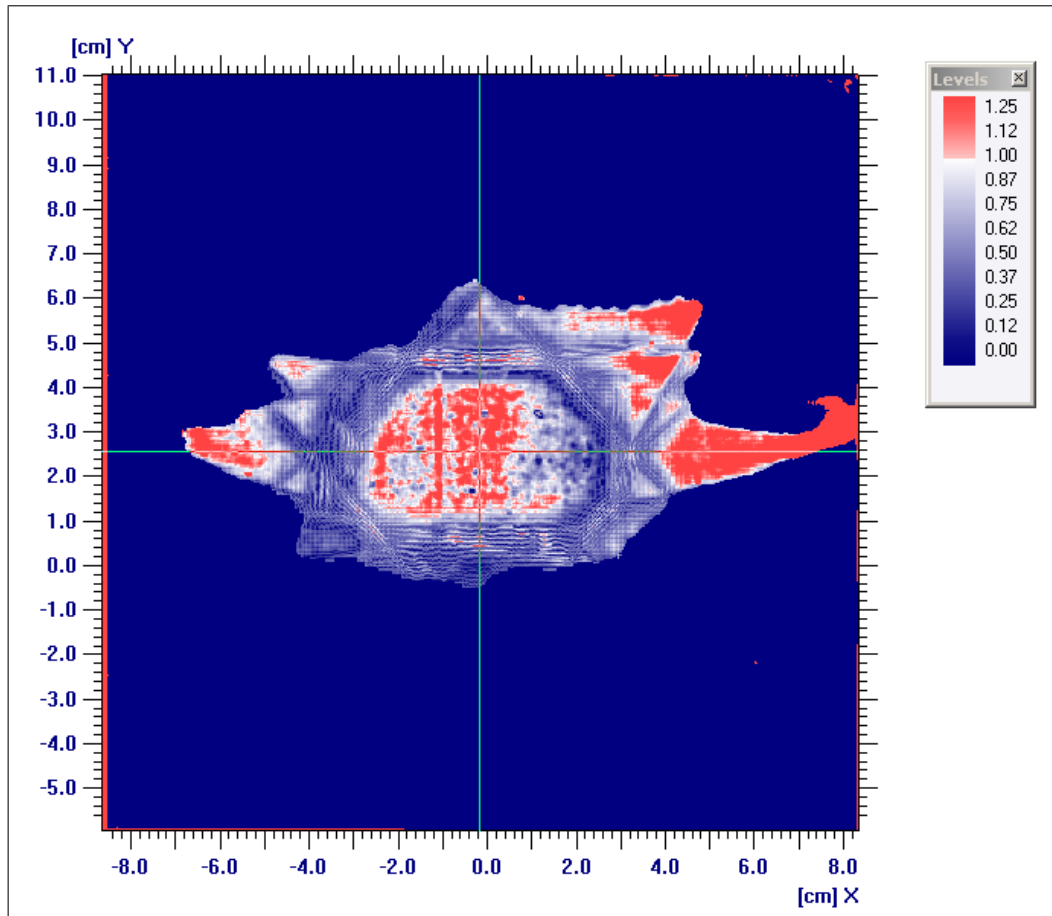. Without obvious high gradient in three dimension, the possibility that a small displacement of the film can cause such big discrepancy is very small. The possibility that the discrepancy is due to the miscalculation of the treatment planning software is also unlikely, because that the same clinical cases are also verified by ion chamber and results conclude that the discrepancy between the measurement and the calculation is at most 2 %. The ion chamber measurement also ruled out the possibility that the treatment plan was not properly delivered due to a malfunction of the MLC. Considering that the dose distribution of clinical IMRT cases are accumulated dose distribution of several fields incident from different angles, the discrepancy may because of different response to different beam incident angle or consequently due to different energy. Although this is not consistent with the designed purpose of the film and has never been reported in the literature, this angular dependence have never been tested in our work. It remains a potential cause. Another possibility is that the radiochromic film responds differently for the dynamic delivery, which would indicate a dose rate dependence. However, a dose rate dependence for non-real time application of Gafchromic EBT film is not reported. But since the dose rate dependence is not tested in our work, we cannot ruled out this possibility. In general, we have ruled out most of the possible reasons which can cause the additional discrepancy. Further investigation of the source of discrepancy in film data is beyond the scope of this work.

Based on this analysis, it is concluded that Gafchromic film dosimetry gives results with discrepancies which are clinically unacceptable. This is because in this project we intended to use the Gafchromic film for absolute dosimetry. This is also the reason 2D Gamma tests of all three cases failed in the central region. We concluded that the Gafchromic film should only be

used for relative dosimetry at this time.

Chapter 6

Conclusion

The first objective of this thesis was to evaluate the performance of Gafchromic EBT film and to establish a relative dosimetry system based on this type of film. While the apparent ease of use of Gafchromic EBT films is appealing, we discovered the following limitations during the course of this work:

1. The darkness of the exposed film, and hence the Optical Density increases with post-exposure time. This increase has been measured, and it is about 2 % of the optical density for the first 15 hours post exposure. The change in Optical Density is negligible after the first 15 hours. Although the magnitude of this change is much smaller when compared with the previous version of Gafchromic film, it is still a factor that needs to be controlled. (See Chapter 3, Section 3.3.1.)

2. The image acquired from a uniformly irradiated film can show large-scale fluctuations in Optical Density that could be as large as 2.5 %. This effect is found to be due to the non-uniformity of the film thickness. (See Chapter 3, Section 3.3.2.)

3. Unlike radiographic film, the signal from radiochromic film is dependent on its orientation during the scanning process. All pieces of film including the calibration films should be scanned in the same orientation.

4. When flatbed scanners are used, the pixel values acquired from the film are also dependent on the location of the film inside the scanner. In general, the peripheral region of the scanning area gives lower pixel values compared to the central region due to the light scattering effect and due to the finite size of the light source. (See Chapter 3, Section 3.2.3.)

In order to determine the overall accuracy of the Gafchromic film dosime-

try system, we measured well defined simple square fields, with well-known dose outputs. Several pieces of film that were cut from a single piece were irradiated using the same field parameters and irradiation condition to different dose levels. The measured doses were compared with the calculated dose. The result indicates the overall uncertainty in dose measurement for the square fields were approximately 2.5 %. This was an indication that the intra-piece variation of the film response contributes approximately 2.5 % error in the dose reading. Inter-piece variation of the film response was tested by comparing three sets of calibration films that were irradiated to the same dose levels. The three separate calibration curves obtained from the three sets of films were compared. The results show that variation in response between different pieces has approximately the same magnitude as within a single piece. (See Chapter 3, Section 3.3.4.)

The second objective of this work was to apply this film dosimetry system together with an ion chamber dosimetry technique for dosimetric validation of a stereotactic IMRT treatment planning system. The following summarizes the results of this work in this respect:

1. Film dosimetry using Gafchromic film showed that in the peripheral region of the irradiated volume, the agreement between the measured dose and the calculated dose is clinically acceptable. However, in the central region where the dose level is above 90 % of the prescribed dose, the measured dose was significantly lower in the three cases we measured. The magnitude of the discrepancy in the central region for one of the cases was as high as 8 %. This is significantly larger than the discrepancy observed during measurements of regular static fields. We have ruled out a number of potential reasons that may cause this effect. (See discussion in Chapter 5, Section 5.3.3.) The actual causes of this effect is yet unclear.

2. From the ion chamber measurement, the dose verification of three clinical cases indicated that for a point dose, the calculated dose agreed with the measured values within 2 %. For individual fields, the discrepancy could

be much larger than this. This is believed to be due to the presence of high dose gradient around the isocenter for individual field. Due to the nature of IMRT each individual field delivers a highly modulated dose but the total dose from all the fields is relatively uniform across the irradiated volume.

3. The angular dependence of the ion chamber response with respect to the incident beam was systematically investigated. Results indicated that the magnitude of this effect was less than 1.0 % in most cases, the largest observed difference being 1.5 %. This was very relevant to the accuracy of stereotactic field verification measurements, as it is often the case that the direction of the incident beam is not perpendicular to the long axis of the ion chamber.

Chapter 7

Future Study

7.1 Gafchromic EBT2 Film

The film manufacturer acknowledges that the intrinsic variation of the thickness of the active layer of the film is in most cases the major contributor to the uncertainty of Gafchromic EBT film dosimetry. Thus a new Gafchromic EBT2 film was introduced with the aim of solving this problem. Gafchromic EBT2 film is manufactured by adding a radiation insensitive yellow color dye to the active layer of the film. The attenuation caused by this yellow dye can be detected primarily in the blue channel and is approximately proportional to the active layer thickness of the film. Because both the red channel signal and the blue channel signal are thickness and dose dependent, if the red channel and blue channel signal can be read together, it is, in principle, possible that the variation in the active layer thickness can be corrected for. Although the basic idea is clear, practical implementation of the yellow dye remains to be done. The manufacturer provides a procedure to make the correction, but further investigation is necessary to verify this method before it can be used. If the thickness variation can be measured and corrected for, the accuracy of Gafchromic film dosimetry may be significantly increased, which is desired for dose verification purpose.

7.2 Monte Carlo Simulation

As mentioned in Chapter 1, Monte Carlo simulation is a useful tool for the purpose of patient-specific dose verification of IMRT treatment plans calcu-

lated by commercial treatment planning systems. This is because the Monte Carlo method calculates the dose from first principles, unlike model-based dose calculation algorithms used in commercial treatment planning systems. For this reason, Monte Carlo simulation has the potential to be the most accurate dose calculation method. Compared with other simplified algorithms, Monte Carlo simulation gives much more accurate results in situations where significant electron disequilibrium exists, for example the presence of air cavities or rapidly changing tissue density.

Compared with measurement-based verification methods, the Monte Carlo simulation method has the following advantages: it produces a three dimensional dose distribution with high resolution and it is much less labor-intensive.

At the Vancouver Cancer Center, Monte Carlo simulation is clinically used for conventional IMRT treatment plan verification. The calculation is carried out in three main steps. The program modules used for the simulation are: BEAMnrc[37], the Virginia code (a simplified MLC simulation code referred here as the Virginia Code as the author is from Medical College of Virginia Hospitals)[38] and DOSXYZnrc[39]. Among them, BEAMnrc and DOSXYZnrc are both EGSnrc[40] based general purpose Monte Carlo simulation programs. BEAMnrc is designed for simulating radiotherapy sources based on the modeling of coupled electron and photon transport. More specifically, BEAMnrc is used for simulating particle interactions inside linac head. The simulation starts from electrons exiting the accelerator vacuum exit window and stops before the particles enter a scoring plane which is located above the MLC. Electron and photon interactions with all components within the linac gantry head are simulated. When the simulation is completed, information including each particle's position, velocity and kinetic energy is saved to a file called a phase space file. The simulation of the MLC is carried out with the Virginia code. BEAMnrc itself is also capable of simulating the MLC, however, because conventional IMRT treatments are dynamically delivered,

a simulation of the dynamic MLC requires extensive calculation and is thus time consuming. The Virginia code, simplifies the simulation. For photons it only considers attenuation and first Compton scattering. Pair production and electron interactions (scattering and Bremsstrahlung) within the MLC are ignored. The simplified modeling significantly increases the calculation speed, while tests show that the accuracy is not significantly reduced. The simulation continues from the phase space file created by BEAMnrc in the first step. The information about the MLC position is (rather than extracted from the treatment plan file) imported from a so-called dynamic log file from the MLC control console, which is a record of the actual MLC performance monitored by build-in sensors (See Chapter 4, Section 4.3.2 for detailed descriptions.) The result of the MLC simulation is saved to another phase space file in the same format. For the last step, the dose distribution is calculated by DOSXYZnrc, which is a general purpose Monte Carlo simulation program for dose distribution calculation. The final three dimensional dose distribution is exported in DICOM format, which is then imported to Varian Eclipse software for comparison with the TPS calculation. The simulation is performed using a 30-node dedicated cluster of 64-bit 2 GHz AMD Opteron processors. The typical calculation time for a single case is approximately 2 hours.

To modify the current Monte Carlo simulation so that it can be applied for dose verification of the stereotactic IMRT technique, the code used in the second step of the Monte Carlo simulation needs to be modified. This is because the BrainLAB m3 micro MLC is used in the stereotactic IMRT beam delivery and the physical dimensions of this MLC is different from the Varian Millennium MLC. The Virginia code should be modified to represent the m3 micro MLC. Noticeably the difference between the m3 MLC and Varian Millennium MLC is not only the size but also the shape and detailed structure of the leaves.

If the Monte Carlo system can be successfully modified and used for

stereotactic IMRT treatment verification, it will be an excellent tool for evaluating dose distributions, considering the accuracy of the current Gafchromic EBT film dosimetry method is not high enough for clinical application.

Bibliography

Bibliography

[1] K. Otto, "Volumetric modulated arc therapy: IMRT in a single gantry arc," *Medical Physics*, vol. 35, pp. 310–317, January 2008.

[2] B. G. Clark, T. Teke, and K. Otto, "Penumbra evaluation of the Varian Millennium and BrainLAB m3 multileaf collimators," *Radiation Oncology*, vol. 66, pp. S71–S75, Nov 2005.

[3] M. McJury, M. Oldham, V. P. Cosgrove, P. S. Murphy, S. Doran, M. O. Leach, and S. Webb, "Radiation dosimetry using polymer gels: methods and applications," *The British Journal of Radiology*, vol. 73, no. 2000, pp. 919–929, 2000.

[4] T. LoSasso, C. S. Chui, and C. C. Ling, "Comprehensive quality assurance for the delivery of intensity modulated radiotherapy with a multileaf collimator used in the dynamic mode," *Medical Physics*, vol. 28, pp. 2209–2219, November 2001.

[5] A. Leal, F. Snchez-Doblado, R. Arrns, J. Rosell, E. C. Pavn, and J. I. Lagares, "Routine IMRT verification by means of an automated Monte Carlo simulation system," *International Journal of Radiation Oncology Biology Physics*, vol. 56, pp. 58–68, May 2003.

[6] T. Bortfeld, W. Schlegel, K. H. Hover, and D. Schulz-Ertner, "Mini and Micro Multileaf Collimators," tech. rep., German Cancer Research Center, 1999.

[7] S. Benedict, R. Cardinale, Q. Wu, R. Zwicker, W. Broaddus, and R. Mohan, "Intensity-modulated stereotactic radiosurgery using dynamic micro-multileaf collimation," *International Journal of Radiation Oncology Biology Physics*, vol. 50, pp. 751–758, July 2001.

[8] S. Espinoza, M. Saboori, S. Forman, C. R. Moorthy, and D. L. Benzil, "Use of stereotactic intensity-modulated radiotherapy in thyroid-related ophthalmopathy," *Journal of Neurosurgery*, vol. 101, pp. 396–401, November 2004.

[9] B. C. Ferreira, M. C. Lopes, and M. Capela, *World Congress on Medical Physics and Biomedical Engineering*, vol. 25/1. Munich, Germany: Springer Berlin Heidelberg, September 2009.

[10] B. Clark, C. Candish, E. Vollans, E. Gete, R. Lee, M. Martin, R. Ma, and M. McKenzie, "Optimization of stereotactic radiotherapy treatment delivery technique for base-of-skull meningiomas," *Medical Dosimetry*, vol. 33, pp. 239–247, April 2008.

[11] F. H. Attix, *Introduction to Radiological Physics and Radiation Dosimetry*. Wiley-Interscience, 1 edition ed., September 1986.

[12] P. Mayles, A. E. Nahum, and J.-C. Rosenwald, *Handbook of Radiotherapy Physics*. Taylor and Francis, first ed., 2007.

[13] H. E. Johns and J. R. Cunningham, *Physics of Radiology*. Charles C. Thomas Publisher, 4th ed., February 1983.

[14] D. I. Thwaites and J. B. Tuohy, "Back to the future : the history and development of the clinical linear accelerator," *Physics in medicine and biology*, vol. 51, no. 13, pp. R343–R362, 2006.

[15] P. Metcalfe, T. Kron, and P. Hoban, *The Physics of Radiotherapy X-Rays from Linear Accelerators*. Medical Physics Publishing Corporation, 1st ed., June 1997.

[16] E. B. Podgorsak, "Stereotactic Irradiation: Historical Perspective and Current Trend," *Journal of Medical Physics*, vol. 26, no. 4, pp. 298–316, 2001.

[17] D. Verellen, N. Linthout, A. Bel, G. Soete, D. V. den Berge, J. D. Haens, and G. Storme, "Assessment of the uncertainties in dose delivery of a commercial system for linac-based stereotactic radiosurgery," *International Journal of Radiation Oncology Biology Physics*, vol. 44, pp. 421–433, May 1999.

[18] Y. C. Lo, C. Ling, and D. A. Larson, "The effect of setup uncertainties on the radiobiological advantage of fractionation in stereotaxic radiotherapy," *International Journal of Radiation Oncology Biology Physics*, vol. 34, pp. 1113–1119, March 1996.

[19] T. Bortfeld, "IMRT: a review and preview," *Physics in Medicine and Biology*, pp. R363–R379, June 2006.

[20] A. Brahme, J. E. Roos, and I. Lax, "Solution of an integral equation encountered in rotation therapy," *Physics in medicine and biology*, vol. 27, pp. 1221–1229, 1982.

[21] A. Niroomand-Rad, C. R. Blackwell, B. M. Coursey, K. P. Gall, J. M. Galvin, W. L. McLaughlin, A. S. Meigooni, R. Nath, J. E. Rodgers, and C. G. Soares, "AAPM Report No.63 Radiochromic Film Dosimetry," tech. rep., AAPM Radiation Therapy Committee Task Group No. 55, Dec 1998.

[22] International Specialty Products Inc., *Effects of Light Scattering by Films on the Performance of CCD Scanners*.

[23] International Specialty Products Inc., *Suggested Procedure QAI 366 Convert the scanner-space values to absorbed dose values*, rev 0.3 ed.

[24] S. Saur and J. Frengen, "GafChromic EBT film dosimetry with flatbed CCD scanner: A novel background correction method and full dose uncertainty analysis," *Medical Physics*, vol. 35, pp. 3094–3101, July 2008.

[25] B. C. Ferreira, M. C. Lopes, and M. Capela, "Evaluation of an Epson flatbed scanner to read Gafchromic EBT films for radiation dosimetry," *Physics in Medicine and Biology*, vol. 54, pp. 1073–1085, Jan 2009.

[26] L. J. van Battum, D. Hoffmans, H. Piersma, and S. Heukelom, "Accurate dosimetry with GafChromic EBT film of a 6 MV photon beam in water: What level is achievable?," *Medical Physics*, vol. 35, Feb 2008.

[27] O. A. Zeidan, S. A. L. Stephenson, S. L. Meeks, T. H. Wagner, T. R. Willoughby, P. A. Kupelian, and K. M. Langen, "Characterization and use of EBT radiochromic film for IMRT dose verification," *Medical Physics*, vol. 33, pp. 4064–4072, 2006.

[28] B. D. Lynch, J. Kozelka, M. K. Ranade, J. G. Li, W. E. Simon, and J. F. Dempsey, "Important considerations for radiochromic film dosimetry with flatbed CCD scanners and EBT GafChromic film," *Medical Physics*, vol. 33, pp. 4551–4556, 2006.

[29] I. S. P. Inc., "EBT Whitepaper," tech. rep., International Specialty Products Inc., August 2007.

[30] I. S. P. Inc., "GafChromic Technical Brief," tech. rep., International Specialty Products Inc., February 2009.

[31] A. Rink, A. Vitkin, I, and D. Jaffray, A, "Intra-irradiation changes in the signal of polymer-based dosimeter (GAFCHROMIC EBT) due to dose rate variations," *Phys. Med. Biol.*, vol. 52, pp. N523–N529, 2007.

[32] "AAPM Report No. 54 Stereotactic Radiosurgery," tech. rep., American Institute of Physics Task Group 42, June 1995.

138

[33] R. K. Rice, J. J. Hansen, G. K. Svensson, and R. L. Siddon, "Measurements of dose distributions in small beams of 6 MV X-rays," *Physics in Medicine and Biology*, vol. 32, pp. 1087–1099, September 1987.

[34] W. U. Laub and T. Wong, "The volume effect of detectors in the dosimetry of small fields used in IMRT," *Medical Physics*, vol. 30, pp. 341–347, March 2003.

[35] E. Pappas, T. G. Maris, A. Papadakis, F. Zacharopoulou, J. Damilakis, N. Papanikolaou, and N. Gourtsoyiannis, "Experimental determination of the effect of detector size on profile measurements in narrow photon beams," *Medical Physics*, vol. 33, pp. 3700–3710, October 2006.

[36] D. A. Low and J. F. Dempsey, "Evaluation of the gamma dose distribution comparison method," *Med. Phys.*, vol. 30, pp. 2455–2464, September 2003.

[37] D. Rogers, B. Walters, and I. Kawrakow, "BEAMnrc Users Manual," tech. rep., Ionizing Radiation Standards, National Research Council of Canada, July 2009.

[38] J. V. Siebers, P. J. Keall, J. O. Kim, and R. Mohan, "A method for photon beam Monte Carlo multileaf collimator particle transport," *Physics in Medicine and Biology*, vol. 47, no. 17, pp. 3225–3249, 2002.

[39] B. Walters, I. Kawrakow, and D. Rogers, "DOSXYZnrc Users Manual," tech. rep., Ionizing Radiation Standards, National Research Council of Canada, July 2009.

[40] I. Kawrakow, E. Mainegra-Hing, D. Rogers, F. Tessier, and B. Walters, "The EGSnrc Code System: Monte Carlo Simulation of Election and Photon Transport," tech. rep., Ionizing Radiation Standards, National Research Council of Canada, Carleton University, Feb 2010.

Appendix A

Source Code

A.1 Matlab Source Code Used to Adjust the Resolution of scanned images

```
%This progam is used to reduce the resolution
%Adjust the parameters if necessary
[fname pname]=uigetfile('*.tif','Select the 300dpi
    input TIFF file');%Change the resolution if needed
tg=imread([pname fname]);
[y x z]=size(tg);

xx=floor(x/3);%Reduced 3 times
yy=floor(y/3);%Reduced 3 times

output=uint16(zeros(yy,xx,z));
for i=1:yy
    for j=1:xx
        for k=1:z
            ave=uint16(median(median(double(tg(((i-1)
                *3+1):i*3,((j-1)*3+1):j*3,k))))));
            output(i,j,k)=ave;
        end
    end
end
```

```matlab
wname=['100dpi_' fname];%Change the resolution if
    needed
imwrite(output,[pname wname]);
```

A.2 Matlab Source Code Used to Calibrate the Film and Convert the Dose Distribution into Omni-pro Compatible Format

```matlab
%Use 6 6x6cm square field to generate calibration curve
%Apply on a measuremtn film and convert it into Omni-
    pro compatible format
%Potiential monification incluedes resulotion and head
    information
%This is a corronal plane version and used raw pixel
    value to calibrate

sq_rd=imread('100dpi_c2.tif');
sq_ave=mean(mean(sq_rd(102:134,102:134,1)));
netod=sq_ave;
dose=0/145;




sq_rd=imread('100dpi_a1.tif');
sq_ave=mean(mean(sq_rd(102:134,102:134,1)));
netod=[netod sq_ave];
dose=[dose 50/145];
```

```matlab
sq_rd=imread('100dpi_a2.tif');
sq_ave=mean(mean(sq_rd(102:134,102:134,1)));
netod=[netod sq_ave];
dose=[dose 100/145];

sq_rd=imread('100dpi_a3.tif');
sq_ave=mean(mean(sq_rd(102:134,102:134,1)));
netod=[netod sq_ave];
dose=[dose 150/145];

sq_rd=imread('100dpi_b1.tif');
sq_ave=mean(mean(sq_rd(102:134,102:134,1)));
netod=[netod sq_ave];
dose=[dose 200/145];

sq_rd=imread('100dpi_b2.tif');
sq_ave=mean(mean(sq_rd(102:134,102:134,1)));
netod=[netod sq_ave];
dose=[dose 250/145];

sq_rd=imread('100dpi_b3.tif');
sq_ave=mean(mean(sq_rd(102:134,102:134,1)));
netod=[netod sq_ave];
dose=[dose 300/145];

sq_rd=imread('100dpi_c1.tif');
sq_ave=mean(mean(sq_rd(102:134,102:134,1)));
netod=[netod sq_ave];
dose=[dose 350/145];
```

```matlab
sq_rd=imread('100dpi_c3.tif');
sq_ave=mean(mean(sq_rd(102:134,102:134,1)));
netod=[netod sq_ave];
dose=[dose 450/145];


sq_rd=imread('100dpi_d1.tif');
sq_ave=mean(mean(sq_rd(102:134,102:134,1)));
netod=[netod sq_ave];
dose=[dose 550/145];


sq_rd=imread('100dpi_d2.tif');
sq_ave=mean(mean(sq_rd(102:134,102:134,1)));
netod=[netod sq_ave];
dose=[dose 700/145];


sq_rd=imread('100dpi_d3.tif');
sq_ave=mean(mean(sq_rd(102:134,102:134,1)));
netod=[netod sq_ave];
dose=[dose 800/145];


netod2=netod;
coef=polyfit(netod2,dose,4);

netod_hires=netod2(1):-0.01:netod2(12);
plot(dose,netod2,polyval(coef,netod_hires),netod_hires)
    ;



xlabel('Dose_(Gy)');
```

```matlab
ylabel('Net_Optical_Density');

[cvfname,cvpname] = uigetfile('*.tif','Select_the_TO_BE
    _CONVERTED_film');
cv=imread([cvpname  cvfname]);



cv_netod=double(cv(:,:,1));
cv_dose=polyval(coef,cv_netod);



cv_dose3=flipud(cv_dose)';
cv_dose2=wiener2(cv_dose3,[5  5]);


cvfname_aux=cvfname(1:length(cvfname)-4);
fidA=fopen([[cvpname  cvfname_aux]  '.opg'],'wt');


% **********************
% Part 1 Create  the  head  (Modify  if  needed)
% **********************
fprintf(fidA,'<opimrtascii>\n');
fprintf(fidA,'\n');
fprintf(fidA,'<asciiheader>\n');
fprintf(fidA,'File_Version:_____3\n');
fprintf(fidA,'Separator:_____","\n');
fprintf(fidA,'Workspace_Name:_____\n');
fprintf(fidA,'File_Name:_____\n');
fprintf(fidA,'Image_Name:_____%s\n',cvfname);
fprintf(fidA,'Radiation_Type:_____Photons\n');
fprintf(fidA,'Energy:_____6.0_MV\n');
```

```
fprintf(fidA , 'SSD:_____\n');
fprintf(fidA , 'SID:_____100.0_cm\n');
fprintf(fidA , 'Field_Size_Cr:_____\n');
fprintf(fidA , 'Field_Size_In:_____\n');
fprintf(fidA , 'Data_Type:_____Abs._Dose\n');
fprintf(fidA , 'Data_Factor:_____1.000\n');
fprintf(fidA , 'Data_Unit:_____mGy\n');
fprintf(fidA , 'Length_Unit:_____cm\n');
fprintf(fidA , 'Plane:_____XY\n');%Important
    !!!!!!


[x,y]=size(cv_dose2);

xres=0.0254;%=100dpi
yres=0.0254;%=100dpi

delta_x=xres*x;
delta_y=yres*y;

startx=-8.5;
starty=-8.5;

%********************************
% Changing no. rows and columns
%********************************
fprintf(fidA , 'No._of_Columns:_____%d\n',x);
fprintf(fidA , 'No._of_Rows:_____%d\n',y);

% *********************
```

```
% Part 2 Create the head (Modify if needed)
% ***********************
fprintf(fidA, 'Number of Bodies:   1\n');
fprintf(fidA, 'Operators Note:     Corr.: Unif.Calib.,
    Bkgnd, Calib Output, Temp., Press.,\n');
fprintf(fidA, '</asciiheader >\n');
fprintf(fidA, '\n');
fprintf(fidA, '<asciibody >\n');
fprintf(fidA, 'Plane Position:     0.0 cm\n');

fprintf(fidA, 'X[cm] , ');%Important !!!!!!
for  i=1:x
    fprintf(fidA, ' %.3f , ', startx+(i-1)*xres);
end
fprintf(fidA, '\nY[cm]\n');%Important !!!!!!

for  j=1:y
    fprintf(fidA, ' %.3f , ', starty+(j-1)*yres);
    for  i=1:x

        fprintf(fidA, ' %d , ', uint16(cv_dose2(i,j)*1000)
            );
    end
    fprintf(fidA, '\n');
end
fprintf(fidA, '</asciibody >\n\n\n');
fprintf(fidA, '</opimrtascii >\n');
fclose(fidA);
```